LOCKHEED MARTIN ENERGY RESEARCH LIBRARIES
3 4456 0515383 8

ORNL-4765 + Addendum
UC-34 – Physics

Cy. 4

AN EVALUATION OF NEUTRON AND GAMMA-RAY-PRODUCTION CROSS SECTIONS FOR LEAD

C. Y. Fu
F. G. Perey

OAK RIDGE NATIONAL LABORATORY
CENTRAL RESEARCH LIBRARY
CIRCULATION SECTION
4500N ROOM 175
LIBRARY LOAN COPY
DO NOT TRANSFER TO ANOTHER PERSON.
If you wish someone else to see this report, send in name with report and the library will arrange a loan.
ORNL-118 (6-97)

OAK RIDGE NATIONAL LABORATORY
operated by
UNION CARBIDE CORPORATION
for the
U.S. ATOMIC ENERGY COMMISSION

Printed in the United States of America. Available from
National Technical Information Service
U.S. Department of Commerce
5285 Port Royal Road, Springfield, Virginia 22151
Price: Printed Copy $3.00; Microfiche $0.95

This report was prepared as an account of work sponsored by the United States Government. Neither the United States nor the United States Atomic Energy Commission, nor any of their employees, nor any of their contractors, subcontractors, or their employees, makes any warranty, express or implied, or assumes any legal liability or responsibility for the accuracy, completeness or usefulness of any information, apparatus, product or process disclosed, or represents that its use would not infringe privately owned rights.

LOCKHEED MARTIN ENERGY RESEARCH LIBRARIES
3 4456 0515383 8

March 17, 1972

ADDENDUM TO ORNL-4765 - AN EVALUATION OF NEUTRON AND GAMMA-RAY-PRODUCTION CROSS SECTIONS FOR LEAD

This addendum describes improvements made to the evaluation documented in the main body of this report.

One of the known deficiencies of the evaluation was the capture cross-section file above thermal. At the time the evaluation was done, we knew that some high-resolution measurements of the capture cross sections for the lead isotopes were in progress at ORELA by Allen et al.[1] Now that the data have become available, we have gone back and performed a reevaluation of the capture cross-section file. With the new data we have been able to improve also the representation of the resonances in the total and elastic-scattering cross-section files.

It did not appear necessary to us to represent explicitly in the file all of the capture resonances reported by Allen et al. (numbering more than 500). Table 1 lists only the capture resonances which could be correlated with observed resonances in the total cross sections and the other capture resonances having areas greater than 5 barn-eV in natural lead. All areas in Table 1 are given in terms of natural lead using isotopic abundances of 0.0124, 0.236, 0.226 and 0.523 for the isotopes 204, 206, 207, and 208 respectively. Our aim was to represent these resonances in both the total and capture cross-section files in such a manner that upon subtraction of these files the resonances would have a reasonable representation in the elastic cross-section file. The remainder of the small capture resonances, together with the 1/v component, were averaged to form a smooth cross section to which the large capture resonances could be added. Total widths and resonance areas in the total cross sections were calculated from resonance parameters compiled in BNL-325 (Ref. 2) and are compared in Table 1 with those

TABLE 1. CORRELATION OF CAPTURE AND TOTAL RESONANCES. ALL AREAS ARE GIVEN IN TERMS OF NATURAL LEAD. E IS IN keV, Γ IN eV, AND A IN BARN-eV

Isotope	Allen			Good			BNL-325			Adopted			
	E	Γ	A_γ	E	Γ	A_T	E	Γ	A_T	E	Γ	A_T	Γ_γ
204				1.690	5	79	1.68	<5.9	135±13	1.685	5	135	
204	2.596	<5.4	0.59	2.485	8	100	2.48	<7.8	138±13	2.485	5	138	0.02
207	3.071	< 7	21	3.070	2	25	3.06		45±10	3.070	2	45	0.93
206	3.365	<6.6	16	3.364	5	74	3.35		140±30	3.360	5	140	0.57
204	8.348	56	10.3	8.374	67	320	8.34	<60	350±60	8.350	56	350	1.5
204	9.635	<19	4.2	9.680	30	61	9.63	<25	91±30	9.635	19	91	0.87
207	10.21	<24	13	10.21	21	61				10.21	21	91	
207	12.40	17	0.34	12.39	24	82	12.1	<25		12.39	17	123	
204	12.88	91	2.7	12.92	77	240	12.9	<55	206±20	12.90	55	220	0.67
206	14.25	<29	5.2	14.24	24	68				14.24	24	102	
207	16.21	<38	17	16.20	44	65				16.20	38	97	
206	16.47	<34	39	16.47			16.4	<20	230±150	16.47	20	230	
207	16.80	60	3.2	16.80	61	730	16.7±0.3	<91	1260±200	16.80	60	1260	0.15
206	19.80	<41	5.9	19.79	49	98				19.79	41	147	
206	19.86	<42	6.1							19.86		↑	
206	21.94	<45	9.4	21.93	33	32				21.93	33	48	
206	25.17	<53	15							25.17		↓	
206	25.49	102	13	25.47	100	1060	25.3±0.4	<59	2300±230	25.47	59	2300	
207	29.46	<72	6.6	29.44	82	320	28.5±0.5	<65	2500±1600	29.44	65	1000	
207	30.54	<75	8.7	30.43	30	60				30.48	30	90	
206	37.57	<80	8.6	36.27	120	400	~35	<58		36.90	58	600	
207	37.82	98	18	37.78	160	650	37.0±0.5	<70		37.80	70	975	
207	41.32	1268	85	41.64	1770	16000	42.8±0.7	1250	20600±2500	41.60	1250	20600	5.0
206	42.20	<90	17							42.20		↑	
206	47.70	<103	2	47.61	220	1200	~46	<73		47.60	73	1800	
206	59.39	<130	11							59.39	130	(11)	
206	64.16	<140	7.5							64.16	140	(7.5)	
206	66.19	116	19	66.22	200	600	66.0±2.0	250	360±220	66.20	116	480	
206	70.50	<155	1.3	71.31	360	2800				71.00	155	4200	
208	77.70	2252	34	78.22	1370	26400	80.0±0.5	1000	27000±2700	78.00	1000	27000	1.26
206	80.63	<180	26							80.63		↑	
206	83.90	134	8.9	86.71	620	1750	85.0±2.0	420	2400±550	85.00	134	2400	
206	88.77	<200	11							88.77	200	(11)	
207	90.40	674	20	90.29	850	3700				90.35	674	3700	
206	92.04	151	5								151	(5)	
206	92.90	149	14								149	(14)	
206	114.9	264	24	115.5	800	1500				115.2	264	1500	
206	118.4	<270	7	117.4	840	5600				117.9	270	5800	
206	125.1	250	29	124.8	620	2400				125.0	250	2400	
206	125.7	166	57	128.0	500	1600	126±1		3500±340	127.0	166	3500	

A2

Table 1 cont.

Isotope	Allen			Good			BNL-325			Adopted			
	E	Γ	A_γ	E	Γ	A_T	E	Γ	A_T	E	Γ	A_T	Γ_γ
206	141.1	409	23	140.2	530	910				140.6	409	910	
206	146.8	400	38								400	(38)	
206	151.7	370	7.3	150.2	1400	6800	151±1		5800±900	151.0	370	6300	
206	170.0	<300	6.4	169.0	1700	2100				169.5	300	2100	
207	181.9	306	64	180.5	1000	1400				181.0	306	1400	
206	199.2	383	26	198.5	1200	1300	197±1		1260±390	198.5	383	1300	

↑(↓) indicates that A_T is probably included in the one given above (below). In such cases only one resonance is given in the cross section file and the capture areas are combined.

obtained from Good's data.[3] The adopted resonance energy, E, total width, Γ, and resonance areas, A_T, are averages of the two sets with some exceptions. Below about 50 keV, the resonance areas in Good's data are generally 50% smaller than those reported in BNL-325. Because Good's measurements have not yet been documented, we adopted the BNL-325 values whenever available and increased by 50% the areas of the other resonances in Good's data. Most of the total widths in Allen et al.'s data are given as upper limits. Because the capture measurements had the better energy resolution, we felt that these upper limits should not be exceeded. Thus when the parameters from BNL-325 and the widths from Good's data gave values of the resonance widths larger than the upper estimates obtained in the capture cross-section measurement, we adopted the later values as the resonance widths. For the capture resonances which had areas greater than 5 barn-eV but could not be correlated with total cross section resonances, the total resonance area A_T was set equal to the capture resonance area A_γ. For some of the resonances for which A_T and Γ appeared reasonably certain, we could extract Γ_γ and these are given in the last column of Table 1. The resonance at 1.685 keV, which is below the lower limit of the capture measurement, is the lowest energy resonance observed so far in the lead isotopes. Since it has the same J^π and approximately the same Γ and A_T as the resonance at 2.485 keV, we adopted the same A_γ for the file.

The average capture cross sections for the lead isotopes, natural lead and the smooth capture cross sections upon which the resonances were built are listed in Table 2. Except for ^{204}Pb above 50 keV, the average capture cross sections for the isotopes are simply a sum of the resonance cross sections in

TABLE 2. AVERAGE CAPTURE CROSS SECTION IN MILLIBARN FOR THE LEAD ISOTOPES AND NATURAL LEAD. THE RIGHTMOST COLUMN GIVES THE SMOOTH CAPTURE CROSS SECTION UPON WHICH THE RESONANCES GIVEN IN TABLE 1 WERE BUILT.

E_n(keV)	204	206	207	208	Pb	σ_b
2-3	65				0.81	0.78
3-4	111	78.5	91.0		41.5	5.0
4-5	81				1.0	1.4
5-6	61				0.76	1.13
6-7	98				1.22	1.57
7-8	13				0.16	0.48
8-9	829				10.3	0.30
9-10	370				4.6	0.70
10-20	70	28.5	13.7	0.29	10.8	1.83
20-30	76	16.0	2.9		5.37	1.14
30-40	59	8.7	12.6	0.10	5.68	2.30
40-50	68	10.5	38.6	0.90	12.5	2.20
50-60	62	5.3			2.02	1.02
60-70	75	13.3	3.4	1.3	5.52	2.97
70-80	50	0.6		6.6	4.21	0.81
80-90	77	21.6	1.5		6.39	1.89
90-100	78	9.6	10.6		5.63	1.83
100-150	73	15.3	4.5	0.24	5.66	2.10
150-200	73	6.3	6.7	0.32	4.07	4.12
200-300	73	4.2	5.3	0.11	3.15	3.6
300-400	69	2.7	1.9	0.11	1.98	3.8
400-500	69	6.7	0.9		2.64	4.2
500-600	69	2.5	(1.6)	0.09	>1.49	4.6
600-700	78	2.7	(10.7)		>1.60	4.3
700-800	91	1.8	(12.9)	2.60	>2.95	3.8
800-900	132		(70.8)	1.04	>2.18	3.5
900-1000						3.3

the given energy interval divided by the energy interval. For ^{204}Pb, above 50 keV, many smaller resonances were not picked up in the analysis; the average cross sections were obtained by summing the experimental data and subtracting from them a smooth time-dependent background.[1] The capture cross-section measurements for ^{207}Pb were seriously contaminated by inelastic scattering above 500 keV, so these data, given in parenthesis in the table, were not included in the average cross sections of natural lead. The last column of Table 2 lists the smooth cross sections upon which the resonances given in Table 1 were built. The smooth cross sections below 150 keV were obtained by subtracting the resonances of Table 1 from the average cross sections and adding a 1/v component based on a previously evaluated cross section of 0.176 barn at 0.0253 eV. Plots[1] of the cumulative sums of the number of resonances versus energy indicated that some of the small resonances, above 100 keV for ^{206}Pb and 200 keV for ^{207}Pb, were not picked up in the analysis. Thus, the average cross section for natural lead above 100 keV is a lower limit which gets worse as the energy increases. Diven et al.[4] have measured capture cross sections for natural lead at seven energies from 175 keV to 1 MeV. Their neutron energy spreads were large enough to justify using their data as the average cross section. The smooth cross sections above 150 keV were then based on the data of Diven et al. Above 1 MeV and below 1 keV the capture cross sections are the same as previously evaluated. Approximately three quarters of the capture cross sections from 1 keV to 200 keV are explicitly given as resonances.

With the exception of the broad 41.60 keV resonance, each resonance was represented in the file by a triangular shape whose area is the resonance area and whose width at the base is equal to 2Γ. If the width were exact, then

the peak cross section in the file would be $\frac{\pi}{2}$ too large. However, since for most resonances we only had an upper limit for the widths, we felt that the above representation was justified. This representation does not reproduce the potential interference in the total cross sections. This drawback should be tolerable considering the large uncertainties in both the widths and the areas of most resonances. Therefore the triangular representation of the resonances appears to be a simple yet realistic one in the present situation.

Total cross sections, except for the new resonance areas listed in Table 1, remain the same as previously evaluated. Elastic-scattering and nonelastic-scattering cross sections were modified accordingly.

The lead evaluation was represented in the ENDF/B-III format. The initial evaluation which was assigned DNA material number 4136 has been adopted by CSEWG, with minor modifications, for the ENDF/B-III set under material 1136. The revisions to the capture cross section file described here have been incorporated in a new tape, submitted to RSIC for inclusion in the DNA evaluated library set and is referred to as Material 4136 Modification 2.

REFERENCES

1. B. J. Allen et al., Capture Cross Sections of the Lead Isotopes, to be published in Physical Review (1972).

2. M. D. Goldberg et al., Neutron Cross Sections, Vol. 11C, Z = 61 to 87, BNL-325, 2nd edition, Supplement No. 2 (1966).

3. W. M. Good, Oak Ridge National Laboratory, private communication (1971).

4. B. C. Diven et al., Radioactive Capture Cross Sections for Fast Neutrons, Phys. Rev. 120, 556 (1960).

ORNL-4765

Contract No. W-7405-eng-26

NEUTRON PHYSICS DIVISION

AN EVALUATION OF NEUTRON AND GAMMA-RAY-PRODUCTION CROSS SECTIONS FOR LEAD

C. Y. Fu and F. G. Perey

MARCH 1972

NOTE: THIS WORK FUNDED BY DEFENSE NUCLEAR AGENCY UNDER SUBTASK No. PC102

OAK RIDGE NATIONAL LABORATORY
Oak Ridge, Tennessee 37830
operated by
UNION CARBIDE CORPORATION
for the
U. S. ATOMIC ENERGY COMMISSION

CONTENTS

Page No.

Abstract 1
1. Introduction 1
2. Previously Available Cross Section Sets 2
2.1. Neutron Cross Sections 2
2.2. Angular Distribution of Secondary Neutrons 3
2.3. Energy Distribution of Secondary Neutrons 3
2.4. Gamma-Ray-Production Cross Sections 4
2.5. Energy Distribution of Secondary Gamma Rays 4
3. General Properties of Lead 5
3.1. Possible Neutron Induced Reactions 5
3.2. Energy Levels and Decay Schemes of the Lead Isotopes 8
3.3. Level Densities of the Lead Isotopes 20
4. Computational Methods and Procedures 23
4.1. Computer Codes 23
4.2. Computational Procedures 28
5. Comparison of Calculation with Experiment 29
5.1. Angular Distribution of Elastic Scattering 31
5.2. Direct-Interaction Contribution to $\sigma_L(n,n')$ 35
5.3. Inelastic-Scattering Exciting Levels 40
5.4. Nonelastic Cross Sections and Components 47
5.5. Energy Distribution of Secondary Neutrons 50
5.6. Gamma-Ray Production 52
6. Evaluation 65
6.1. Total Cross Sections 66
6.2. Elastic-Scattering Cross Sections 68
6.3. Nonelastic-Scattering Cross Sections 74
6.4. Inelastic-Scattering Cross Sections 74
6.5. $\sigma(n,2n)$ and $\sigma(n,3n)$ 75
6.6. Capture Cross Sections 75
6.7. Angular Distribution of Secondary Neutrons 78
6.8. Energy Distribution of Secondary Neutrons 81

Page No.

6.9. Gamma-Ray-Production Cross Sections 81
6.10. Angular Distribution of Secondary Gamma Rays 82
6.11. Energy Distribution of Secondary Gamma Rays 82
6.12. Photon Interaction Cross Sections 86
7. Conclusion and Discussions 86
8. Acknowledgements 88

AN EVALUATION OF NEUTRON AND GAMMA-RAY-PRODUCTION CROSS SECTIONS FOR LEAD

C. Y. Fu* and F. G. Perey

ABSTRACT

A survey was made of the available information on neutron and gamma-ray-production cross section measurements of lead. Evaluated nuclear data sets in the ENDF/B format were prepared for lead covering the energy range from 0.00001 eV to 20.0 MeV. The cross section sets were based on experimental results available to June 1971 and on nuclear model calculations. This evaluation received MAT. No. 4136 in the DNA Library and 1136 for CSEWG.

1. INTRODUCTION

An investigation has been made of the neutron interaction mechanisms with lead. Particular emphasis was given to understanding the neutron and gamma-ray-production cross sections for this element. Being magic nuclei, the lead isotopes have been studied considerably concerning their nuclear properties such as level spins and parities and gamma-ray branching ratios. These properties aid in the understanding of the neutron and gamma-ray-production cross sections.

An extensive literature survey has been made to obtain information on the neutron and gamma-ray-production cross sections for lead. The survey is believed to be reasonably complete for information available to June 1971.

Complete sets of neutron and gamma-ray-production cross sections have been prepared in the ENDF/B format.[1,2] These data sets also include descriptions of the energy and angular distributions of the secondary neutrons and gamma rays. These cross section sets contain data for incident neutrons in

*University of Tennessee, Knoxville, Tennessee

the range between 0.00001 Ev and 20.0 MeV. For a small part the evaluated cross sections were obtained from measured data. In most cases the experimental information was not sufficient to define the cross sections in the entire energy region; the cross sections were interpolated, extrapolated, or predicted using nuclear model calculations. The techniques used in the model calculation and the procedures employed in the evaluation are described in this report.

2. PREVIOUSLY AVAILABLE CROSS SECTION SETS

This section is written primarily for those who have done neutron and/or gamma-ray transport calculations in materials containing natural lead with the previous evaluations. One may wish to know what part of the cross sections he has used is adequate or inadequate for a specific problem.

There are two major evaluations for natural lead, namely, that of Atomic's Weapons Research Establishment of the United Kingdom in 1961[3,4] and that of the United Nuclear Corporation in 1964.[5] The former has been translated into ENDF/B formats and is most commonly used.[6] The latter contains the only complete set of gamma-ray spectra resulting from (n,xγ) reactions.[7] Although the present evaluation is an entirely new one and completely independent of the earlier evaluations, for certain specific problems the earlier cross section sets may be just as good as the newly evaluated sets. The judgement is of course left with the user. This section attempts to help the user make a judgement as to whether recalculation of certain problems, in whole or in part, is necessary.

2.1. Neutron Cross Sections

Recent measurements with much improved techniques have shown a great many new resonances in the total cross sections. The gross structure of

the total cross sections agrees quite well with the previous evaluations. However, many of the newly observed resonances have peaks and valleys differing from the gross structure by as much as one barn. This may bear some significance in neutron transport calculations.

Changes in (n,γ), (n,n') and (n,2n) cross sections were small; except the level excitation cross sections in (n,n') reaction were given in much more detail. (n,3n) cross sections have been added.

Elastic-scattering cross sections, as the total cross sections, contain many more resonance structures than those previously reported.

2.2. Angular Distribution of Secondary Neutrons

The angular distributions of elastically scattered neutrons are given for five neutron energies in the AWRE evaluation and for 378 energies in the UNC report. The present evaluation, in terms of the first four Legendre expansion coefficients, agrees with the latter to within 20% above 1 MeV and 30% below 1 MeV.

The angular distributions of secondary neutrons from inelastic excitation of 35 levels up to 4.4 MeV have been added.

2.3. Energy Distribution of Secondary Neutrons

The energy distributions of secondary neutrons from elastic scattering, and inelastic scattering exciting the discrete levels, may be obtained analytically from the angular distributions. Thus the situation here is the same as in the above section.

The energy distribtuions of secondary neutrons from (n,n' continuum) and from (n,2n) reactions are believed to be much improved. Those from (n,3n) reactions are also included.

2.4. Gamma-Ray-Production Cross Sections

The gamma-ray-production cross sections from (n,xγ) reactions proposed in this evaluation are considerably larger than those in the UNC report. An average deviation of approximately two barns exists in the neutron energy region above 5 MeV. The shapes of the cross sections in the two cases are also different, especially above 14 MeV.

The gamma-ray-production cross sections from (n,γ) reactions are also larger than those in the UNC report above 1 keV of neutron energy. This will be explained in the next section.

2.5. Energy Distribution of Secondarv Gamma Rays

The energy distributions of secondary gamma rays from (n,xγ) reactions deviate substantially from those given in the UNC report, both in spectral shapes and in neutron energy dependence.

The thermal-neutron-capture spectrum was assumed in the UNC work, due to the lack of alternatives, to be valid for captures of all energy neutrons. Here this assumption is relaxed somewhat by introducing one fast-neutron-capture gamma-ray spectrum for use with the capture of neutrons above 1 keV. The fast-neutron-capture spectrum has larger gamma-ray multiplicity than the thermal-neutron-capture spectrum, thus giving larger gamma-ray-production cross sections.

The present evaluation was based on more up-to-date data and more sophisticated calculations than the earlier evaluations. However, reevaluation will be necessary as more and better data become available.

3. GENERAL PROPERTIES OF LEAD

3.1. Possible Neutron Induced Reactions

The element lead has four naturally occurring isotopes. The fractional abundances, the isotopic masses[8] and the thermal neutron activation cross sections[8,9] of the naturally occurring isotopes are given in Table 1. In cases where analysis has to be made with respect to each isotope, the contribution from ^{204}Pb is sometimes ignored. In such cases the effective fractional abundances, given in parenthesis in Table 1, are used.

The three lead isotopes ^{206}Pb, ^{207}Pb, and ^{208}Pb are end products of the three naturally occurring radioactive chains and may be present in abnormal amounts in particular samples. A few percent variations in relative abundances from those given in Table 1 are not uncommon.[4]

Numerous neutron interactions with the lead isotopes are energetically possible for neutrons with energies less than 20 MeV, the upper energy limit of this study. The Q-values[10,11] and residual nuclei for all allowed reactions are given in Table 2.

Although all of the reactions listed in Table 2 were considered for their possible contributions to the cross sections of lead, not all of these reactions were included in the final data sets. Reactions with charged-particle emission, strongly inhibited by the Coulomb barrier, were found to make negligible contributions and thus were ignored.

Reactions like (n,n'γ), (n,2nγ), and (n,3n) have to be considered separately for each isotope. Both the neutron cross sections and the resulting gamma-ray spectra for these reactions depend heavily on model calculations. They are thus the most time consuming part of the evaluation.

Table 1. Properties of the Naturally Occurring Lead Isotopes

Isotope	Fractional Abundance	Isotopic Mass+	Thermal Neutron Activation Cross Section (barns)
^{204}Pb	0.0124(0.0)*	203.97304	0.655±0.05
^{206}Pb	0.236(0.24)	205.97447	0.0305±0.008
^{207}Pb	0.226(0.23)	206.97590	0.709± 0.01
^{208}Pb	0.523(0.53)	207.97665	0.0005

+Mass of natural lead may be set equal to 207.21±0.03 amu in the ^{12}C scale.

*Effective abundances used in cases where the contribution from ^{204}Pb is neglected.

Table 2. Reaction Q Values and Residual Nuclei for Lead Isotopes

Reaction	Q Values (keV) and Residual Nuclei			
	^{204}Pb	^{206}Pb	^{207}Pb	^{208}Pb
(n,γ)	+6734.4±12.0 Pb 205	+6733.1±6.7 Pb 207	+7376.0±6.9 Pb 208	+3944.8±9.3 Pb 209
(n,n')	-899.0±0.0 Pb 204	-803.0±0.0 Pb 206	-570.0±0.0 Pb 207	-2615.0±0.0 Pb 208
(n,p)	-17.5±11.3 Tl 204	-741.8±7.5 Tl 206	-652.5±8.6 Tl 207	-4211.1±7.7 Tl 208
(n,np)	-6646.0±8.0 Tl 203	-7265.0±6.0 Tl 205	-7476.0±6.0 Tl 206	-8034.0±9.0 Tl 207
(n,2n)	-8244.4±14.4 Pb 203	-8085.7±10.1 Pb 205	-6733.1±6.7 Pb 206	-7376.0±6.9 Pb 207
(n,d)	-4420.5±10.6 Tl 203	-5043.8±9.2 Tl 205	-5250.5±7.8 Tl 206	-5804.1±8.5 Tl 207
(n,t)	-5859.5±24.4 Tl 202	-6320.8±9.2 Tl 204	-5519.5±9.4 Tl 205	-6369.1±7.7 Tl 206
(n,^{3}He)	-4622.9±10.0 Hg 202	-5957.2±7.5 Hg 204	-7147.9±100.1 Hg 205	-7663.5±21.5 Hg 206
(n,α)	+8195.7±10.6 Hg 201	+7122.4±8.3 Hg 203	+7887.7±7.8 Hg 204	+6054.1±100.1 Hg 205
(n,nα)	+1969.3±10.0 Hg 200	+1135.0±7.5 Hg 202	+389.3±8.6 Hg 203	+511.7±7.7 Hg 204
(n,3n)	-15174.0±38.0 Pb 202	-14816.0±4.3 Pb 204	-14817.0±7.0 Pb 205	-14110.0±3.0 Pb 206

3.2. Energy Levels and Decay Schemes of the Lead Isotopes

Understanding the properties of the energy levels and decay schemes of the lead isotopes is very important when trying to analyze the (n,n'), (n,2n), and (n,3n) cross sections and the resulting gamma rays. The energy levels and gamma-ray branching ratios for ^{206}Pb, ^{207}Pb, and ^{208}Pb as used in the theoretical analysis are given in Tables 3-5 and Figs. 1-3.

For ^{206}Pb the energy levels are mostly those given in Nuclear Data Sheets.[12] Those taken from other sources[13-16] are indicated in the comments of Table 3. Above 2 MeV levels predicted by the shell-model calculations of Alburger and Pryce[15] were added. The same calculation was used to assume spins and parities for observed levels for which spins and parities had not been known. Most of the energy levels in ^{206}Pb below 3.7 MeV may be interpreted as two-neutron-hole states on a doubly magic core ^{208}Pb. Around 3.8 MeV, two-proton-quasi particle and four-neutron-quasi particle states are likely to set in. The two-neutron-hole states were calculated by Alburger and Pryce[15] assuming single-hole states of ^{207}Pb to be: $P^{-1}_{1/2}$ at 0.0 MeV, $f^{-1}_{5/2}$ at 0.570 MeV, $P^{-1}_{3/2}$ at 0.870 MeV, $i^{-1}_{13/2}$ at 1.634 MeV, and $h^{-1}_{9/2}$ at 2.35 MeV. The last single-hole state was mistaken at that time (1954) and has since been proved to be $f^{-1}_{7/2}$ (Ref. 17). The calculation was modified accordingly before it was entered into Table 3. However, the modification did not change any states as calculated by Alburger and Pryce[15] below 3 MeV. Their calculation was thought to be trustworthy because six of the predicted levels have been experimentally verified since the publication of their paper. The 3^- state at 2.634 MeV has been identified as the lowest vibrational state,[18] and the 2^+ state at 4.128 the lowest rotational state.[16] These two collective states will need special care in the cross section analysis.

This page left blank intentionally.

Table 3. Energy Levels of ^{206}Pb

Level	Excitation Energy (MeV)	Spin and Parity Established	Spin and Parity Assumed	Comments
1	0.0	0^+		
2	0.803	2^+		
3	1.175	0^+		
4	1.341	3^+		
5	1.462	2^+		
6	1.682	4^+		
7	1.700	1^+		
8	1.762	(2^+)	2^+	
9	1.998	4^+		
10	2.160		2^+	A
11	2.200	7^-		B
12	2.210		3^+	C
13	2.250		1^+	C
14	2.385	6^-		
15	2.500		0^+	C
16	2.526		3^-	D
17	2.634	3^-		
18	2.783	5^-		
19	2.800		3^+	C
20	2.820		4^+	E
21	2.940		4^-	E
22	3.017	6^-		
23	3.050		2^+	C
24	3.125	(6^+)	5^+	D
25	3.200		4^+	E
26	3.250		6^-	E
27	3.280	5^-		
28	3.300		1^-	C
29	3.404	5^-		
30	3.453	(3^-)	3^-	F
31	3.500		3^+	C
32	3.560	(5^-)	5^-	F

Table 3 continued

Level	Excitation Energy (Mev)	Spin and Parity Established	Spin and Parity Assumed	Comments
33	3.600		5^+	C
34	3.708		5^-	I
35	3.721		2^+	G
36	3.750		4^+	C
37	3.776	(5^-)	5^-	F
38	3.900		6^+	C
39	3.961		4^-	I
40	4.005		3^-	H
41	4.075		4^-	H
42	4.125		4^-	I
43	4.128	(2^+)	2^+	F
44	4.191		5^-	H
45	4.253		5^-	I
46	4.259		6^-	H
47	4.368	(4^+)	4^+	F
48	4.382		6^-	I
49	4.386	(6^+)	6^+	F

A. Assumed by Lind and Day,[13] and also by Cranberg et al.[14] in their calculations.

B. The assignment 7^- at 2.2 MeV was not consistent with the inelastic scattering measurement of Cranberg et al.,[14] so they used 2^+ for this level in their analysis. The two states 3^+ and 1^+ predicted by Alburger and Pryce[15] near 2.2 MeV tend to resolve this dilemma.

C. Calculated levels by Alburger and Pryce.[15]

D. Tentative assignment proposed by Alburger and Pryce.[15]

E. Level observed by Cranberg et al.,[14] spin assumed with the calculation of Alburger and Pryce.[15]

F. Observed levels and tentative spins by Saudinos et al.[16]

G. Level observed by Saudinos et al.,[16] spin assumed with the calculation of Alburger and Pryce.[15]

H. Levels observed by Saudinos et al.,[16] spins assumed to be those of four-quasi particle states: $(p_{1/2})^{-2}\ (f_{5/2})^{-1}\ (g_{9/2})^{1}$.

I. Two-proton-quasi particle states assumed to be the same as in ^{208}Pb (see Table 5).

Table 4. Energy Levels of ^{207}Pb

Level	Excitation Energy(MeV)	Spin and Parity Established	Spin and Parity Assumed	Comments
1	0.0	$1/2^-$		
2	0.570	$5/2^-$		
3	0.898	$3/2^-$		
4	1.633	$13/2^+$		
5	2.340	$7/2^-$		
6	2.624	$5/2^+$		
7	2.662	$7/2^+$		
8	2.726	$9/2^+$		
9	3.057		$3/2^+$	A
10	3.180		$11/2^+$	A
11	3.202		$5/2^+$	A
12	3.222		$13/2^+$	A
13	3.267		$7/2^+$	A
14	3.298	$1/2^+$		A
15	3.382	$(9/2^+,11/2^+)$	$9/2^+$	A
16	3.409	$9/2^-$		
17	3.426		$3/2^+$	B
18	3.471		$5/2^+$	B,D
19	3.499	$(11/2^+)$	$11/2^+$	C
20	3.503		$7/2^+$	B,D
21	3.522		$9/2^+$	B,D
22	3.580		$7/2^+$	E
23	3.620		$9/2^+$	E
24	3.632		$5/2^+$	E
25	3.645		$11/2^+$	D,E
26	3.725		$9/2^+$	D,F
27	3.817		$11/2^+$	F,G
28	3.854		$3/2^+$	G,H
29	3.891		$9/2^+$	G,I
30	3.989		$5/2^+$	G,H
31	4.040		$7/2^+$	J,H
32	4.060		$9/2^+$	J,H
33	4.089	$(3/2^-)$		K,G
34	4.113	$(15/2^-)$		L,G
35	4.120		$11/2^+$	J,H
36	4.127	$(5/2^-)$		K,G
37	4.140		$5/2^+$	J,M
38	4.160		$7/2^+$	J,M
39	4.181		$9/2^+$	G,M
40	4.200		$11/2^+$	J,M
41	4.220		$7/2^-$	J,N
42	4.240		$9/2^-$	J,N
43	4.260		$11/2^-$	J,N
44	4.288	$(7/2^-,9/2^-)$	$7/2^-$	G
45	4.300		$11/2^+$	J,O
46	4.310		$9/2^+$	J,O
47	4.314		$7/2^+$	O
48	4.339	$(11/2^-)$		G
49	4.380	$(13/2^-)$		G
50	4.388	$(5/2^+)$		P

Table 4 continued

Table 4 - footnotes

A. Assumed configuration $^{208}Pb(3^-,2.615) \times {}^{207}Pb(f^{-1}_{5/2},0.570)$. The symbol x stands for "coupling". The 3.180 and 3.222 MeV states are observed to decay to the $13/2^+$ state, and are, therefore, assigned to be $11/2^+$ and $13/2^+$ respectively.

B. Assumed configuration $^{208}Pb(3^-,2.615) \times {}^{207}Pb(p^{-1}_{3/2},0.898)$.

C. Probably $(i\ 11/2)^1$ (Ref. 17).

D. Energy levels observed by Grosse et al.[19]

E. Assumed configuration $^{206}Pb(2^+,0.803) \times {}^{207}Pb(g_{9/2},2.726)$. The state $^{206}Pb(2^+,0.803)$ has the dominant neutron configuration $(p_{1/2})^{-2}$ (Ref. 15).

F. Assumed configuration $^{208}Pb(5^-,3.702) \times {}^{207}Pb(p^{-1}_{1/2},0.0)$. The state $^{208}Pb(5^-,3.702)$ has the dominant neutron configuration $(g_{9/2},f^{-1}_{5/2})$ (Ref. 13).

G. Levels observed by Saudinos et al.[16]

H. Assumed configuration $^{206}Pb(3^+,1.338) \times {}^{207}Pb(g_{9/2},2.726)$. The state $^{206}Pb(3^+,1.338)$ has the dominant neutron configuration $(p^{-1}_{1/2},f^{-1}_{5/2})$ (Ref. 15).

I. Assumed configuration $^{206}Pb(0^+,1.165) \times {}^{207}Pb(g_{9/2},2.726)$. The state $^{206}Pb(0^+,1.165)$ has the dominant neutron configuration $(f_{5/2})^{-2}$ (Ref. 15).

J. Energy levels not observed but added from core coupling considerations.

K. Proposed by Saudinos et al.[26] to have the dominant configuration $^{208}Pb(2^+,4.076) \times {}^{207}Pb(p^{-1}_{1/2},0.0)$. The state $^{208}Pb(2^+,4.076)$ is collective.[13]

L. Probably $(j_{15/2})^1$ (Ref. 17)

M. Assumed configuration $^{206}Pb(2^+,1.462) \times {}^{207}Pb(g_{9/2},2.726)$. The state $^{206}Pb(2^+,1.462)$ has the dominant neutron configuration $(p^{-1}_{1/2},P^{-1}_{3/2})$ (Ref. 15).

N. Assumed $^{208}Pb(3^-,2.615) \times {}^{207}Pb(i^{-1}_{13/2},1.633)$.

O. Assumed $^{206}Pb(2^+,0.803) \times {}^{207}Pb(i^{-1}_{11/2},3.499)$.

P. Probably $(d_{5/2})^1$ (Ref. 17).

Table 5. Energy Levels of ^{208}Pb

Level	Excitation Energy(MeV)	Spin and Parity Established	Spin and Parity Assumed	Comments
1	0.0	0^+		
2	2.615	3^-		
3	3.198	5^-		A
4	3.475	4^-		A
5	3.708	5^-		B
6	3.920	(6^-)	5^-	C
7	3.946	(≥ 4)	5^-	F^+
8	3.961	(4^-)	4^-	C
9	3.998		6^-	B
10	4.038	(7^-)	7^-	B
11	4.050	(4)	4^-	B
12	4.076	2^+		Coll.
13	4.125	$4^-,5^-$	4^-	D
14	4.161	$(5)^-$	5^-	E
15	4.204	$5^-,6^-$	6^-	F
16	4.231	(2^-)	2^-	B^+
17	4.243	(2^--4^-)	3^-	B^+
18	4.253	(3^--5^-)	5^-	D
19	4.316	$(5)^-$	4^-	E
20	4.323	4^+		Coll.
21	4.357	(4^-)	3^-	E
22	4.382	$(6)^-$	6^-	D
23	4.435	(6^+)		Coll.
24	4.480	$(6)^-$	6^-	E
25	4.608	$(8)^+$	8^+	G
26	4.650		3^-	K*
27	4.698	$(3)^-$	3^-	D
28	4.720		4^-	K*
29	4.740		5^-	K*
30	4.760		6^-	K*
31	4.780		3^-	L*
32	4.800		3^+	M*
33	4.820		4^+	L*
34	4.839	(1)	2^+	M^+
35	4.859	0^+		pairing vibration
36	4.863	$(7)^+$	7^+	G
37	4.910	$(4-10)^+$	4^+	I
38	4.920		4^+	M*
39	4.934	(2^+)	2^+	I^+
40	4.953	(4-6)	5^+	M^+
41	4.974	$(3)^-$	3^-	H
42	5.010		4^-	N*
43	5.038	$(2)^-$	2^-	H
44	5.060		3^+	I*
45	5.077	$(5-10)^+$	5^+	I
46	5.095		5^-	N*
47	5.127	$(2)^-$	2^-	O^+
48	5.140		6^+	M*
49	5.162		1^+	I^+

Table 5 continued

Level	Excitation Energy (Mev)	Spin and Parity Established	Assumed	Comments
50	5.180		6^+	N*
51	5.200	$(8-10)^+$	6^+	I
52	5.211	$(8-10)^+$	7^+	I
53	5.220		4^-	O*
54	5.236	0^+		
55	5.245	$(2)^-$	3^-	0^+
56	5.260		5^-	O*
57	5.281	0^-		J
58	5.288	1^-		J

A-O: Particle-hole configurations.

\+ Assumed particle-hole configuration for observed levels.

* Assumed level and configuration

A. $^{209}Pb(g_{9/2},0.0) \times {}^{207}Pb(p^{-1}_{1/2}, 0.0)$. A constant energy gap $\Delta_n = 3.34$ MeV is assumed for all neutron configurations.

B. $^{209}Pb(g_{9/2},0.0) \times {}^{207}Pb(f^{-1}_{5/2}, 0.57)$.

C. $^{209}Bi(h_{9/2},0.0) \times {}^{207}T\ell(s^{-1}_{1/2}, 0.0)$. A constant energy gap $\Delta_p = 3.83$ MeV is assumed for all proton configurations.

D. $^{209}Bi(h_{9/2}, 0.0) \times {}^{207}T\ell(d^{-1}_{3/2}, 0.351)$.

E. $^{209}Pb(g_{9/2}, 0.0) \times {}^{207}Pb(p^{-1}_{3/2}, 0.898)$.

F. $^{209}Pb(i_{11/2}, 0.782) \times {}^{207}Pb(p^{-1}_{1/2}, 0.0)$.

G. $^{209}Pb(j_{15/2}, 1.428) \times {}^{207}Pb(p^{-1}_{1/2}, 0.0)$.

H. $^{209}Pb(d_{5/2}, 1.570) \times {}^{207}Pb(p^{-1}_{1/2}, 0.0)$.

I. $^{209}Bi(h_{9/2}, 0.0) \times {}^{207}T\ell(h^{-1}_{11/2}, 1.341)$.

J. $^{209}Pb(s_{1/2}, 2.041) \times {}^{207}Pb(p^{-1}_{1/2}, 0.0)$.

K. $^{209}Pb(i_{11/2}, 0.782) \times {}^{207}Pb(f^{-1}_{5/2}, 0.570)$.

L. $^{209}Bi(f_{7/2}, 0.900) \times {}^{207}T\ell(s^{-1}_{1/2}, 0.0)$.

M. $^{209}Pb(g_{9/2}, 0.0) \times {}^{207}Pb(i^{-1}_{13/2}, 1.633)$

N. $^{209}Pb(i_{13/2}, 0.782) \times {}^{207}Pb(p^{-1}_{3/2}, 0.898)$.

O. $^{209}Bi(f_{7/2}, 0.900) \times {}^{207}T\ell(d^{-1}_{3/2}, 0.351)$.

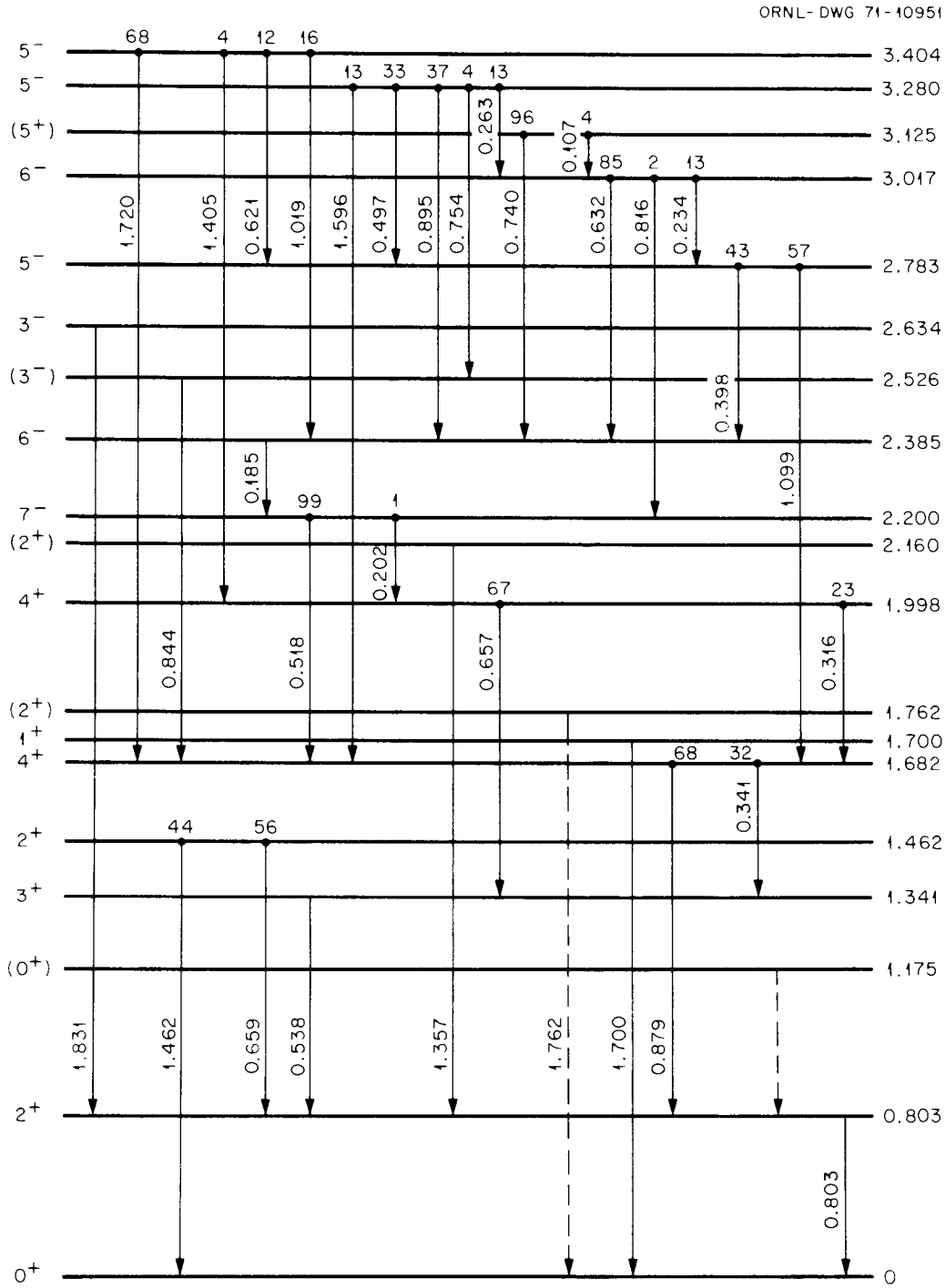

Fig. 1. ^{206}Pb level diagram with gamma-ray branching ratios.

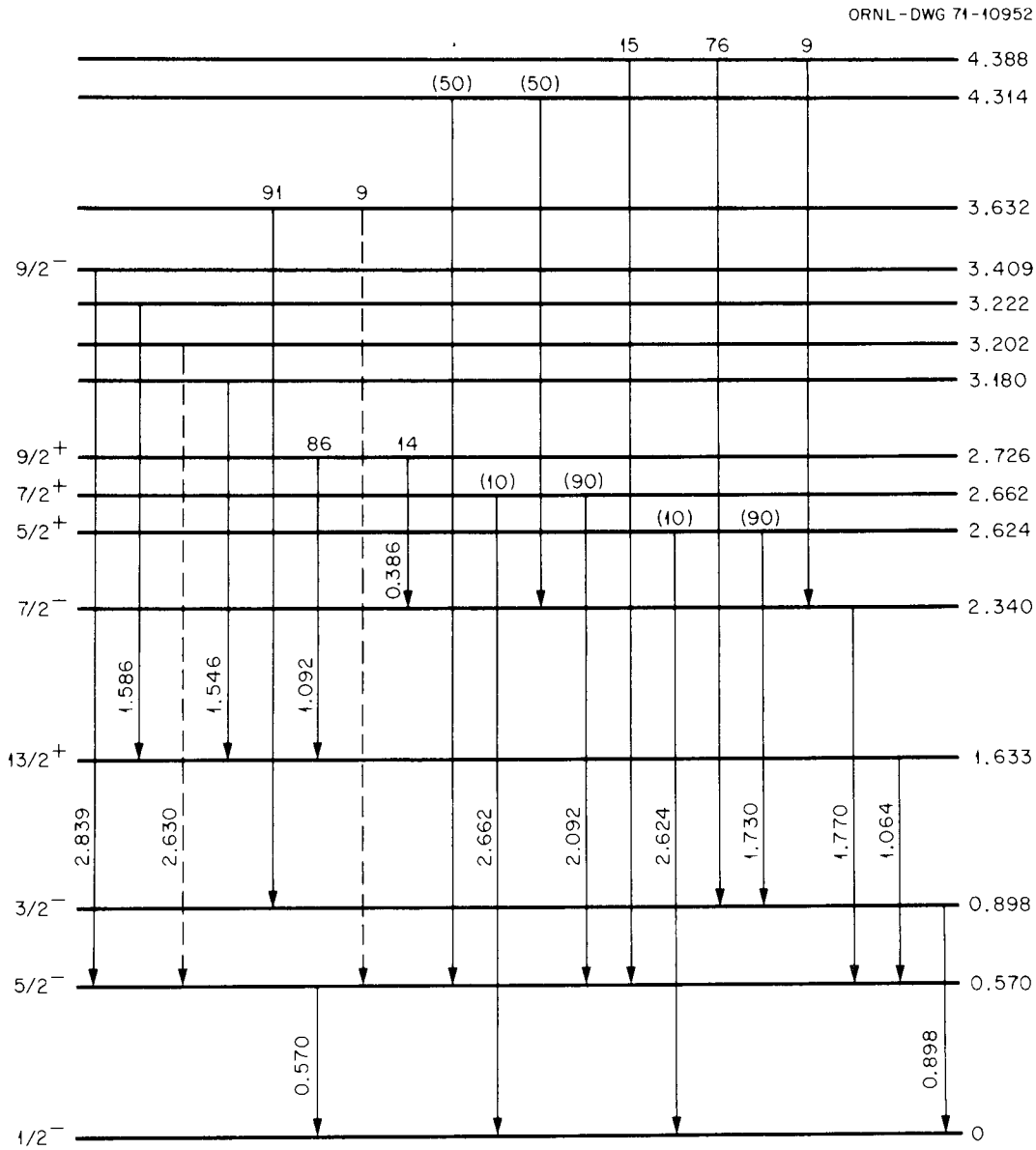

Fig. 2. ^{207}Pb level diagram with gamma-ray branching ratios.

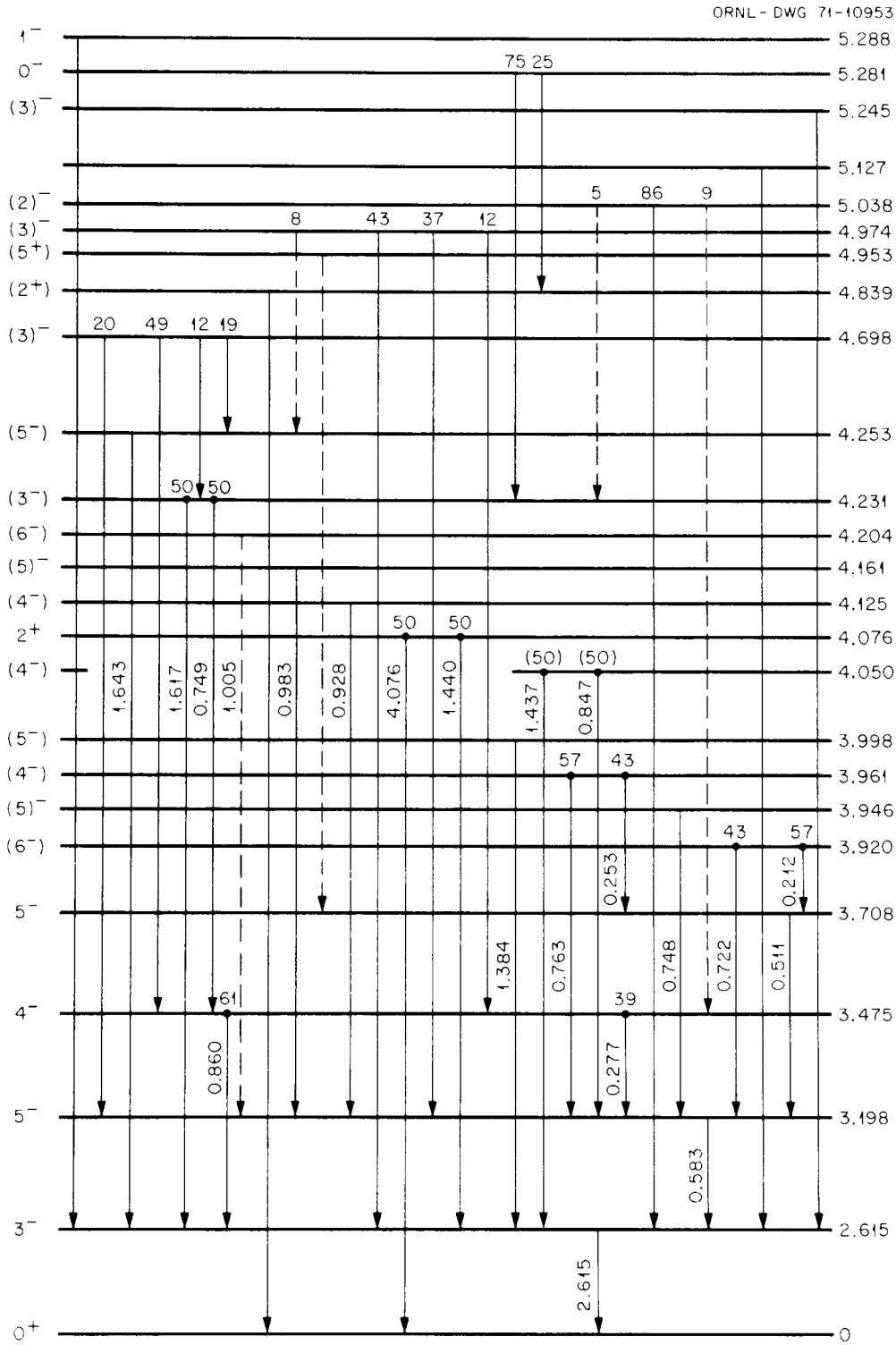

Fig. 3. ^{208}Pb level diagram with gamma-ray branching ratios.

The gamma-ray branching ratios for ^{206}Pb (Fig. 1) were taken from Nuclear Data Sheets.[12]

The energy levels, spins, and parities of ^{207}Pb below 3 MeV were obtained from Nuclear Data Sheets.[17] Between 3 and 4 MeV 21 levels have been observed, but only a few have spin and parity assignments. We followed the core coupling picture of Grosse et al.[19] in obtaining spin and parity assignments for these levels. Details of such assignments are given in the comments of Table 4. While this approach is by no means accurate, it is believed to be far closer to the true spin and parity distribution than that represented by a level density formula. For example, 20 of the 21 levels between 3 and 4 MeV are predicted to have positive parity. The levels $5/2^+$ at 2.624 MeV and $7/2^+$ at 2.662 MeV have the dominant configuration ^{208}Pb(3^-, 2.615) x ^{207}Pb ($P^{-1}_{1/2}$,0.0), and are therefore collective.

The gamma-ray branching ratios for ^{207}Pb (Fig. 2) were mostly taken from Nuclear Data Sheets.[17] The branching ratios from the levels at 2.624 and 2.662 MeV were assumed on the basis that transitions observed in more than one reaction were stronger than those observed in only one reaction.

Besides the vibrational state (3^-, 2.615 MeV) and the rotational band (2^+, 4.076 MeV; 4^+, 4.23 MeV, etc.), nearly all excited states below 5.3 MeV in ^{208}Pb are two-quasi particle admixtures.[20] Both neutron and proton configurations are almost equally likely because the nucleus is doubly magic. The energy levels, spins, and dominant particle-hole configurations below 5.3 MeV in ^{208}Pb are listed in Table 5. For excitation energies less than 4.6 MeV, all possible two-quasi particle states with spins less than or equal to 6 match the observed levels very well. Above 4.6 MeV approximately half of the allowed spins and/or configurations are not yet observed

but are added. The single-particle and single-hole states were taken from the neighboring add-A nuclei; namely, ^{209}Pb and ^{207}Pb for neutron configurations, and ^{209}Bi and ^{207}Tl for proton configurations. The energy gaps were taken to be Δ_n = 3.34 MeV for the neutron pair, and Δ_p = 3.83 for the proton pair. For details see the comments in Table 5.

The decay scheme of ^{208}Pb (Fig. 3) was mostly reconstructed from Nuclear Data Sheets.[20] The gamma-ray branching ratio from decay of the 4.231 MeV level was taken from Nellis et al.[21] We also followed their assumption for the branching ratio from the level at 4.050 MeV.

For the calculation of gamma-ray-production cross sections, branching ratios not known experimentally were filled by assuming E1 selection rule. If a level could not be deexcited by E1 transition, then Mλ or Eλ transitions were also allowed with the smallest possible λ. An exception to these rules were the decays of the rotational band heads in ^{206}Pb and ^{207}Pb near 4 MeV for which we assumed 50% deexcitation to the ground states and 50% by the above selection rules. This was based on the observed transitions of the rotational band head in ^{208}Pb and on the relatively large B(Eλ) values observed for these states, which indicated that ground-state transitions were allowed. Energy considerations ($E_\gamma^{2\lambda+1}$) also tend to favor transitions of the rotational members to the ground states than to the band heads. Thus the 50% transition to the ground states were also assumed for the rotational members. The deformation parameters β_λ, which are related to the B(Eλ) values and are needed for later use, are listed in Table 6.[22,23]

3.3. Level Densities of the Lead Isotopes

The level densities of the lead isotopes, needed for analyzing the (n,n'), (n,2n) and (n,3n) cross sections and the resulting gamma rays, may

Table 6. Deformation Parameters β_γ

Isotope	Level	λ	Deformation Parameter β_γ Reported (Ref.)	Adopted
^{206}Pb	2^+(0.803)	2	0.037(22), 0.078(16)	0.037
	4^+(1.682)	4	0.042(16)	
	3^-(2.634)	3	0.12±0.02 (18)	0.12
			0.115(16)	
	5^-(3.776)	5	0.077(16)	
	2^+(2.128)	2	0.063(16)	
	4^+(4.368)	4	0.068(16)	
	6^+(4.386)	6	0.060(16)	
^{207}Pb	$5/2^+$(2.624)	3	0.072(17)	
	$7/2^+$(2.662)	3	0.087(17)	
	$3/2^-$(4.089)	2	0.040(17)	
	$5/2^-$(4.127)	2	0.045(17)	
	$7/2^-$(4.288)	4	0.062(17)	
	$11/2^-$(4.339)	6	0.043(17)	
	$13/2^-$(4.380)	6	0.048(17)	
^{208}Pb	3^-(2.615)	3	0.084-0.150(20)	0.12
			0.12(16)	
	5^-(3.198)	5	0.072(20)	
	5^-(3.708)	5	0.034(20)	
	2^+(4.076)	2	0.058(20)	
	4^+(4.323)	4	0.066(20)	
	6^+(4.425)	6	0.057(20)	
Pb	2.7±0.1	3	0.11±0.02(18)	0.114*
	2.5±0.2		0.12±0.01(23)	
	4.1±0.3	2,4,6	0.10±0.01(23)	

*Adjusted to fit 8 MeV and 14 MeV inelastic-scattering data simultaneously.

be described by the Gilbert and Cameron[24] scheme, as extended by Penny[25]

$$\rho(E,I,\pi) = 1/2\ \omega(E)\ e(E,I) \tag{1}$$

$$e(E,I) = e^{-I^2/2ct} - e^{-(I+1)^2/2ct}, \tag{2}$$

$$\omega(e) = \begin{cases} \frac{1}{T}\, e^{(E-E_o)/T} & ;\ E_c \leq E \leq E_x\ , \quad (3a) \\ e^{2\sqrt{aU}}/12\sqrt{2ac}\ at^3 ; & E>Ex, \quad (3b) \end{cases}$$

where

$$U = E - \Delta = at^2,$$

$$\Delta = \text{pairing correction}^{24}$$

$$E_c = \text{continuum cut-off energy.}$$

The parameters c, a, T, and E_o are determined from experimental evidences discussed below.

Theoretical considerations have led to the formula[24]

$$c = 0.0888\ aA^{2/3}. \tag{4}$$

One may use Eq. (4) to determine "c" from a given "a" or from experiment.

For ^{207}Pb and ^{208}Pb, "a" is determined from the resonance spacings. Gilbert and Cameron[24] quoted the values a = 7.7 $\pm$ 1.0 for ^{207}Pb and a = 6.77 $\pm$ 0.8 for ^{208}Pb from analysis of s-wave neutron resonances. Baba[26] gave corresponding values of $10.98\ ^{+0.54}_{-0.20}$ and $10.28\ ^{+0.47}_{-0.33}$ from **analysis** of both s-wave and p-wave neutron resonances. These discrepancies in "a" lead to differences in level densities (based on Eq. (3b)) by factors of 14 and 22 near the neutron separation energies in ^{207}Pb and ^{208}Pb respectively. These large discrepancies result mainly from uncertainties in assigning "ℓ" values to the resonances. Therefore the values of "a"

resulting from analysis of both s- and p-wave resonances should be more trustworthy.

At very low energies, the level densities should be consistent with the direct level counts of the discrete levels given in the last section. One may then obtain E_o and T by solving Eq. (3a) with the requirements that it is equal to the level density obtained from counting discrete levels at very low energies and those from Eq. (3b) near the neutron separation energy.

There exist no resonance data in ^{206}Pb. Gilbert and Cameron[24] predicted a set of level density parameters for ^{206}Pb based on their semi-empirical scheme. The nuclear temperature (T = 0.96) they predicted was found to be consistent with the neutron evaporation data of Cranberg et al.[14] We also adopted Gilbert and Cameron's parameters for ^{205}Pb and ^{204}Pb. Fig. 4 and Table 7 summarize the proposed level densities. One should keep in mind that these level densities were obtained from insufficient experimental evidences. They should be modified as new evidences become available.

4. COMPUTATIONAL METHODS AND PROCEDURES

The theoretical calculations provide the most reliable way of extrapolating and interpolating the data to energies and angles not available in the experiment. In this section we list the computer codes used and the computational procedures adopted. Details of calculated data will be given later in conjunction with the discussions of experimental data.

4.1. Computer Codes

There are four computer codes available for the present calculation. The first three codes are much more general than outlined below.

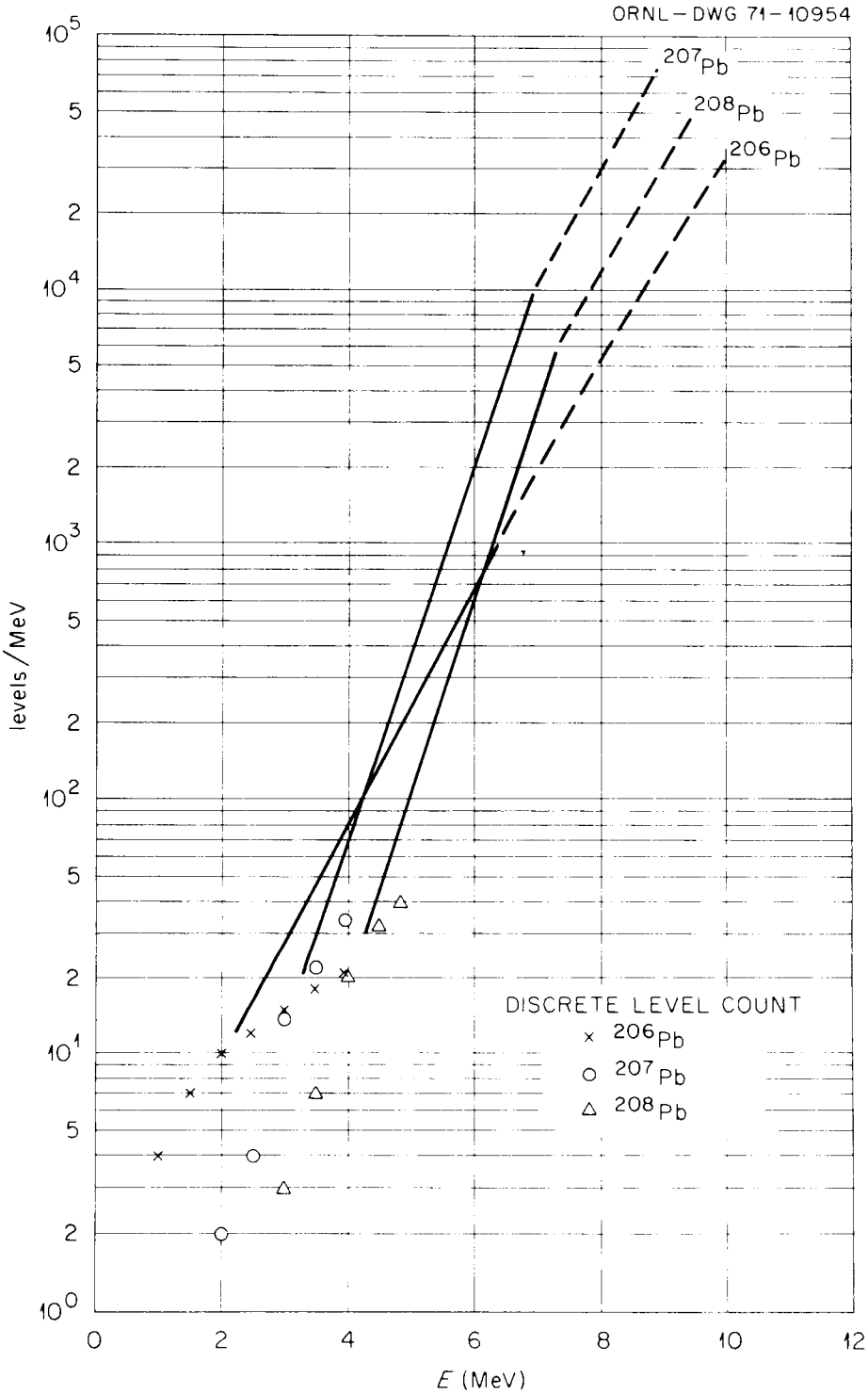

Fig. 4. Level densities of the lead isotopes.

Table 7. Level Density Parameters for the Lead Isotopes

Lead Isotope	Δ (MeV)	a (MeV^{-1})	E_o (MeV)	T (MeV)	C	E_c (MeV)	E_x (MeV)
204	1.54	12.91	0.96	0.63	26.6	0	4.5
205	0.83	11.18	-0.58	0.825	30.4	0	5.5
206	1.24	9.32	-0.18	0.96	24.9	2.2	6.4
207	0.83	10.98	1.86	0.59	28.8	3.3	6.9
208	1.21	10.28	2.64	0.58	26.2	4.3	7.4

GENOA[27] is an optical model[28] search code. It fits simultaneously several sets of data by means of an average optical model potential. The optical model potentials and parameters are defined by

$$Vf_v(r) + iWf_w(r) + U\,\vec{\ell}\cdot\vec{\sigma}\,f_u(\gamma)$$

where

$$f_v(r) = [1 + \exp\,(\frac{r-R_v}{a_v})]^{-1}, R_v = r_v A^{1/3},$$

$$f_w = 4\,\exp\,(\frac{r-R_w}{a_w})\,[1 + \exp\,(\frac{r-R_w}{a_w})]^{-2},\ R_w = r_w A^{1/3},$$

$$f_u = (\frac{h}{2Mc})^2\,\frac{1}{a_u r}\,\exp\,(\frac{r-R_u}{a_u})\,[1 + \exp\,(\frac{r-R_u}{a_u})]^{-2},\ R_u = r_u A^{1/3},$$

where M is the pion mass. GENOA may be used not only to provide an optimum set of optical model parameters but also to calculate total cross sections, reaction cross sections, shape elastic cross sections, and angular distributions.

HELGA[29] employs the Hauser-Feshbach model[30] with Porter-Thomas width fluctuation corrections[31] for scattering and binary reaction cross sections. Continuum states can be included in competition with discrete states. Gamma-ray-production cross sections and energy distributions of secondary gamma rays can be calculated for the discrete states. Optical model parameters from GENOA (but without spin-orbit dependence), level structures and gamma-ray branching ratios given in the last section are used as inputs. Gamma-ray

branching ratios not known experimentally are calculated with simple assumptions concerning the multipolarities of gamma-ray transitions.

JULIE[32] is a distorted-wave-Born approximation[33] code which may be used to calculate the direct-interaction contributions to inelastic scattering exciting the collective states described in the last section. Optical model parameters from GENOA and the deformation parameters given in Table 6 are needed for the calculation.

NNNGAM[34] is a code developed specifically for the present purpose. It may be used to calculate the energy distributions of secondary gamma rays and gamma-ray-production cross sections for (n,n'), (n,2n) and (n,3n) reactions. The code was based largely on the statistical-model theory of neutron reactions and scattering[35] and the gamma-ray cascade theory of Troubetzkoy.[36] However, two variations were made. First, the statistical model is used to determine the excitation of both the continuum states and the discrete states only if incident neutron energy is sufficiently high. If the incident neutron energy is low (1 or 2 MeV above the highest discrete level), the excitation of the discrete states is redistributed according to the calculations with HELGA and JULIE. The second variation involved gamma-ray branching ratios. Gamma-ray cascades are made spin- and parity-dependent. Discrete-to-discrete branching ratios, if not known experimentally, are filled by E1 selection rules. Levels that cannot be deexcited by E1 transitions are allowed to decay by $M\lambda$ or $E\lambda$ transitions with the smallest possible λ. Continuum-to-discrete transitions are assumed to be dipole with the weight $\{\exp[-I^2/2\ ct] - \exp[-(I+1)^2/2\ ct]\}$ where I is the spin of a discrete level. The code also contains a method for approximating gamma-ray yield from (n,3n) reactions by those of (n,2n) reactions

involving the same residual nucleus and employing the concept of modified level density (see Section 5.6).

4.2. Computational Procedures

The four codes outlined above are obviously inter-dependent. The calculated cross sections from all four codes were based on the same set of input data. The input data, apart from those selected for determining the optical model parameters, were obtained from experimental evidences not directly related to cross sections. The calculated cross sections formed a consistent set.

First the angular distributions of elastic-scattering cross sections were surveyed. A set of data covering incident neutron energies from 1 MeV to 15 MeV was selected based on the relative merits of experimental technique and data reduction. The data above 7 MeV may be considered predominantly shape elastic and were used in the search code GENOA to find the initial set of optical model parameters. The total cross sections and nonelastic cross sections were not fitted but were used as checks. Many sets of optical model parameters have been used in the literature, each set best fitting certain cross sections for certain energy ranges. Two sets of parameters were found satisfactory at this step. They were:

1. The local potential equivalent[37] to the nonlocal potential of Perey and Buck.[28] This set has been widely used.

2. The set proposed by Zafiratos _et al._[38] which best fits their angular distribution of neutron scattering from lead at 7 MeV.

These two sets of optical model parameters were then used in HELGA for the compound-nucleus portion of inelastic-scattering cross sections and in JULIE for the direct-interaction portion. Upon comparison with experiment

the first set of parameters was found to be far superior to the second set for these cross sections.

The angular distributions of compound elastic cross sections below 8 MeV generated by HELGA with the first set of optical-model parameters were fed back to GENOA. Fits to the cross sections above 4 MeV were good but became increasingly worse as the energy got lower. Small improvement in fitting low-energy differential elastic cross sections resulted in substantial worsening in inelastic cross sections. Thus attention was shifted to fitting inelastic cross sections, altering only the potential depths. This resulted in a fixed set of optical model parameters, as shown in Table 8. Several iterations were made with the above procedures in obtaining this set of parameters.

The level excitation cross sections from HELGA and JULIE below 7 MeV were used as input to NNNGAM for computing gamma-ray spectra and production cross sections. The gamma-ray spectra and production cross sections below the continuum cut-off (4.4 MeV) were generated directly from HELGA. The continuum cut-offs, E_c, of the three major lead isotopes are smaller than 4.4 MeV (see Table 7). From E_c to 4.4 MeV the discrete level excitation cross sections were weighted by the level densities for use in forming the gamma-ray cascade. For computing gamma-ray yields, all the levels below 5.3 MeV in ^{208}Pb were used so that the known level properties and gamma-ray branching ratios could be fully utilized.

5. COMPARISON OF CALCULATION WITH EXPERIMENT

It will become clear that the data situation in lead is such that heavy reliance has to be placed with calculation to obtain complete cross section sets. In this section we compare calculated cross sections with

Table 8. Fixed Optical Model Parameters

Real well depth V	47.0 - 0.25 E_n MeV
Imaginary well depth W	3.5 + 0.43 E_n MeV
Spin-orbit well dpeth U	6.0 MeV
Real well radius r_v	1.25 F
Imaginary well radius r_w	1.25 F
Spin-orbit well radius r_u	1.25 F
Real well diffuseness a_v	0.65 F
Imaginary well diffuseness a_w	0.47 F
Spin-orbit well diffuseness a_u	0.65 F

measured data wherever feasible. In some cases, calculations define the cross sections better than curves drawn through data. In some other cases, computed data are adopted due to the lack of better alternatives.

Fig. 5 presents a concise picture of some of the calculated cross sections to be discussed in detail. This includes $\sigma(n,x\gamma)$, $\sigma(n,x)$, $\sigma(n,n')$, $\sigma_L(n,n')$, $\sigma_C(n,n')$, $\sigma(n,2n)$, and $\sigma(n,3n)$. The subscripts L and C stand for level and continuum respectively. $\sigma_L(n,n')$ is composed of compound-nucleus and direct-interaction contributions. All these cross sections will be discussed and/or compared with experimental data in the order of calculation. Angular distribution of elastic scattering will be presented first.

5.1. Angular Distribution of Elastic Scattering

Fig. 6 compares optical model calculations with the experimental data at 7 MeV and near 14.6 MeV. Three different sets of experimental data[39,40,41] were used to cover the entire angles of scattering near 14.6 MeV. These data were chosen from relative merits of experimental and data-reduction techniques. Many more measurements have been made near 14 MeV and have been summarized in in BNL-400 (Ref. 42). The measurement by Zafiratos _et al._[38] at 7 MeV is believed to be an excellent one and has helped in defining the optical model parameters. However, the comparison shown in Fig. 6 does not represent best fit to these data because consideration in inelastic scattering has altered the optical potential strengths somewhat from the values best fitting these data.

Fig. 7 compares optical model calculations with data at 4 MeV and 5 MeV. The comparison at 5 MeV seems inconclusive. The measurement by Buccino _et al._[43] at 5 MeV is for radiogenic lead and the data of Hill[44,45] are given

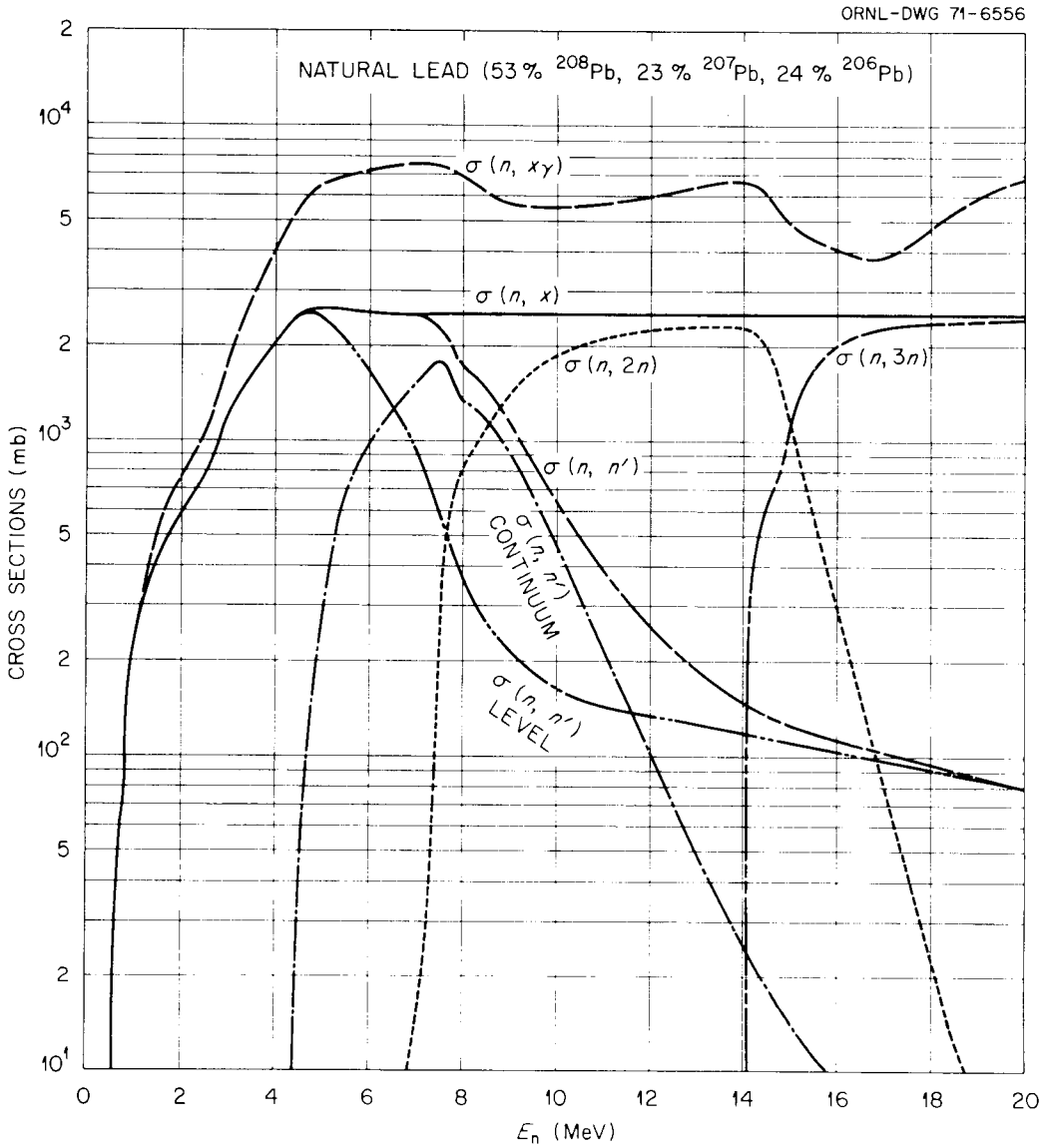

Fig. 5. A concise presentation of some calculated cross sections.

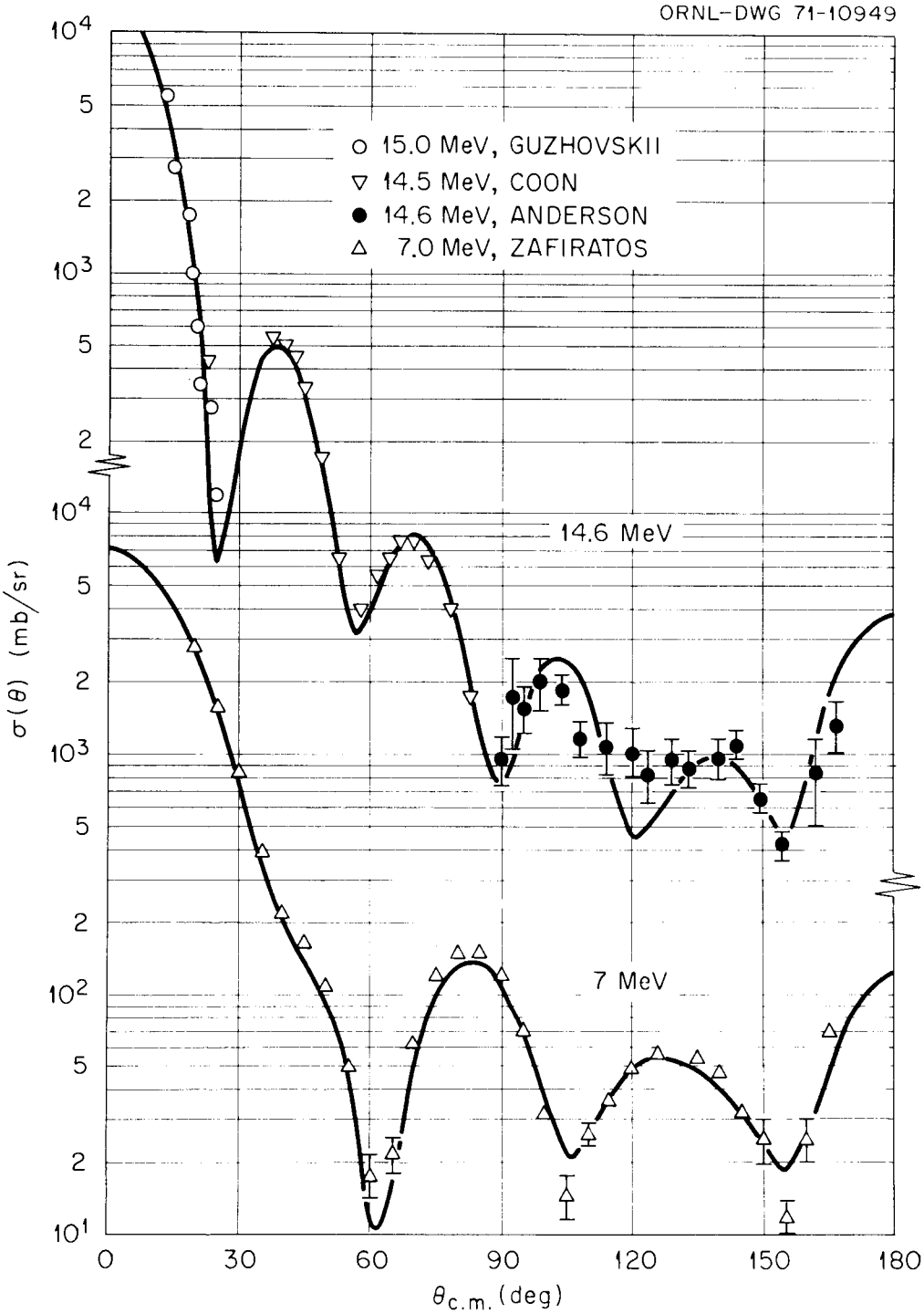

Fig. 6. Comparison of calculation with experiment for the angular distributions of elastic scattering at 7 MeV and 14.6 MeV.

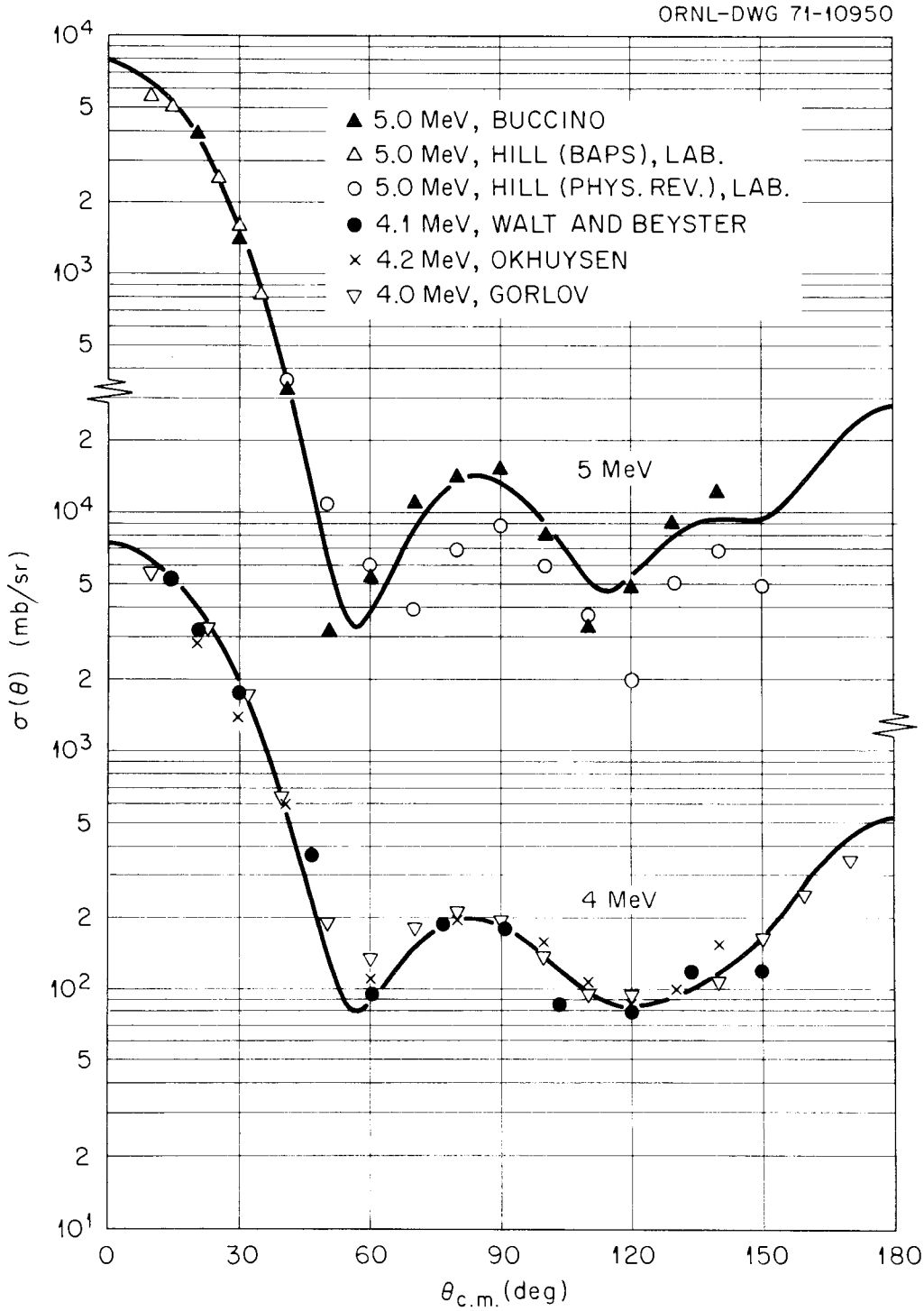

Fig. 7. Comparison of calculation with experiment for the angular distributions of elastic scattering at 4 MeV and 5 MeV.

in laboratory angles. These two sets of data disagree substantially. Converting the Hill's data to center of mass system makes the disagrement slightly worse. The good agreement of optical model calculations with measurements at 4 MeV and 7 MeV has led us to assume that the calculation is more trustworthy than either of the measurements at 5 MeV. The 4 MeV data were taken from Walt and Beyster,[46] Okhuysen et al.[47] and Gorlov et al.[48]

It should be noted that the comparisons shown in Figs. 6 and 7 are given in the absolute sense. The optical model calculations, above 5 MeV, will be used to represent the normalized angular distributions of elastic scattering. The magnitude of elastic scattering cross sections will be determined by other means.

5.2. Direct-Interaction Contribution to $\sigma_L(n,n')$

Angular distributions of the direct-interaction contribution to $\sigma_L(n,n')$ were calculated with JULIE with the fixed optical model parameters. Fig. 8 compares these calculations with the available data for the vibrational (2.6 MeV) states at 8 MeV and 14 MeV and for the rotational (4.1 MeV) states at 14 MeV for natural lead. A deformation parameter of 0.114 was found reasonable, as compared with quoted values of 0.11 (Ref. 18) and 0.12 (Ref. 23), for the vibrational states. At 8 MeV and above compound-nucleus contributions to these levels are negligible.

Calculations with JULIE have been made over the entire energy range for all the levels for which the deformation parameters are appreciably large, as listed in Table 6. The direct-interaction components of $\sigma_L(n,n')$ are shown in Figs. 9, 10, and 11 for levels in ^{206}Pb, ^{207}Pb, and ^{208}Pb respectively. The corresponding angular distributions were fitted by Legendre polynomials to be merged with the compound-nucleus components which will be discussed next.

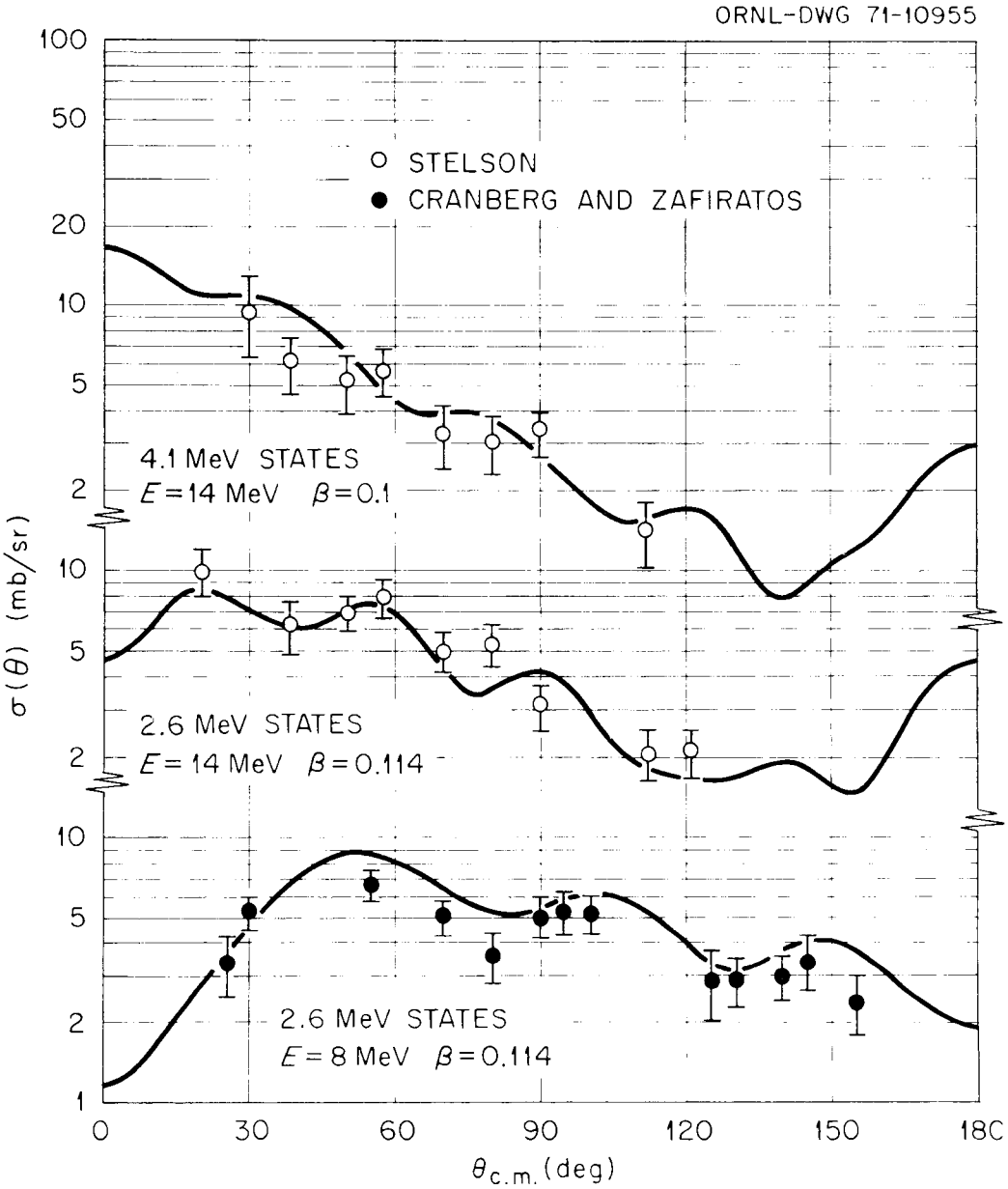

Fig. 8. Comparison of calculation with experiment for the angular distributions of direct-inelastic scattering at 8 MeV and 14 MeV.

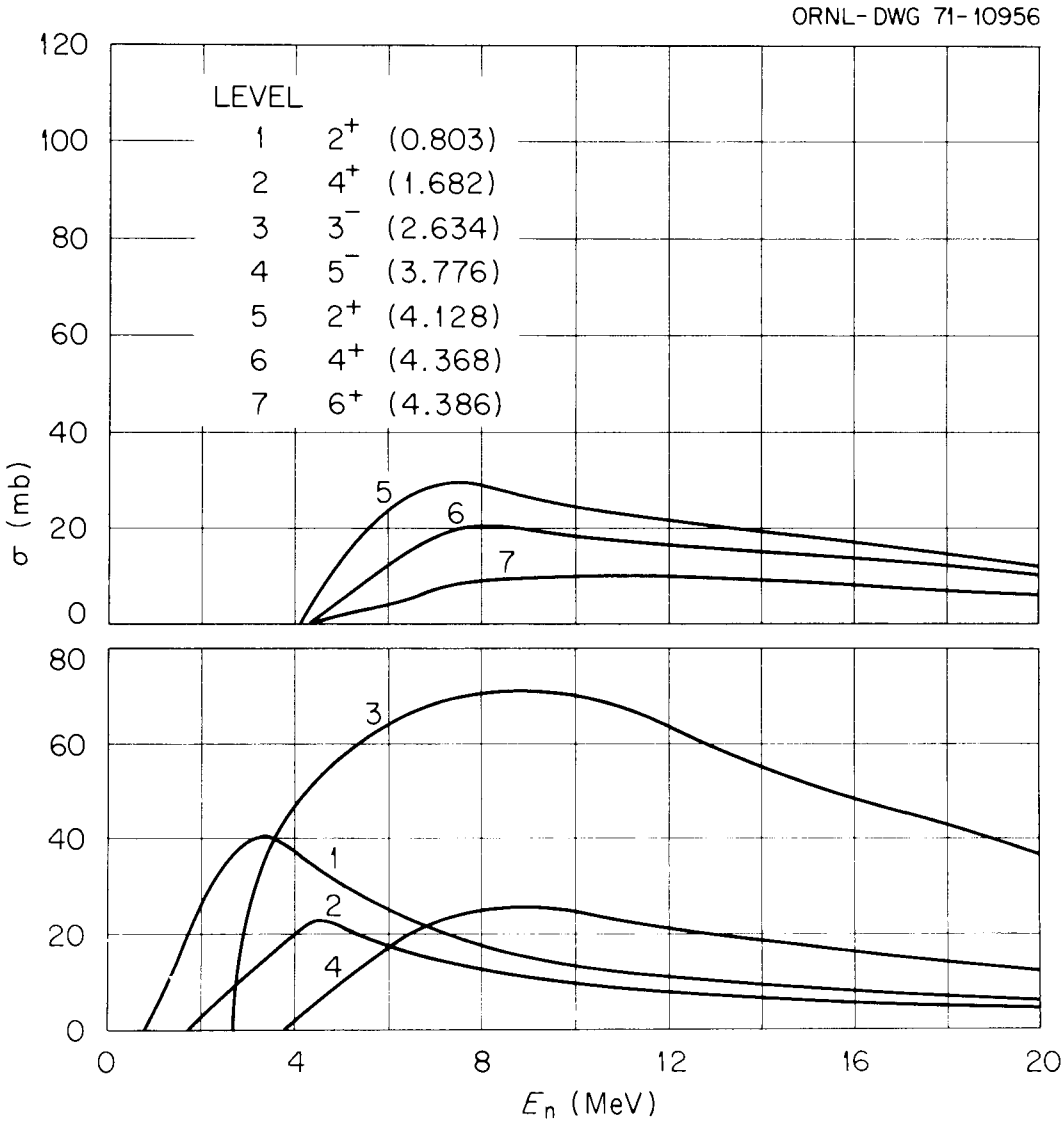

Fig. 9. Calculated direct-inelastic scattering cross sections for ^{206}Pb.

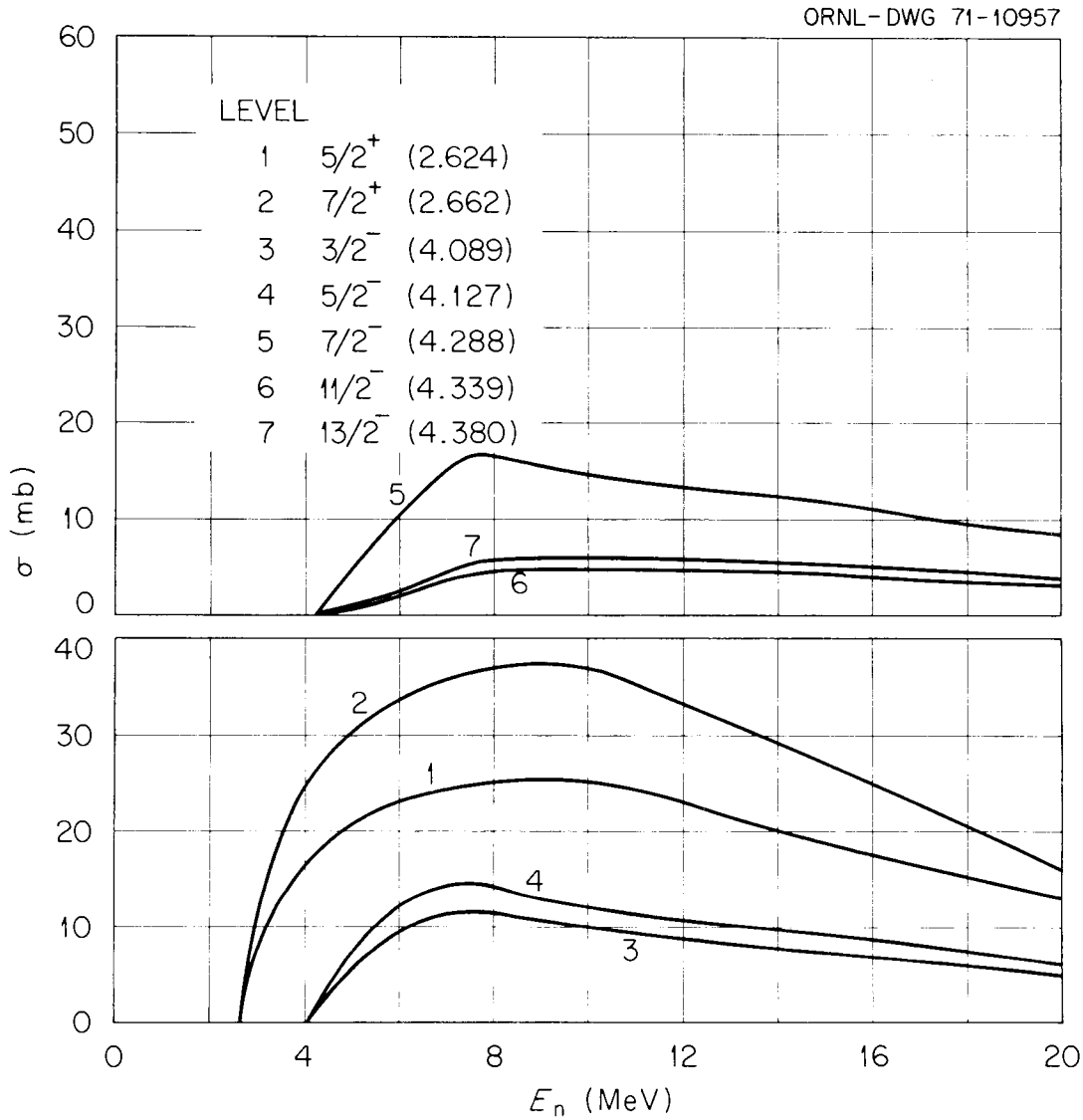

Fig. 10. Calculated direct-inelastic scattering cross sections for ^{207}Pb.

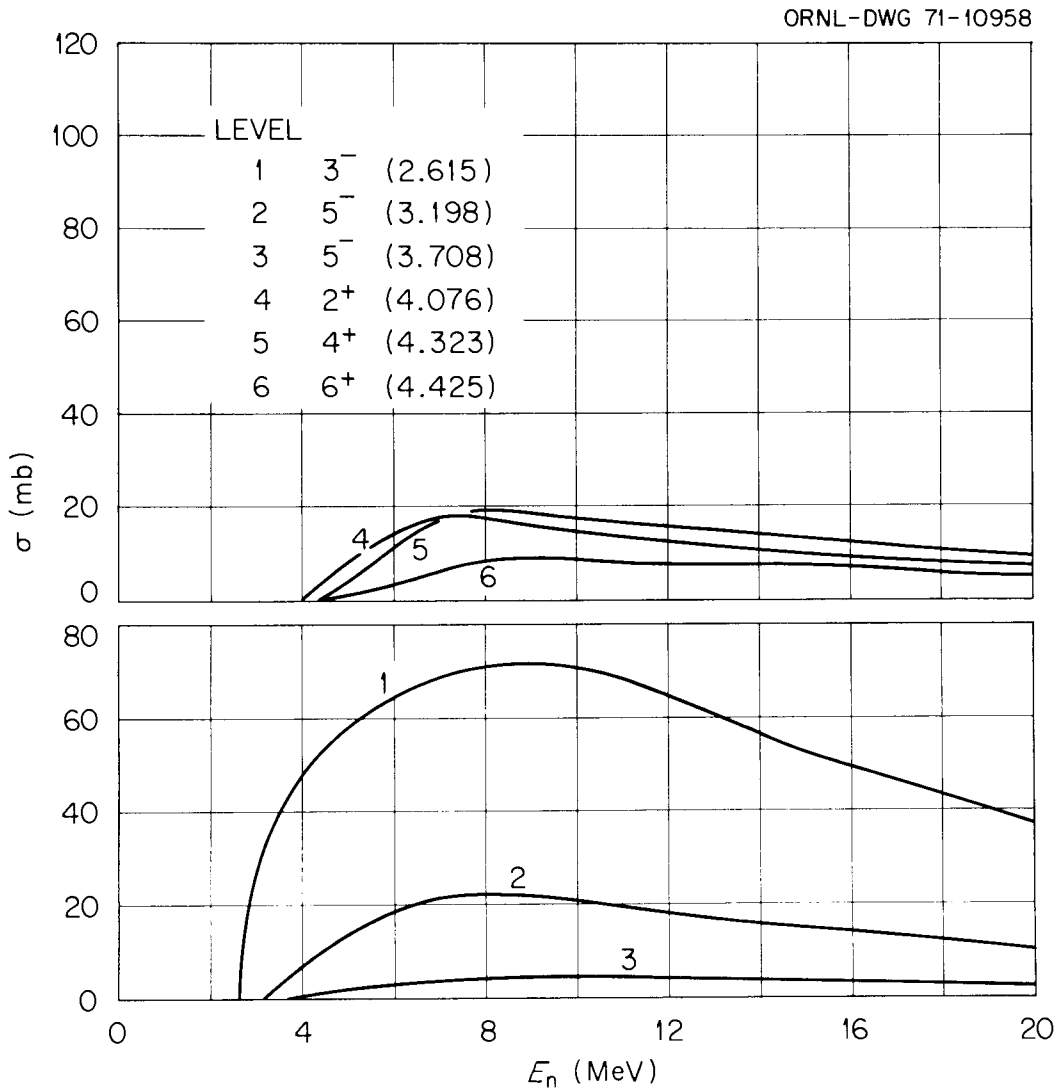

Fig. 11. Calculated direct-inelastic scattering cross sections for ^{208}Pb.

5.3. Inelastic-Scattering Exciting Levels

Fig. 12 compares calculation with the measurement of Towle and Gilboy[49] for inelastic-scattering cross sections for the three lowest excited states in ^{208}Pb. The agreement is reasonably good except for one datum near 4.5 MeV for the 2.615 MeV level. The calculated cross sections for exciting the 2.615 MeV level is depressed above 4.0 MeV because of intense competitions from other levels. The dashed curves are for compound-nucleus contributions alone.

Fig. 13 shows similar comparison for ^{207}Pb for levels up to 3.43 MeV. The measurement, taken at a scattering angle of 50°, is due to Cranberg et al.[14] The quoted error is $\pm 10\%$. Fig. 14 compares differential cross sections for the three lowest excited states. The agreement is generally good. For the 1.633 MeV level, good agreement in Fig. 13 and poor agreement in Fig. 14 indicate possible inconsistency in the data. It may be noted that $\sigma(E)$ is approximately equal to $4\pi\sigma(50^{\circ},E)$.

Figs. 15, 16, and 17 serve the same purpose for ^{206}Pb. The groupings of levels in ^{207}Pb and ^{206}Pb were made such that all levels in the closest vicinity of an observed excitation energy were included for that excitation.

The small humps near 4 or 5 MeV in the calculated excitation cross sections mark the turning-off of the width-fluctuation correction. This was a drawback in the computational scheme, but fortunately, its effect was small and it influenced only the lowest few levels.

The calculation was performed for all the discrete levels up to 4.4 MeV. The sum of these cross sections, weighted by the isotopic abundances, define $\sigma_L(n,n')$ shown in Fig. 5.

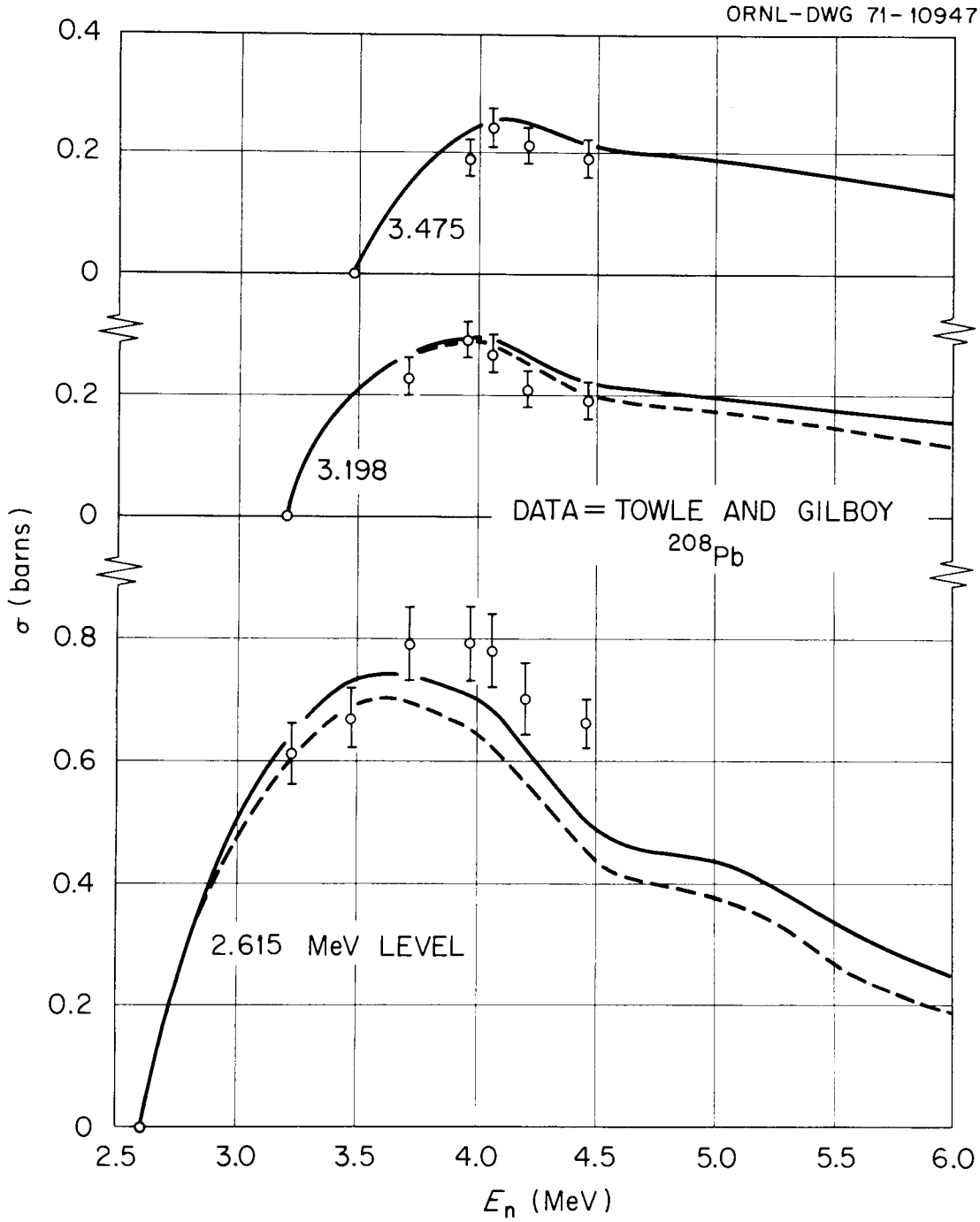

Fig. 12. Comparison of calculation with experiment for the inelastic level excitation cross sections in ^{208}Pb.

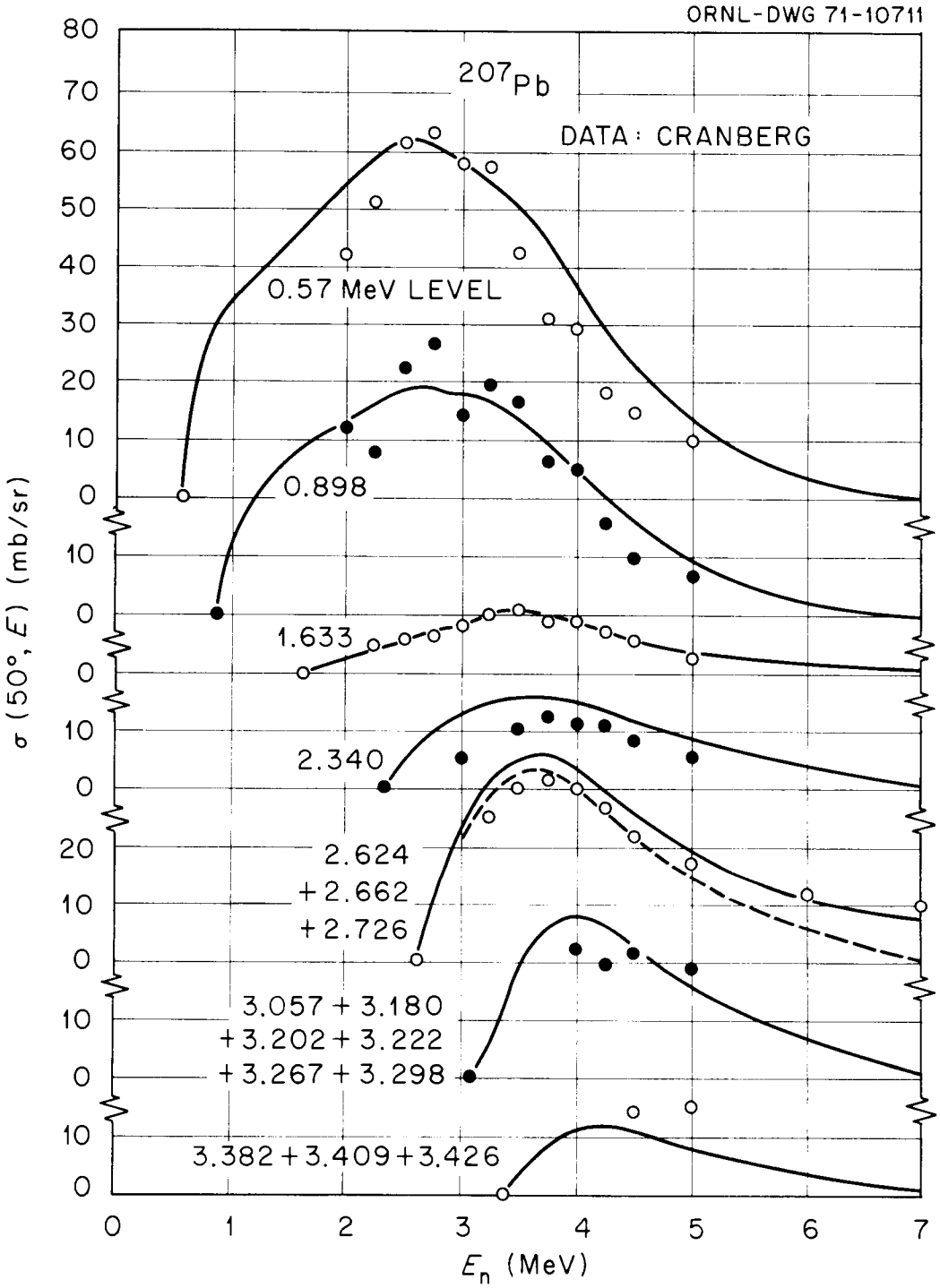

Fig. 13. Comparison of calculation with experiment for the inelastic level excitation cross sections in ^{207}Pb.

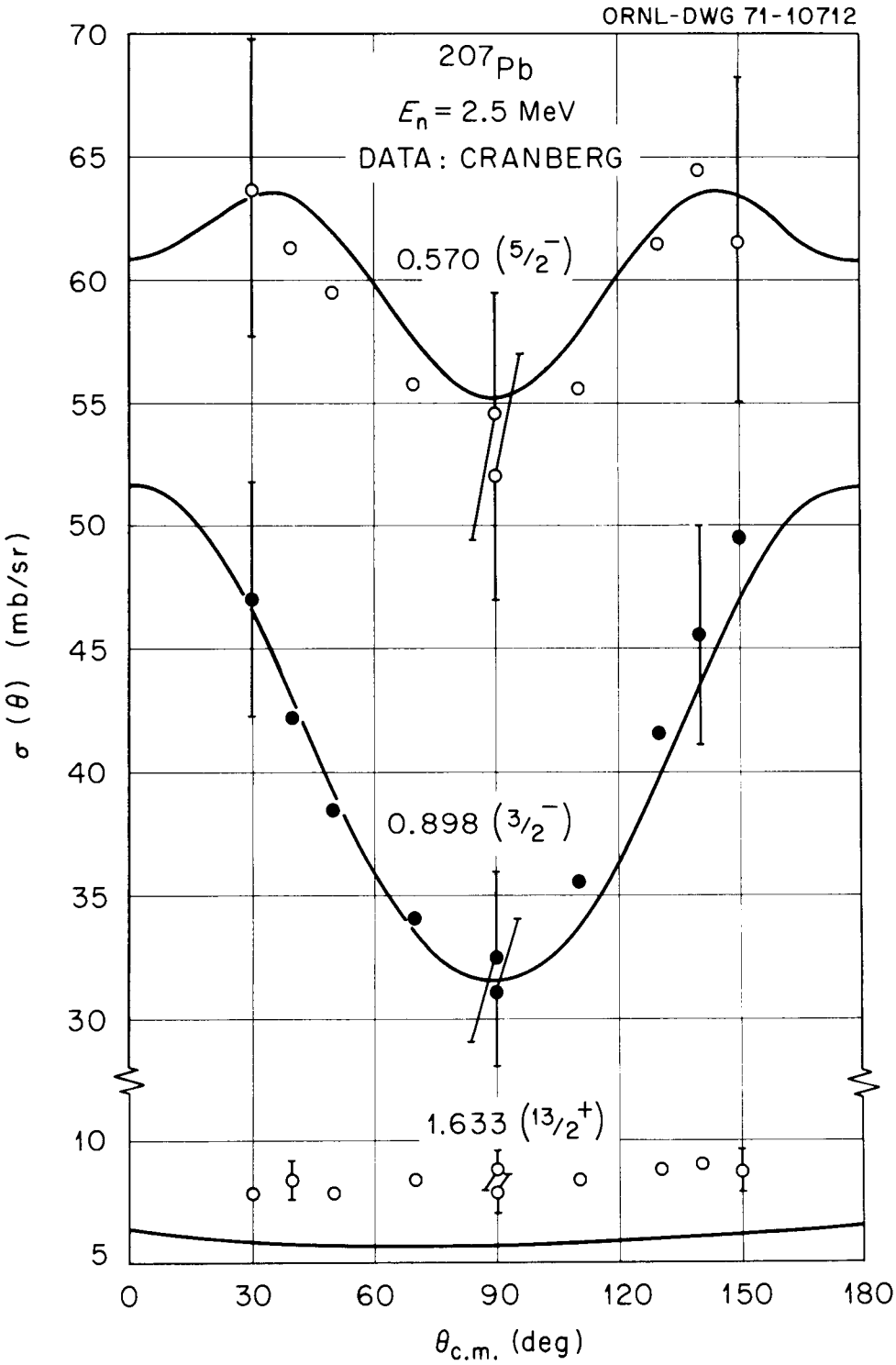

Fig. 14. Comparison of calculation with experiment for the angular distributions of inelastic level excitations in ^{207}Pb for E_n = 2.5 MeV.

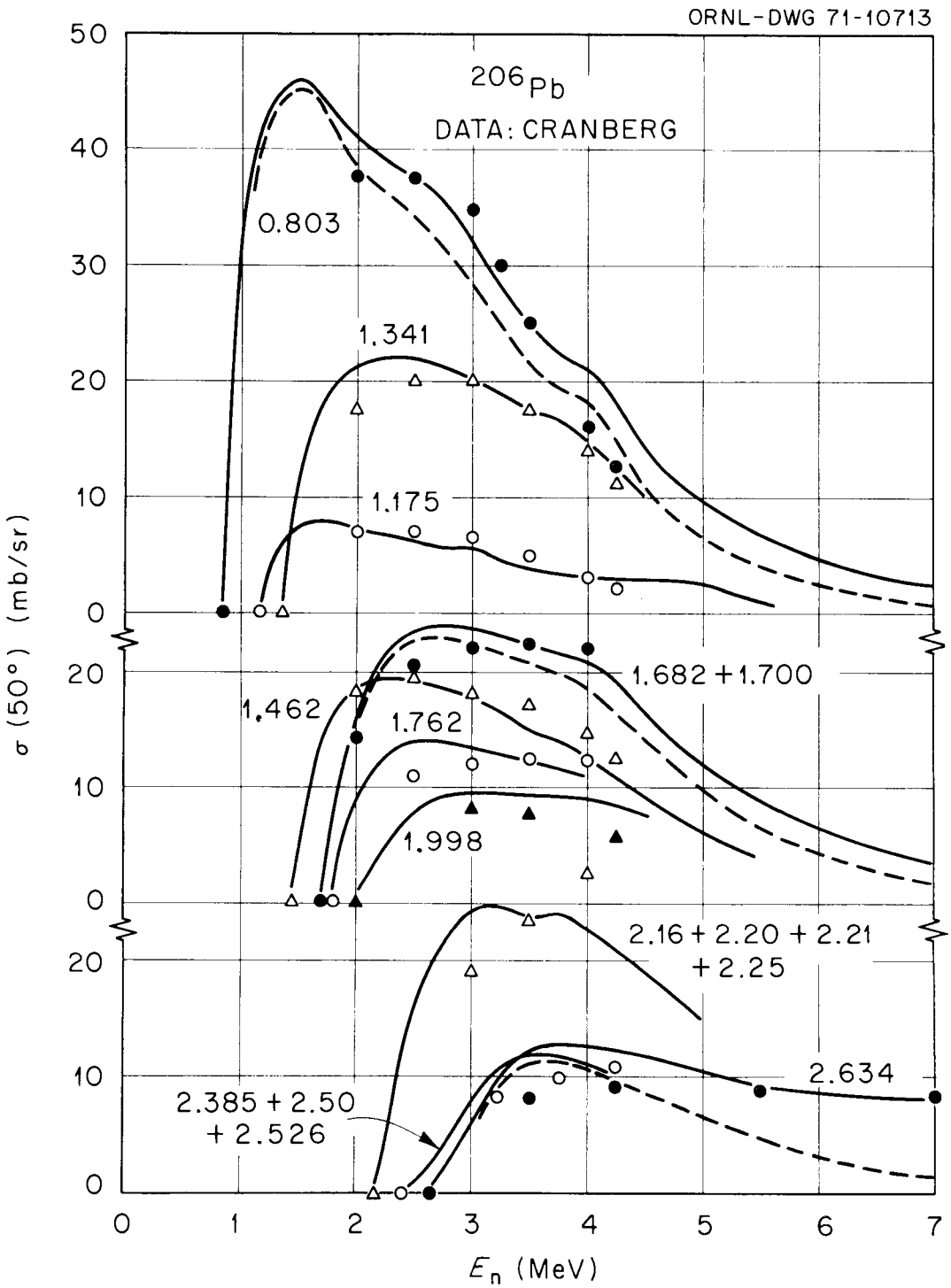

Fig. 15. Comparison of calculation with experiment for the inelastic level excitation cross sections in ^{206}Pb.

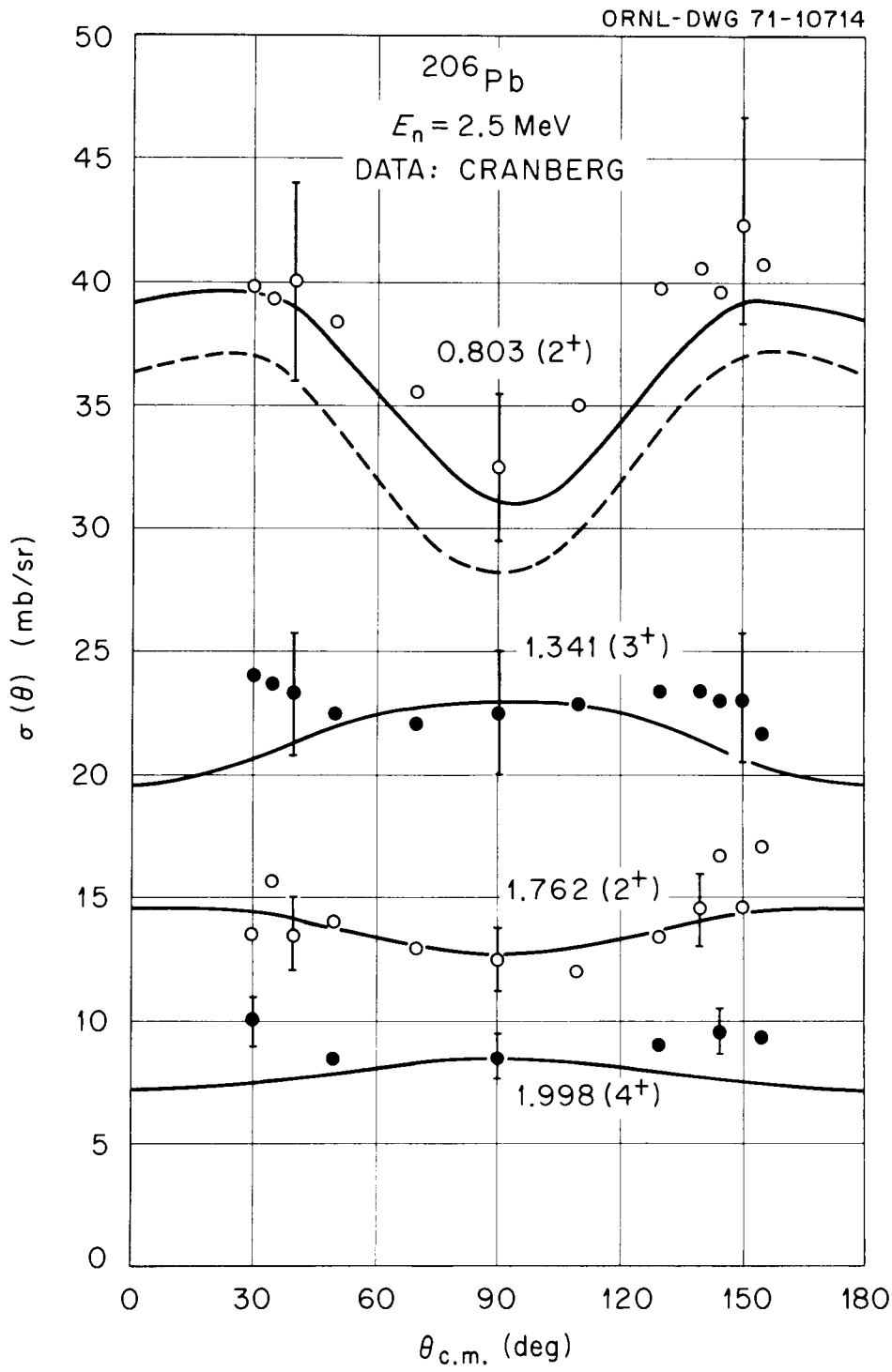

Fig. 16. Comparison of calculation with experiment for the angular distributions of inelastic level excitations in ^{206}Pb for E_n = 2.5 MeV.

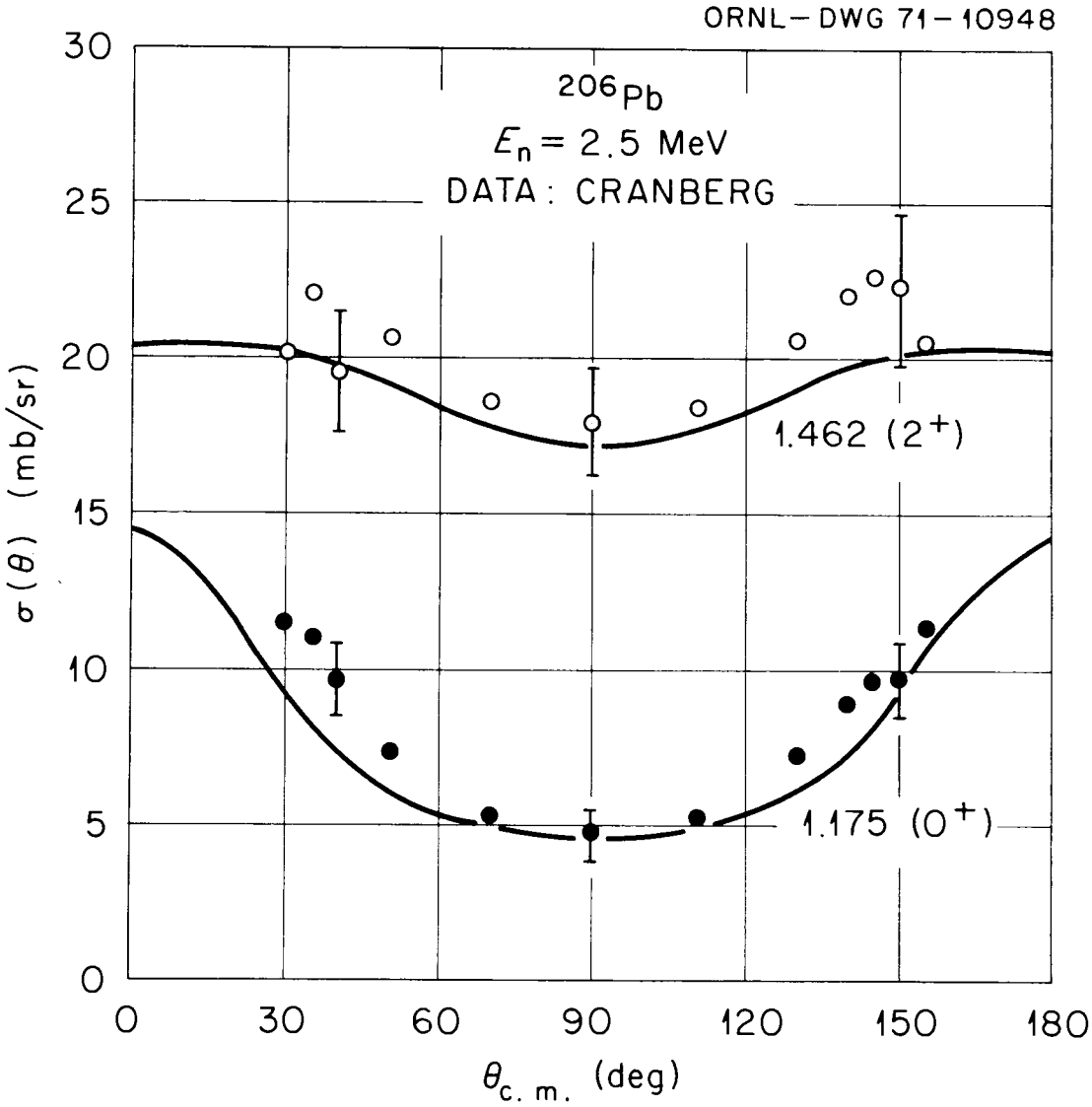

Fig. 17. Comparison of calculation with experiment for the angular distributions of inelastic level excitations in ^{206}Pb for E_n = 2.5 MeV.

5.4. Nonelastic Cross Sections and Components

Above the (n,n') threshold (0.573 MeV), the capture cross sections are smaller than 4 mb and above 3 MeV they are less than 1 mb. Coleman[50] has measured (n,α) cross section for ^{208}Pb to be 1.58 ± 0.24 mb at 14.5 MeV. Other cross sections for the emission of charged particles are believed to be small. Therefore, the nonelastic cross sections above the (n,n') threshold are composed mainly of (n,n'), (n,2n) and (n,3n) reactions.

Up to 8 MeV, the nonelastic cross sections were calculated with HELGA. The (n,n') thresholds in the three major isotopes mark a three-step rise of the (n,n') cross sections in the low-energy region. From 8 MeV to 20 MeV, the nonelastic cross sections were computed with GENOA. The ratios of the compound-nucleus components of (n,n') cross sections to the sum of (n,2n) and (n,3n) cross sections were calculated with NNNGAM. Given nonelastic cross sections and the direct-interaction part of the (n,n') cross sections, the rise of the (n,2n) cross sections and the decline of the (n,n') cross sections above the (n,2n) threshold were then defined. The (n,3n) cross sections were calculated with the Pearlstein formalism[51] with level densities defined previously. All calculations were performed for each of the three major isotopes so that the effects of different reaction thresholds in the isotopes were included properly. The contributions of ^{204}Pb to these cross sections were ignored.

The calculated σ(n,X) and σ(n,n') are compared with available data in Fig. 18. For σ(n,X) the data were taken from LA-1429 as given in CSISRS,[52] Walt and Barschall,[53] Beyster *et al.*,[54] Beyster, Walt and Salmi,[55] Strizhak,[56] Taylor *et al.*,[57] Pasechnik,[58] Degtyarev,[59] Bonner and Slattery,[60] Degtyarev and Nadtochii,[61] Chatterjee and Ghose,[62] and Coon *et al.*[40] Not shown in

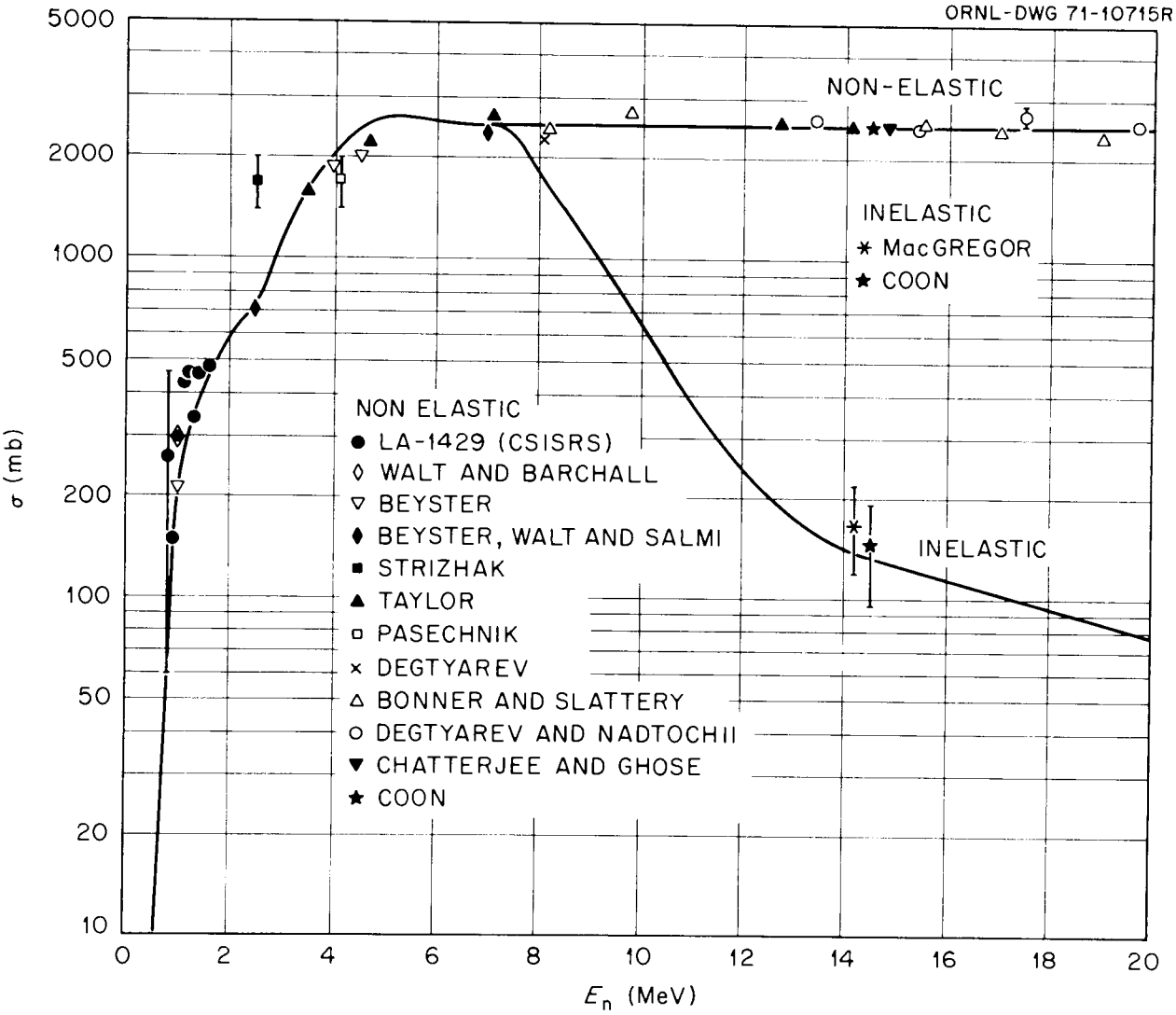

Fig. 18. Comparison of calculation with experiment for nonelastic and inelastic scattering cross sections.

the figure are seven single values of $\sigma(n,X)$ near 14 MeV which have been tabulated in BNL-325 (Ref. 9). The average of these values well defines a $\sigma(n,X)$ of 2.5 $\pm$ 0.02 barns near 14 MeV.

MacGregor[63] measured $\sigma(n,n') = 170 \pm 50$ mb at $E_n = 14.2$ MeV for $E_{n'} = 9 - 14$ MeV. Coon et al.[40] measured $\sigma(n,n') = 88 \pm 30$ mb at $E_n = 14.5$ MeV for $E_{n'} = 9 - 14$ MeV and $\theta = 40^o - 180^o$. The scattered neutrons of energies from 9 to 14 MeV correspond to the excitation of levels below 5 MeV which result dominantly from direct interactions for incident neutrons above 14 MeV. Therefore, the contribution to $\sigma(n,n')$ in the $\theta = 0^o - 40^o$ region was estimated from the calculation given in Section 5.2 to be 59 $\pm$ 15 mb. This was added to Coon's datum to give $\sigma(n,n') = 147 \pm 45$ mb at $E_n = 14.5$ MeV for $E_{n'} = 9 - 14$ MeV. The scattered neutrons below 9 MeV result mainly from compound nucleus formation, and their contributions to $\sigma(n,n')$ obtained in the NNNGAM calculation were found to be 16 mb at 14.2 MeV and 12 mb at 14.5 MeV. These corrections, well within the experimental errors, were not applied to the data. From analysis of gamma-ray cascades, Jönsson[64] obtained the upper limit of $\sigma(n,n')$ at 15.5 MeV to be 820 $\pm$ 270 mb and the lower limit 650 $\pm$ 100 mb. These values seemed to be too big by a factor of ten and were not entered into Fig. 18. $\sigma_C(n,n')$ is obtained by subtracting $\sigma_L(n,n')$ from $\sigma(n,n')$.

Several measurements have been made for $\sigma(n,2n)$ near 14 MeV which are tabulated below:

E_n(MeV)	σ (mb)	Reference
14	1800 $\pm$ 200	65
14	2300 $\pm$ 190	66
14	2180 $\pm$ 200	67
14	1760 $\pm$ 40	68
14.1	2740 $\pm$ 200	69
15.5	1700 $\pm$ 280	64

The last entry was obtained from the limits 1850 ± 110 mb and 1680 ± 270 mb, estimated by the author from analyzing measured gamma rays. It is seen that the discrepancies among various measurements at 14 MeV are large, and one can hardly argue for or against a calculated value of 2358 mb at 14 MeV and the $\sigma(n,2n)$ curve shown in Fig. 5. However, the calculated $\sigma(n,2n)$ is consistent with measured $\sigma(n,X)$ and $\sigma(n,n')$.

No measurements have been made of $\sigma(n,3n)$.

5.5. Energy Distribution of Secondary Neutrons

The energy distribution of secondary neutrons from (n,n' continuum), (n,2n), and (n,3n) reactions may be derived from the level densities with the statistical-model theory[35] and the LeCouteur theory[70] for neutron cascade. The energy distribution of the "first" neutron may be represented by an evaporation spectrum

$$f(E_n \rightarrow E_n') \sim E_n' \, e^{-E_n'/\theta_1}$$

where the temperature θ_1 is equal to T in the level density formula given by Eq. (3a). Corresponding to Eq. (3b) the temperature is given approximately by

$$\theta_1 \sim \left(\frac{E_n - \Delta}{a}\right)^{1/2} \quad \text{if } E_n - \Delta \gg E_n'.$$

Eq. (3b) was used first to obtain the temperature, θ_1, above 8 MeV for the lead isotopes. The temperature in the energy region from the (n,n') continuum cut-off (4.4 MeV) to 8 MeV was extrapolated from that above 8 MeV and the extrapolation was required to go through a temperature defined by Eq. (3a) near 6 MeV. The temperature for natural lead is shown in Fig. 19, together with some measured values taken from Mathur *et al.*,[71] Huber *et al.*,[72] and

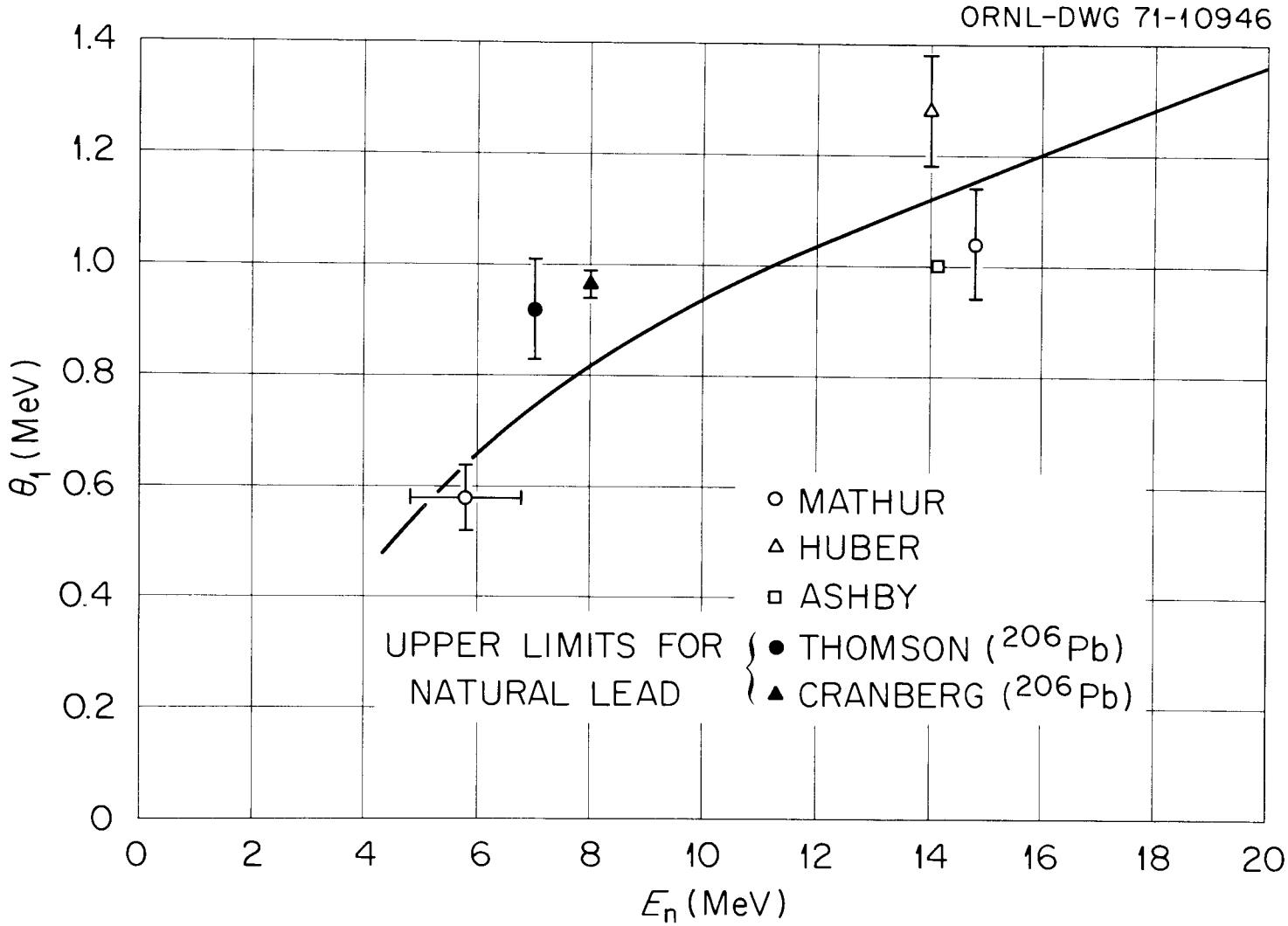

Fig. 19. Comparison of calculation with experiment for the nuclear temperature of the first neutron emitted in (n,n' continuum), (n,2n) and (n,3n) reactions in natural lead.

Ashby et al.[69] Two data points are given for ^{206}Pb which represent upper limits for natural lead. These were taken from Thomson[73] and Cranberg et al.[14]

After emitting the first neutron, the nucleus is cooled down and subsequent neutrons are emitted with smaller temperatures. LeCouteur[70] has shown that the energy distribution of the sum of two or more cascade neutrons may be represented by

$$f(E_n \rightarrow E_n') \sim (E_n')^{5/11} e^{-12 E_n'/11 \theta_1}.$$

This representation is not allowed by the ENDF/B format, but it is quite close to a Maxwellian distribution. Therefore, the energy distribution of secondary neutrons for (n,2n) and (n,3n) reactions were given as Maxwellian distributions with the temperature $11 \theta_1/12$.

5.6. Gamma-Ray Production

The gamma-ray-production cross sections and energy distributions of secondary gamma rays for (n,n') reactions up to 4.4 MeV were calculated using HELGA with the level properties and gamma-ray branching ratios given previously. Above 4.4 MeV, they were calculated with NNNGAM. The code NNNGAM provides gamma-ray multiplicities and energy distributions for (n,n'), (n,2n), and (n,3n) reacitons. The calculated gamma-ray multiplicities were multiplied by the evaluated $\sigma(n,X)$ to obtain the gamma-ray production cross sections. The code does not treat the neutron cascade in (n,3n) reactions, but $\sigma(n,3n\gamma)$ can be calculated with an approximate method to be described below. Gamma-ray cascades in ^{205}Pb and ^{204}Pb were treated as continua using level densities given in Table 7.

The excitation of the residual nucleus in $^{A}Pb(n,3n)$ reaction was approximated by $^{A-1}Pb(n,2n)$ reaction with E_n replaced by $E_n - E_b(A)$ and $a(A-1)$ by $a^*(A-1)$, where $E_b(A)$ is the separation energy of the last neutron in nucleus A and the new level density parameter a^* is defined below.

The temperature of the first neutron in $^{A}Pb(n,3n)$ reaction is given by

$$\theta_1 \approx \left[\frac{E_n - \Delta(A)}{a(A)}\right]^{1/2} .$$

Assuming an evaporation spectrum, the mean energy of the first neutron is $2\theta_1$. The temperature of the second neutron in $^{A}Pb(n,3n)$ reaction may then be approximated by

$$\theta_2 \approx \left[\frac{E_n - \Delta(A-1) - E_b(A) - 2\theta_1}{a(A-1)}\right]^{1/2}.$$

Comparing this with the temperature of the first neutron in $^{A-1}Pb(n,2n)$ reaction with an incident neutron of energy $E_n - E_b(A)$,

$$\left[\frac{E_n - E_b(A) - \Delta(A-1)}{a(A-1)}\right]^{1/2},$$

it is seen that the approximation of $^{A}Pb(n,3n)$ by $^{A-1}Pb(n,2n)$ with energy $E_n - E_b(A)$ results in a neutron spectrum which is harder than the real one and a gamma-ray spectrum which is too soft by the same amount of energy. One can easily compensate this drawback by changing the level density parameter $a(A-1)$ to $a^*(A-1)$ with the relation,

$$a^*(A-1) = a(A-1) \left[\frac{E_n - E_b(A) - \Delta(A-1)}{E_n - E_b(A) - (A-1) - 2\theta_1}\right].$$

Some of the calculated results are compared with available data in Figs. 20 - 28. Figs. 20, 21, and 22 are for some of the discrete gamma lines in ^{206}Pb, ^{207}Pb, and ^{208}Pb respectively. For ^{206}Pb experimental data were taken from Bostrom et al.,[74] Lind and Day,[13] Boring et al.,[75] Kiehn and Goodman,[76] Day,[77] and Morgan et al.[78] Only representative data are shown for Lind and Day's measurements. For ^{207}Pb data were obtained from Day[77] and Morgan et al.[78] For ^{208}Pb data were derived from the measurement of Nellis[21] which superseded earlier measurements of Texas Nuclear Corporation.[74,78] Figs. 23 - 27 display the energy distributions for E_n = 4.5, 5.5, 6.5, 7.5, and 8.5 MeV. Fig. 28 shows the total gamma-ray-production cross sections $\sigma(n,x\gamma)$. Corresponding data were taken from Perkin,[79] Howerton and Plechaty,[80] Scherrer et al.,[81] and Battat et al.[82] Most of the data shown in these figures are designated as $4\pi\sigma(\theta)$ where θ is the laboratory angle for which the measurement was made. In making comparisons of these data with calculations, the question of the anisotropy of the gamma-ray angular distribution always arises. Table 9 (Ref. 83) provides the anisotropies, $\sigma(0^o)/\sigma(90^o)$, for some of the gamma rays from inelastic scattering. This information makes the comparisons shown in Figs. 20 - 28 more meaningful. For instance, the calculated cross sections for the production of 0.803 MeV gamma rays are in better agreement with the $4\pi\sigma(94^o)$ of Lind and Day[13] than that indicated in Fig. 20 because $\sigma(0^o)/\sigma(90^o)$ is 1.25, and the data $4\pi\sigma(94^o)$ should be moved approximately 12% higher to be comparable with the calculation. For similar reasons, the comparison for E_γ = 0.538 MeV is worse than that indicated in the figure.

In Fig. 22 the experimental data were obtained by integrating the differential cross sections measured by Nellis[21] except for E_γ = 0.76 MeV for which the data are $4\pi\sigma(90^o)$.

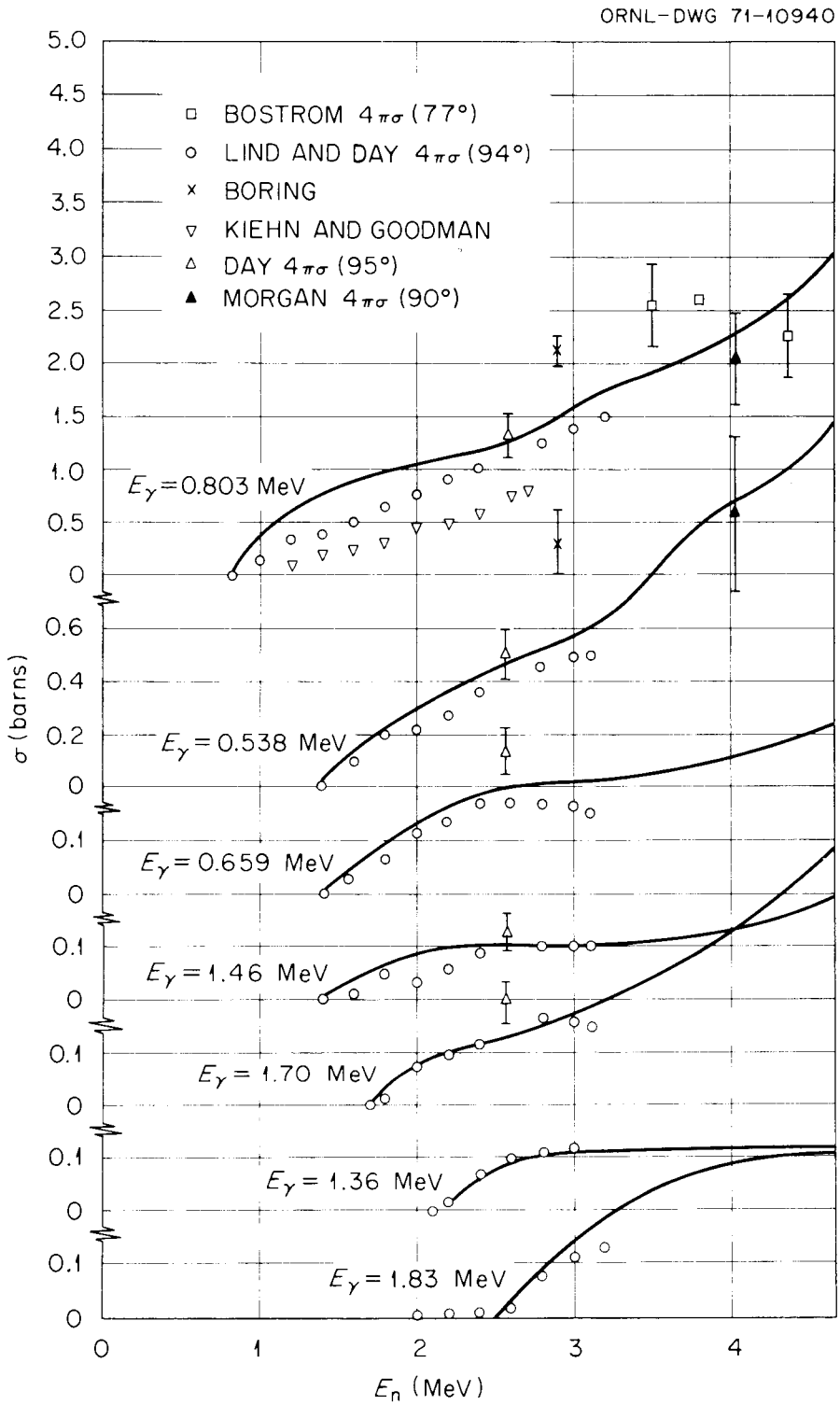

Fig. 20. Comparison of calculation with experiment for the production cross sections of discrete gamma rays in ^{206}Pb.

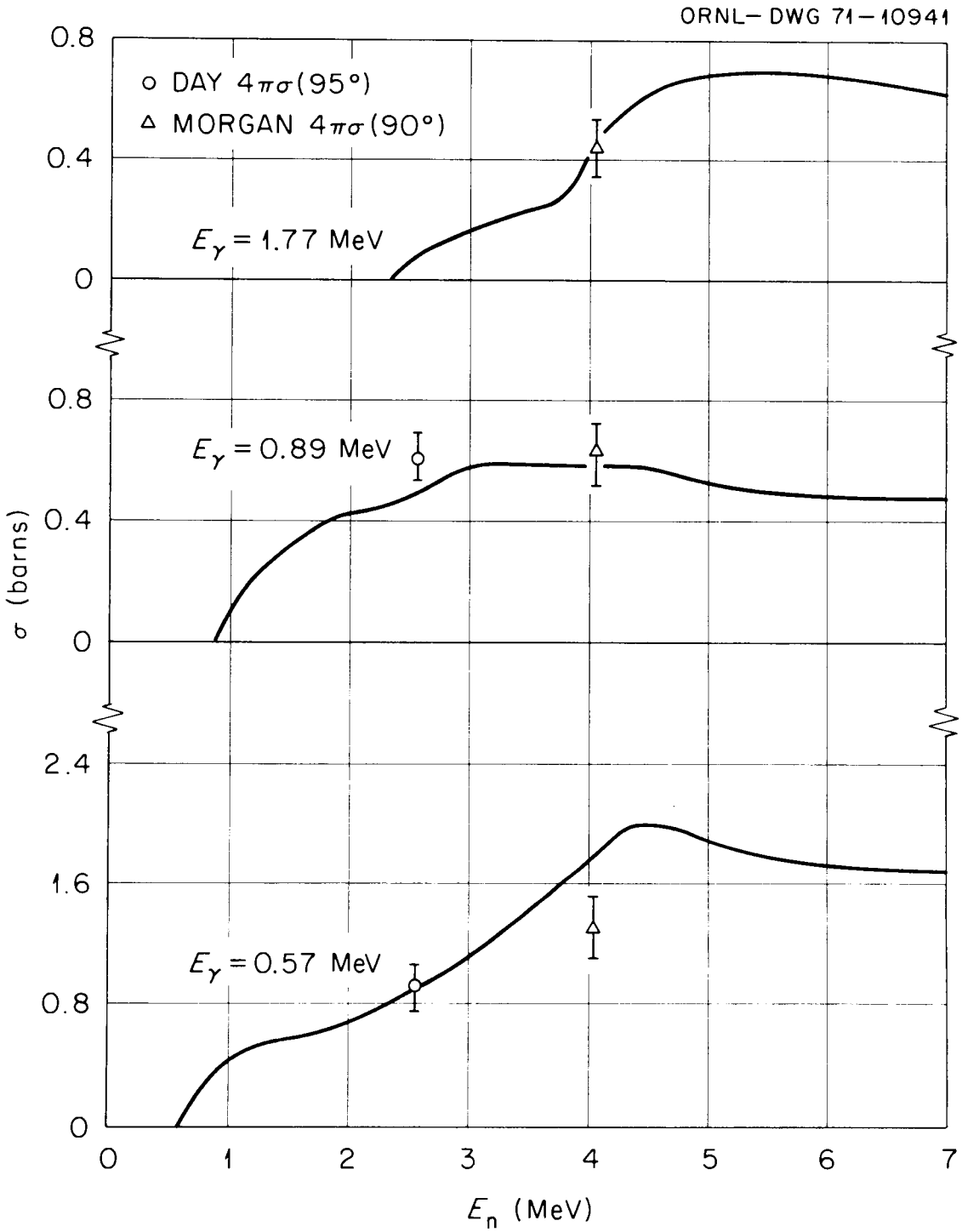

Fig. 21. Comparison of calculation with experiment for the production cross sections of discrete gamma rays in ^{207}Pb.

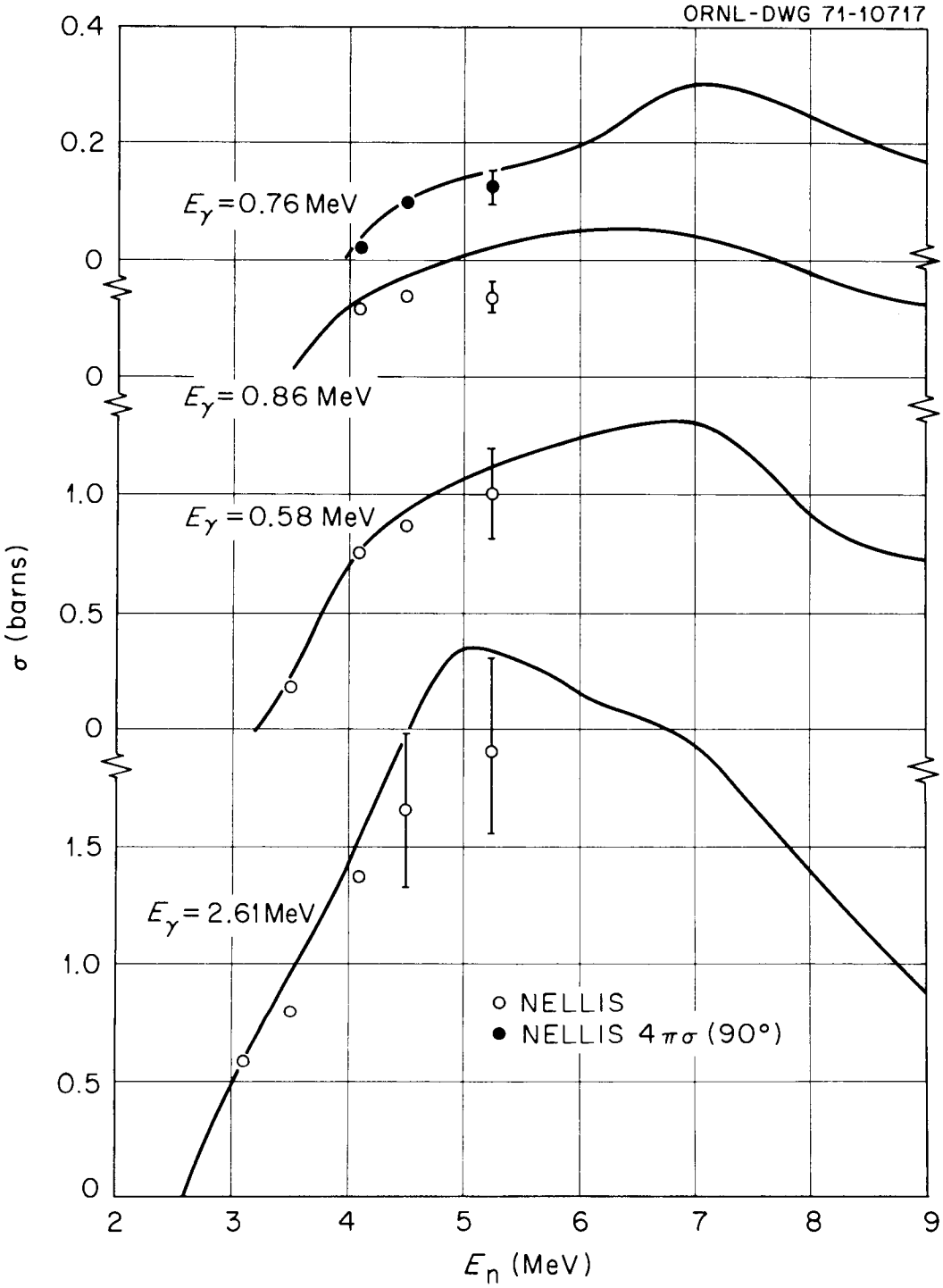

Fig. 22. Comparison of calculation with experiment for the production cross sections of discrete gamma rays in ^{208}Pb.

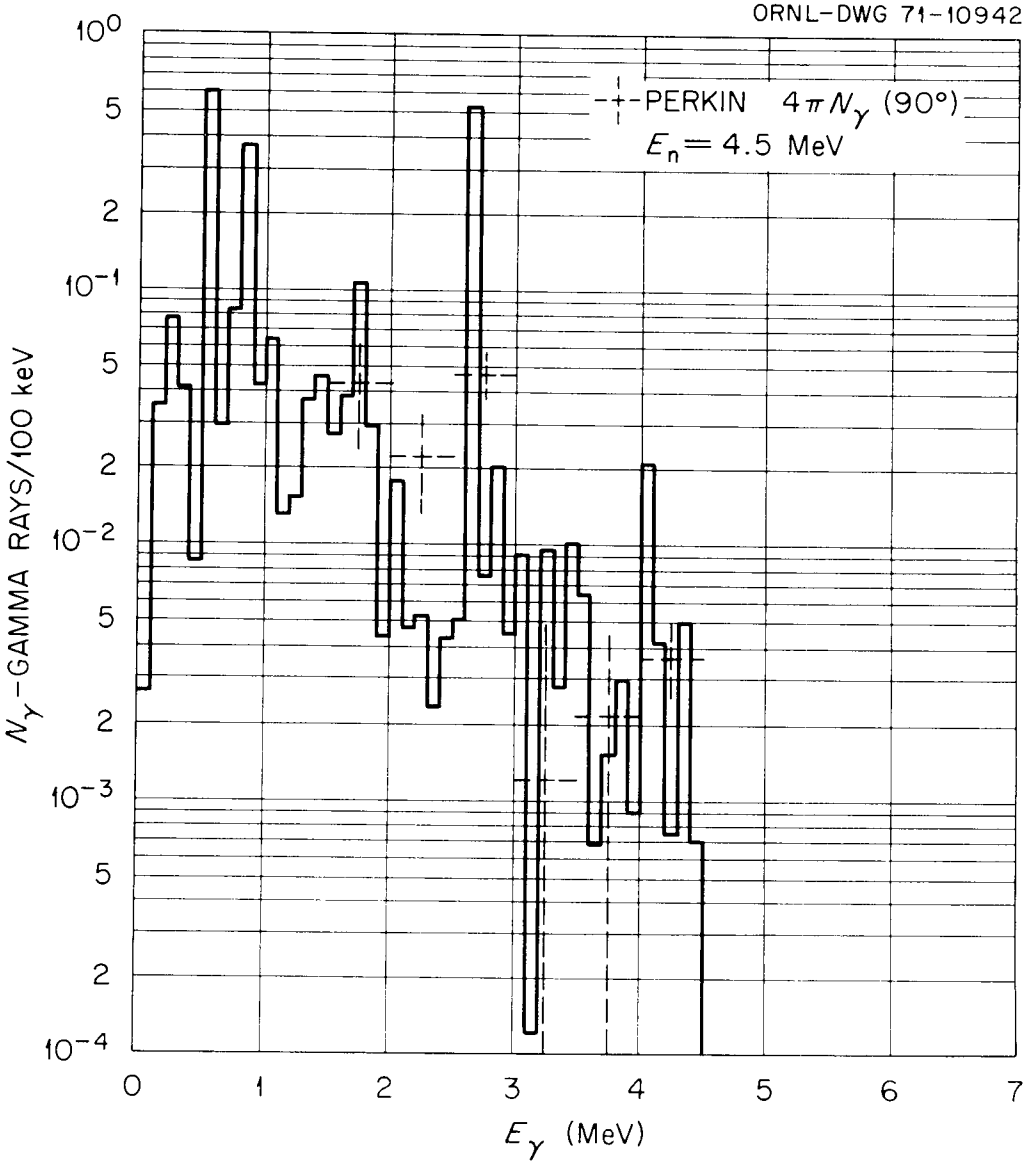

Fig. 23. Comparison of calculation with experiment for the gamma-ray yield spectrum from inelastic scattering of 4.5 MeV neutrons with natural lead.

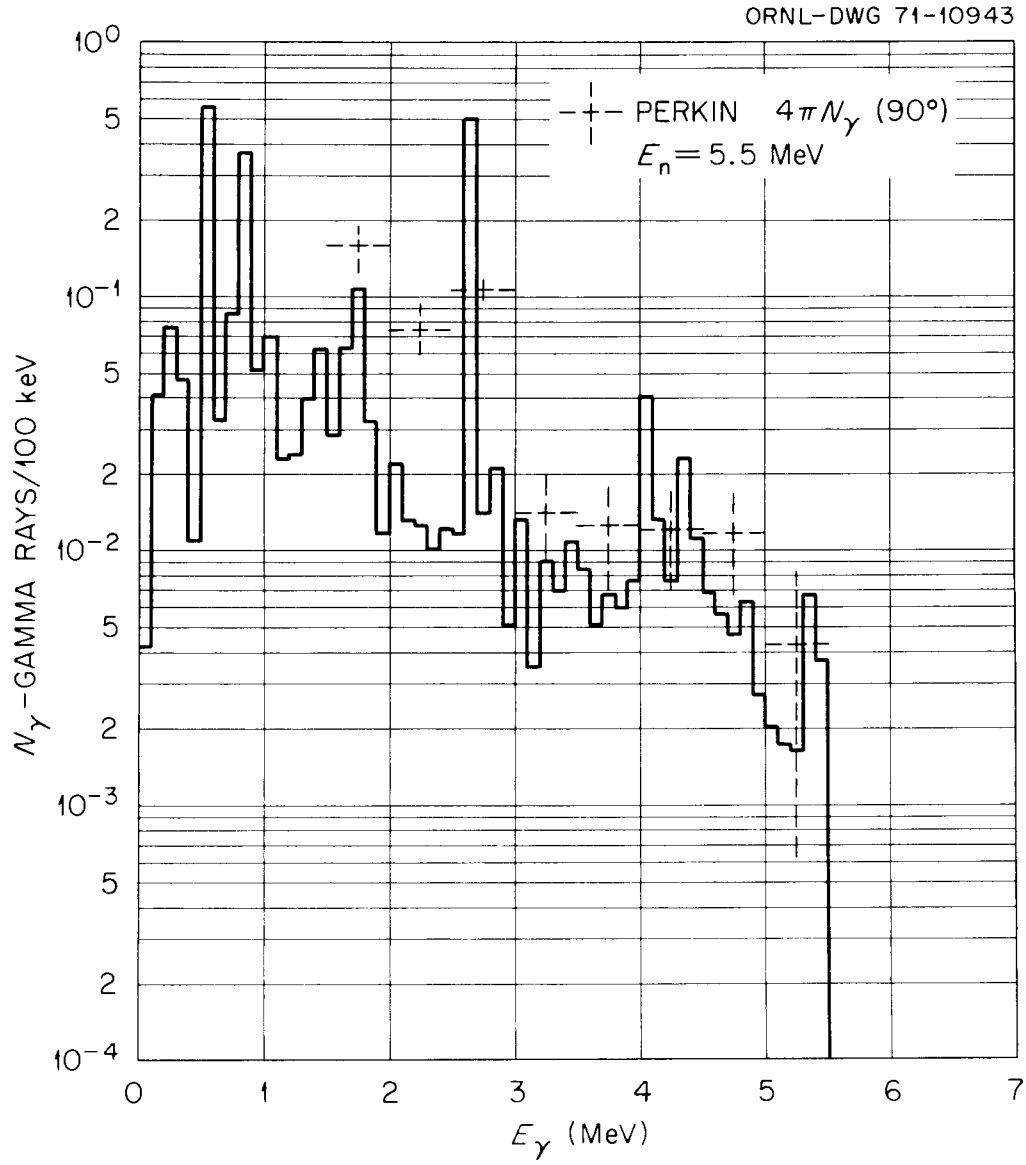

Fig. 24. Comparison of calculation with experiment for the gamma-ray yield spectrum from inelastic scattering of 5.5 MeV neutrons with natural lead.

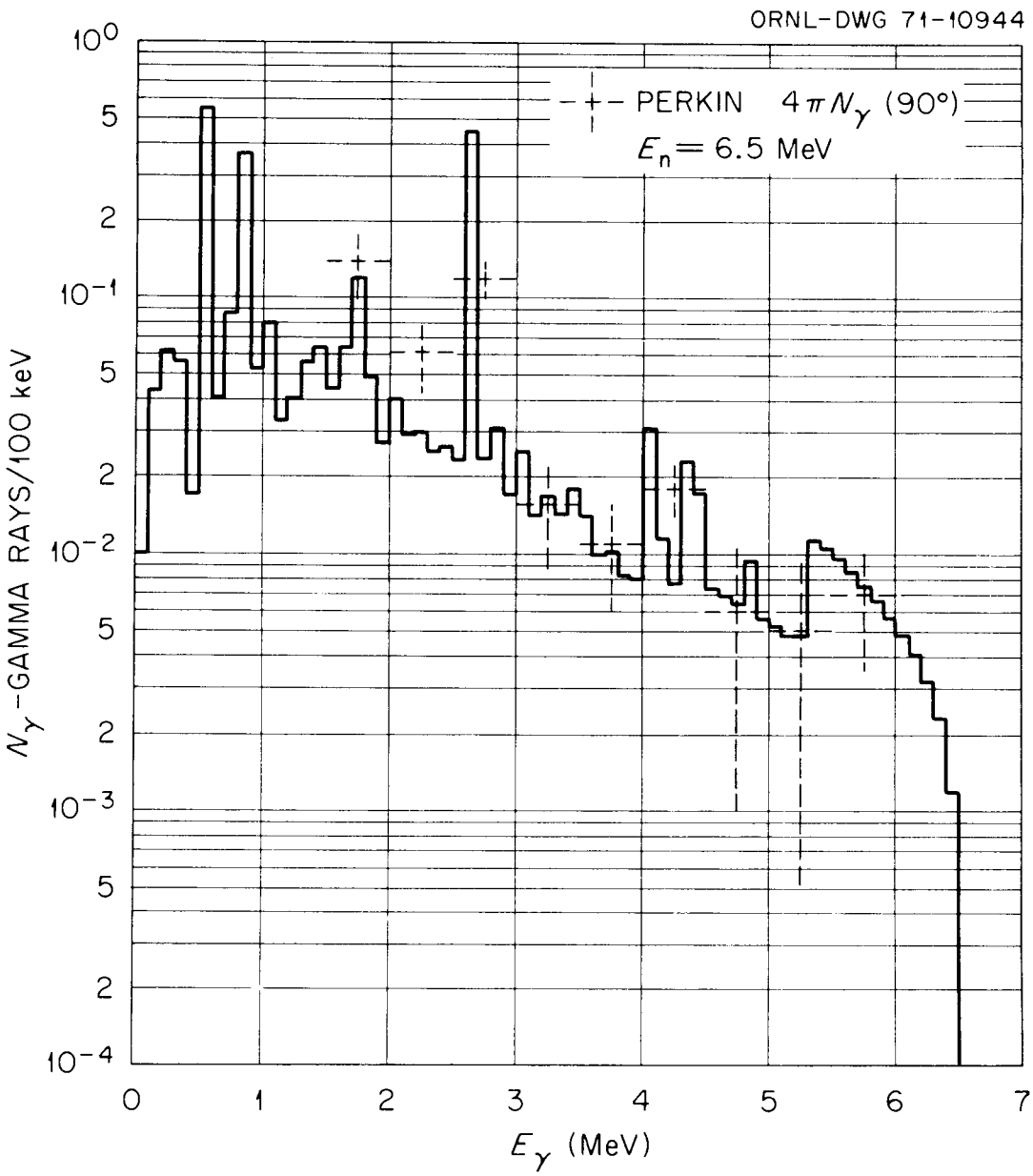

Fig. 25. Comparison of calculation with experiment for the gamma-ray yield spectrum from inelastic scattering of 6.5 MeV neutrons with natural lead.

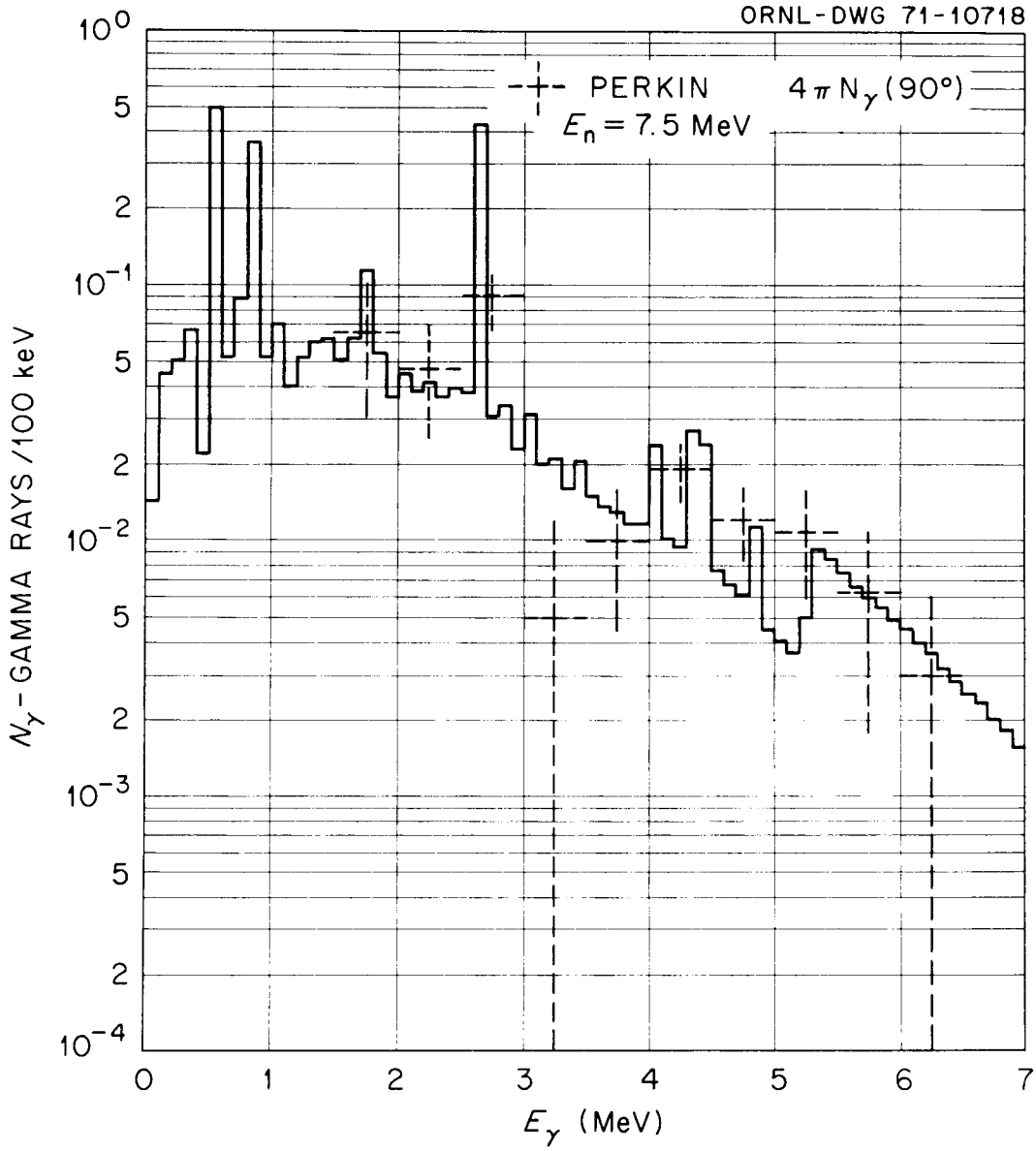

Fig. 26. Comparison of calculation with experiment for the gamma-ray yield spectrum from (n,n') and (n,2n) reactions of 7.5 MeV neutrons with natural lead.

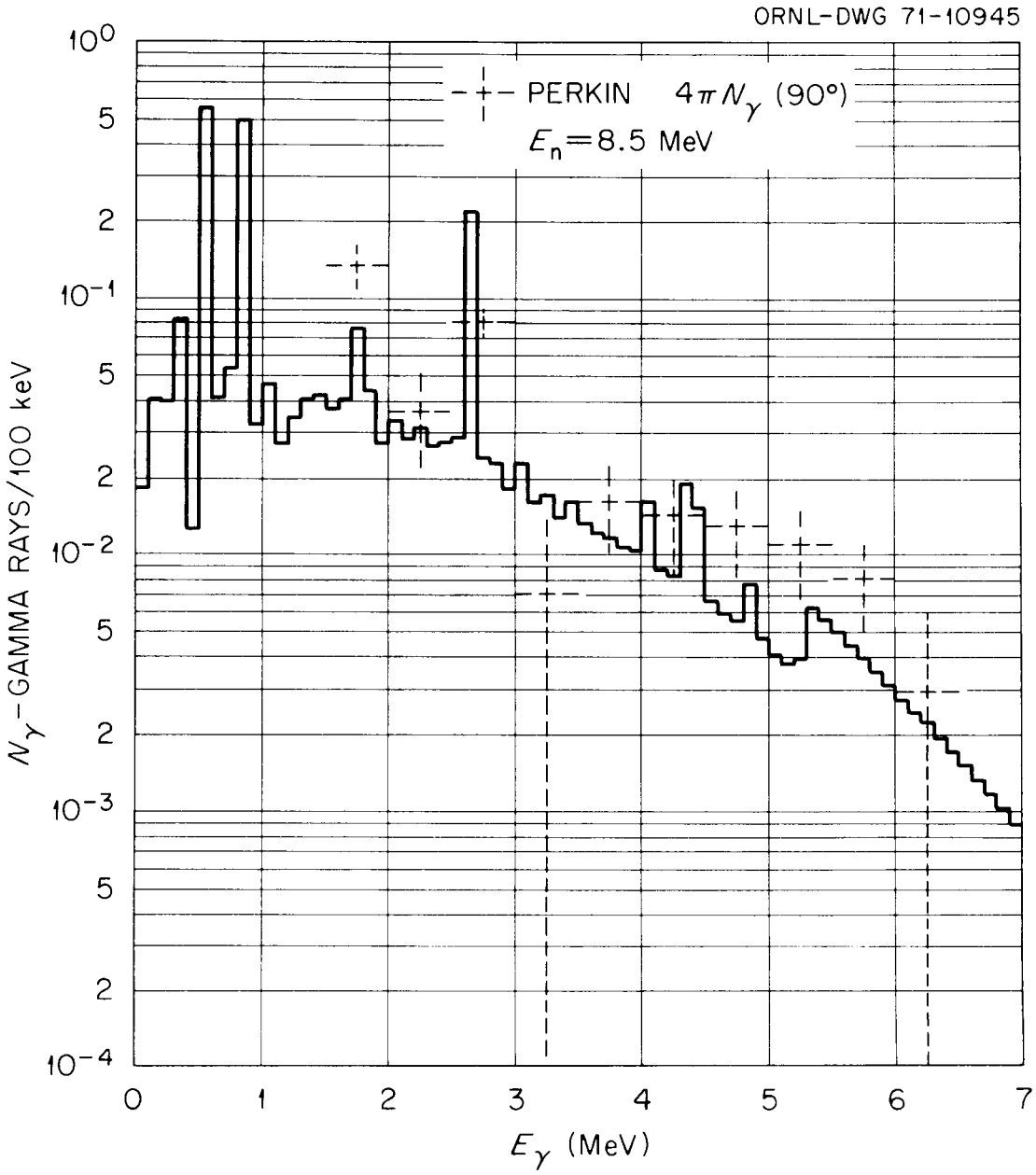

Fig. 27. Comparison of calculation with experiment for the gamma-ray yield spectrum from (n,n') and (n,2n) reactions of 8.5 MeV neutrons with natural lead.

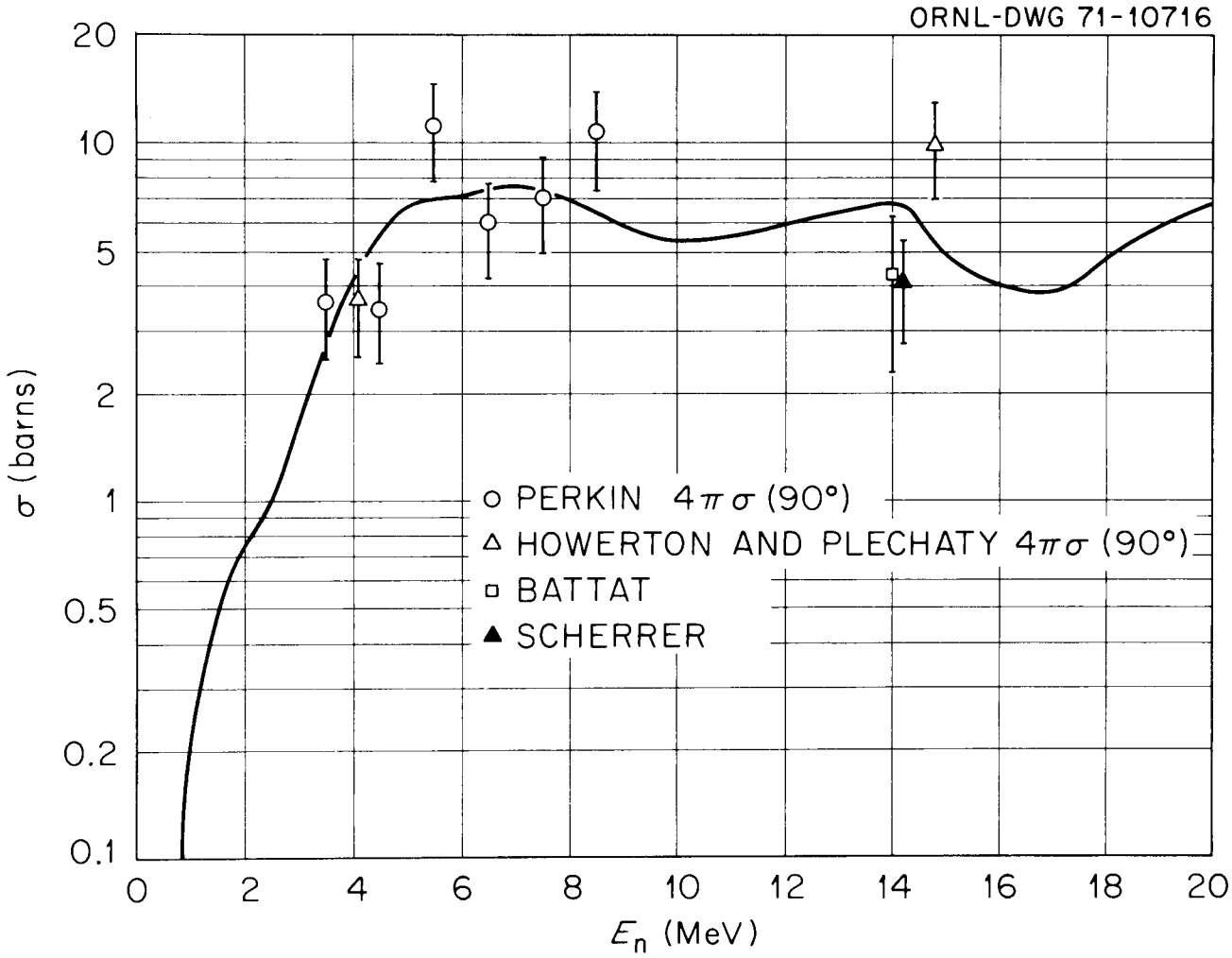

Fig. 28. Comparison of calculation with experiment for the total gamma-ray production cross sections for the sum of (n,n'), (n,2n), and (n,3n) reactions.

Table 9. Anisotropy of Gamma Rays from Inelastic Scattering

Isotope	E_γ(MeV)	E_n(MeV)	$\sigma(0^\circ)/\sigma(90^\circ)$ $\pm 10\%$	Reference
^{206}Pb	0.538	4.1	0.7	83
	0.803	4.1	1.25	83
^{207}Pb	0.89	4.1	0.85	83
	1.77	4.1	0.75	83
	2.634	4.1	1.3	83
^{208}Pb	0.58	3.5	1.6	83
		4.1	1.2	83
		4.1	1.6	21
		4.5	1.2	21
		5.2	1.2	21
	0.86	4.1	0.8	83
		4.1	0.7	21
		4.5	0.7	21
		5.2	0.7	21
	2.615	3.0	1.8	83
		3.1	1.7	21
		3.5	1.8	83
		3.5	1.9	21
		4.1	1.8	83
		4.1	1.9	21
		4.5	1.8	83
		5.2	1.8	83
Natural Lead	All Gamma Rays	3.7	1.3	74
		4.2	1.35	74
		4.7	1.15	74

In Figs. 23 - 27 the gamma-ray yields are given as "number of gamma rays per 100 keV bin Perkin's $d\sigma(90^{o})/dE_{\gamma}$ (Ref. 79) were reduced to the same unit using the evaluated $\sigma(n,X)$.

In Fig. 28 some of the measured production cross sections do not cover the entire gamma-ray energy. Perkin[79] measured the production cross sections for $E_{\gamma} > 1.5$ MeV. From the calculation the contributions of gamma rays for $E_{\gamma} < 1.5$ MeV to the total production cross sections are 67.6%, 62.5%, 58.4%, 42.1%, 51.1%, and 61.4% for E_n = 3.5, 4.5, 5.5, 6.5, 7.5, and 8.5 MeV respectively. The same percentages were applied to Perkin's data to obtain the data shown in the figure. The contributions of the gamma rays for $E_{\gamma} <$ 1.5 MeV to the total production cross sections are largely due to the strong lines of E_{γ} = 0.803 MeV in ^{206}Pb and E_{γ} = 0.570 MeV in ^{207}Pb and E_{γ} = 0.58 MeV in ^{208}Pb. The data obtained from the tabulation of Howerton and Plechaty[80] and the measurement of Scherrer et al.[81] do not include the gamma rays of an energy smaller than 0.5 MeV. The errors caused by the omission of these low-energy gamma rays are well within the quoted errors and, therefore, these data need not be corrected. The large production cross sections of Perkin's at E_n = 5.5 and 8.5 MeV are due mainly to the gamma rays in the energy interval $1.5 < E_{\gamma} < 2.0$, as seen from Figs. 24 and 27. These gamma rays have abnormally large intensities and do not seem to be consistent with the gamma-ray spectra at other incident neutron energies.

6. EVALUATION

In Section 5 it was seen that most of the calculated data were strongly favored by the experimental information. In these cases, calculations provide complete and consistent sets of cross sections. In this section attention is

given to the reactions and the energy ranges for which calculations are not feasible and evaluation has to rely solely on experimental information and, in certain special situations, on educated guesses.

6.1. Total Cross Sections

Below 1 keV there has been no new measurement for the total cross sections since the publication of BNL-325 (Ref. 84). The total cross sections from 0.00025 eV to 1 keV were taken from BNL-325 (Ref. 84) with the 296°K data. From 10^{-5} eV to 0.00025 eV the total cross sections were extended from the above data by assuming that they are proportional to the capture cross sections.

From 0.47 MeV to 20 MeV the total cross sections were taken from the data of R. B. Schwartz.[85] In this energy region measurements of total cross sections are numerous and are available from RNL-325 (References 84 and 9) and the CSISRS data library.[52] Schwartz's data were adopted because 1) the agreement with most of the other data sets is very good, 2) the energy resolutions are small and many new resonances are reasonably well-defined and, 3) the data cover the entire energy region from 0.47 MeV to 20 MeV while other data sets cover only a section of this region.

In the energy range 1 keV to 470 keV, the situation is much less clear-cut than the above two ranges and some difficulties are present. The available data[86-88] are listed in Table 10. Good's data[88] cover the entire energy range and display more detailed resonance structures than the other data sets. In terms of resonance structures, Good's data agree reasonably well with those of Newson _et al_.[86] and Bilpuch _et al_.[87] However, in terms of absolute magnitude, his data are substantially higher than all

Table 10. Total Cross Sections Considered for the Evaluation in the Range 1 keV to 470 keV

Energy Range (keV)	Data Points	Year	Reference
18 - 960	110	1949	Wisconsin(52)
12 - 80	99	1953	Duke(52)
0.2 - 20.5	76	1958	BNL(52)
300 - 750	330	1961	Duke(52)
15 - 50	104	1961	Newson(86)
50 - 360	900	1961	Bilpuch(87)
1 - 1000	10900	1971	Good(88)

the others in certain sections of energy. For instance, near 470 keV Good's data are approximately 1 barn higher than those of Wisconsin,[52] Duke (1961),[52] and Schwartz.[85] Therefore, we adopted Good's data for the resonance structures but adjusted their magnitude to obtain reasonable agreement with most of the available data. From 1 keV to 10 keV, the magnitude was based on BNL-325 (Ref. 84). From 10 keV to 20 keV, the magnitude was based on the average of the data of Newson, Wisconsin, and BNL[52] which agree better among one another than with Good's data. From 20 keV to 50 keV, the magnitude was based on that of Newson. From 50 keV to 65 keV, the magnitude was more or less the average of Bilpuch's and the Wisconsin data. From 65 keV to 200 keV, Good's data agree reasonably well with those of Bilpuch and Wisconsin. From 200 to 300 keV, Good's data agree well with Bilpuch's, but the Wisconsin data are somewhat too low. Therefore, Good's data were unchanged from 65 to 300 keV. From 300 to 470 keV, the magnitude was based on the data of Duke, Bilpuch, and Wisconsin.

The final total cross sections were prepared by taking the intersections of straight lines drawn through the data points on a log-log scale for the range 10^{-5} eV to 1.69 keV and on a linear-linear scale for the range 1.69 keV to 20 MeV. The evaluated total cross sections are displayed in Figs. 29 to 35.

6.2. Elastic-Scattering Cross Sections

The evaluated elastic-scattering cross sections were obtained by subtracting the nonelastic-scattering cross sections from the total cross sections. The result is compared with available data in Fig. 36. The data of Fowler *et al.*,[89] Becker *et al.*,[90] Pasechnik *et al.*,[91] Brugger *et al.*,[92] Buccino *et al.*,[43] and Zafiratos *et al.*[38] were obtained by

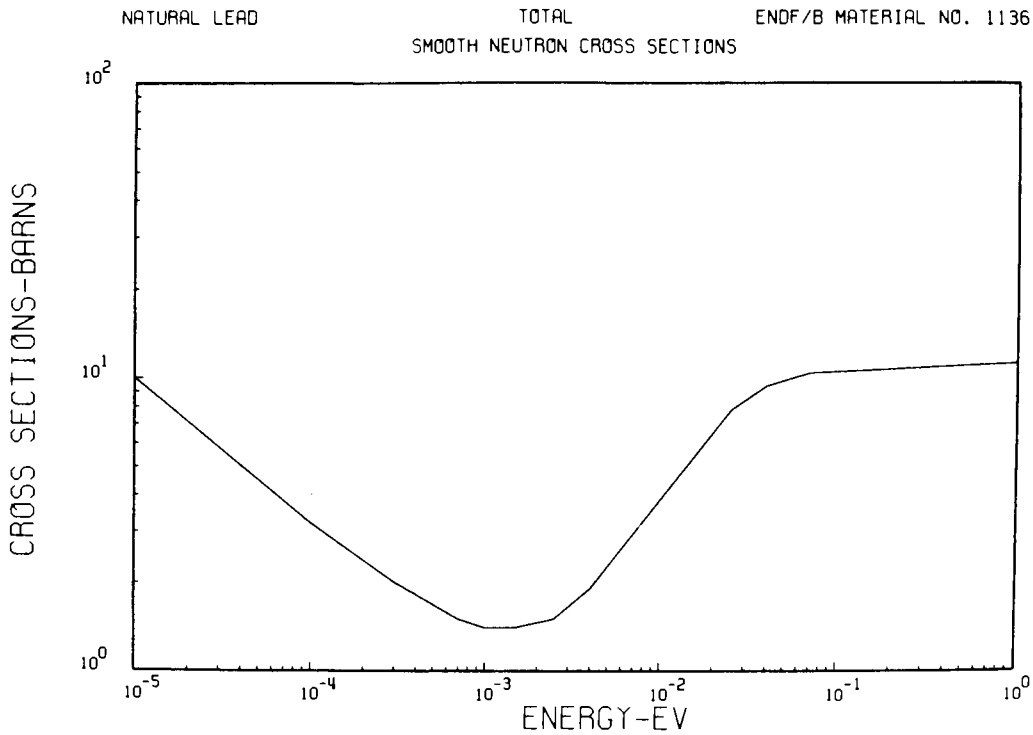

Fig. 29. Smoothed total cross sections from 0.00001 eV to 1 eV.

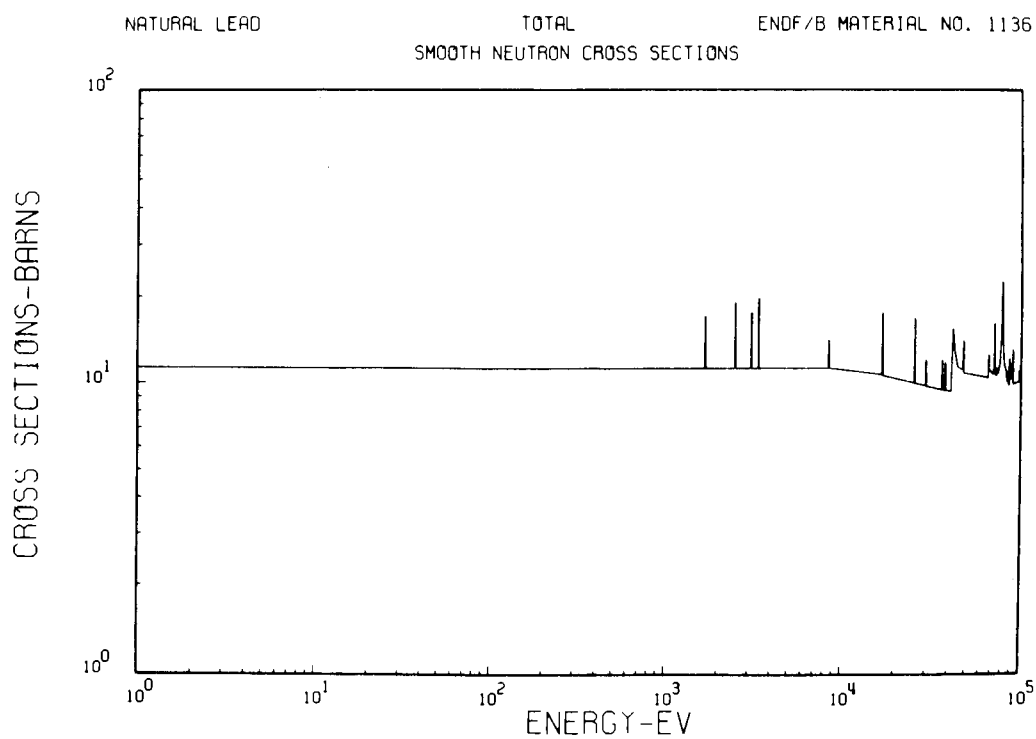

Fig. 30. Smoothed total cross sections from 1 eV to 100 keV.

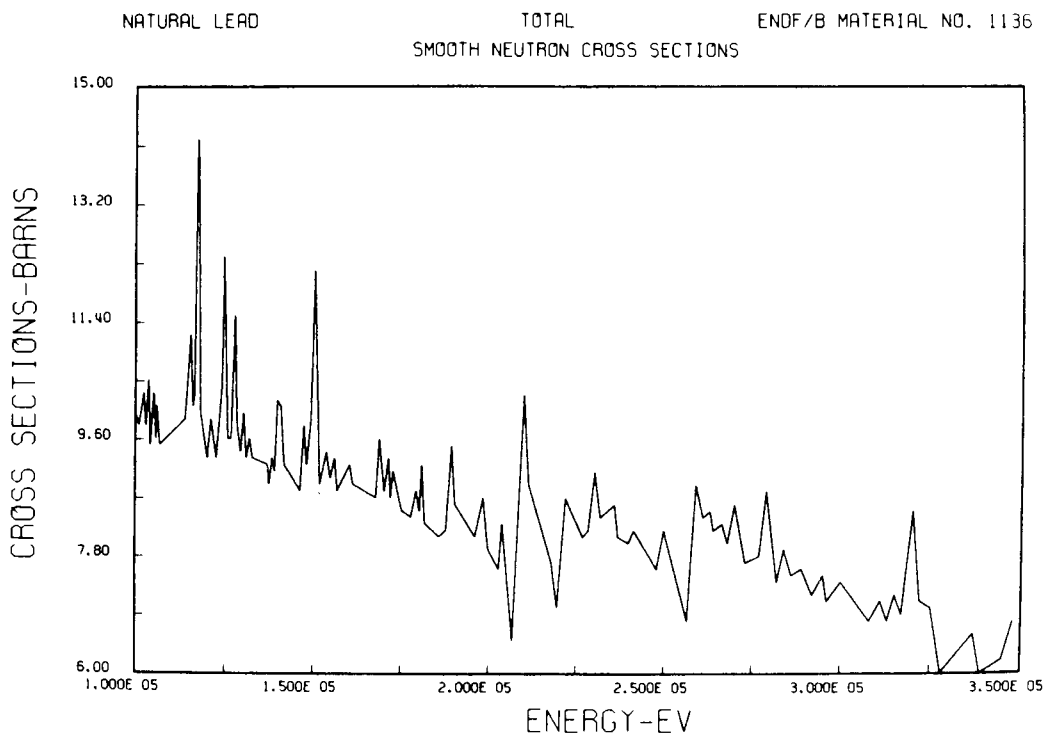

Fig. 31. Smoothed total cross sections from 100 keV to 350 keV.

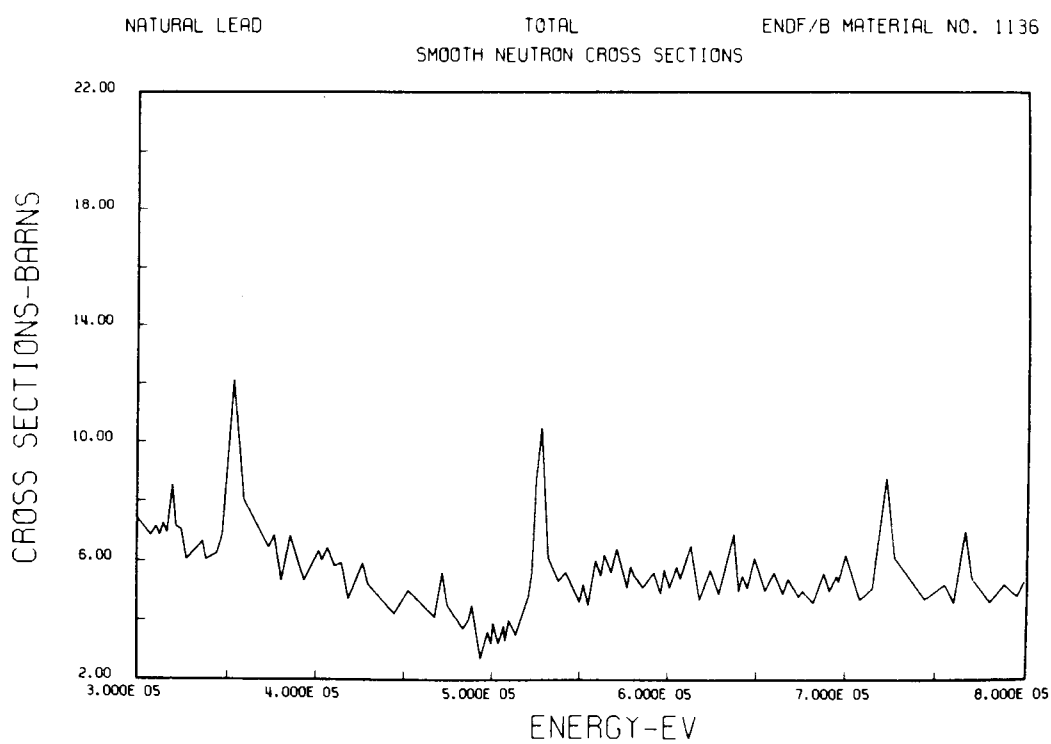

Fig. 32. Smoothed total cross sections from 300 keV to 800 keV.

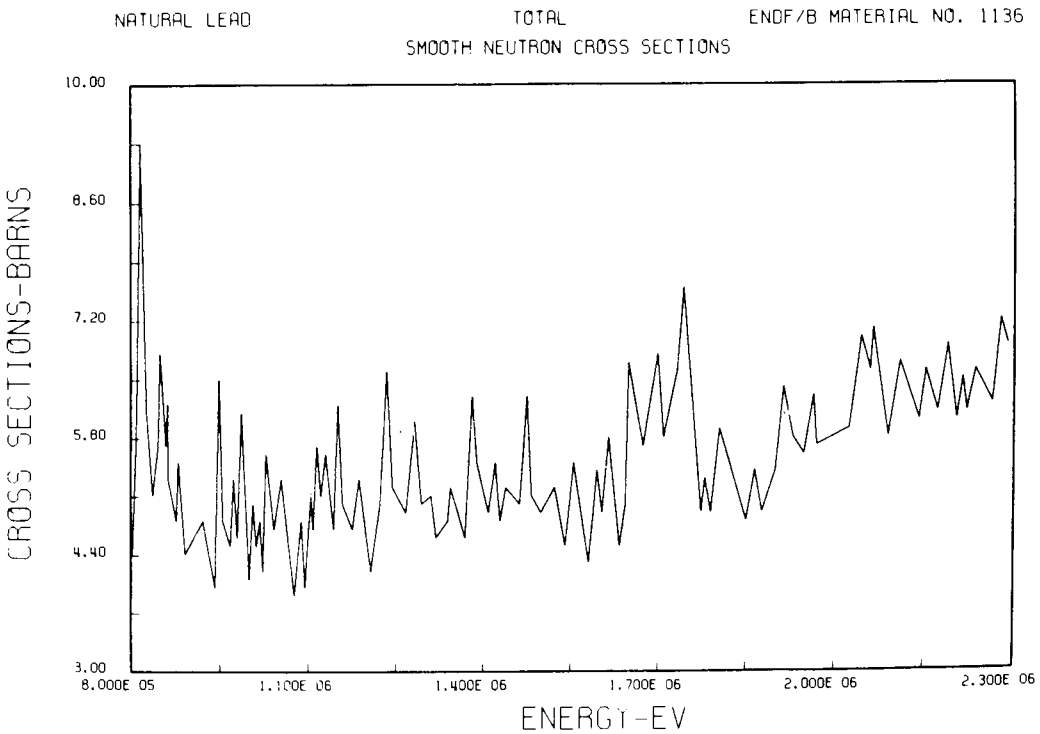

Fig. 33. Smoothed total cross sections from 800 keV to 2.3 MeV.

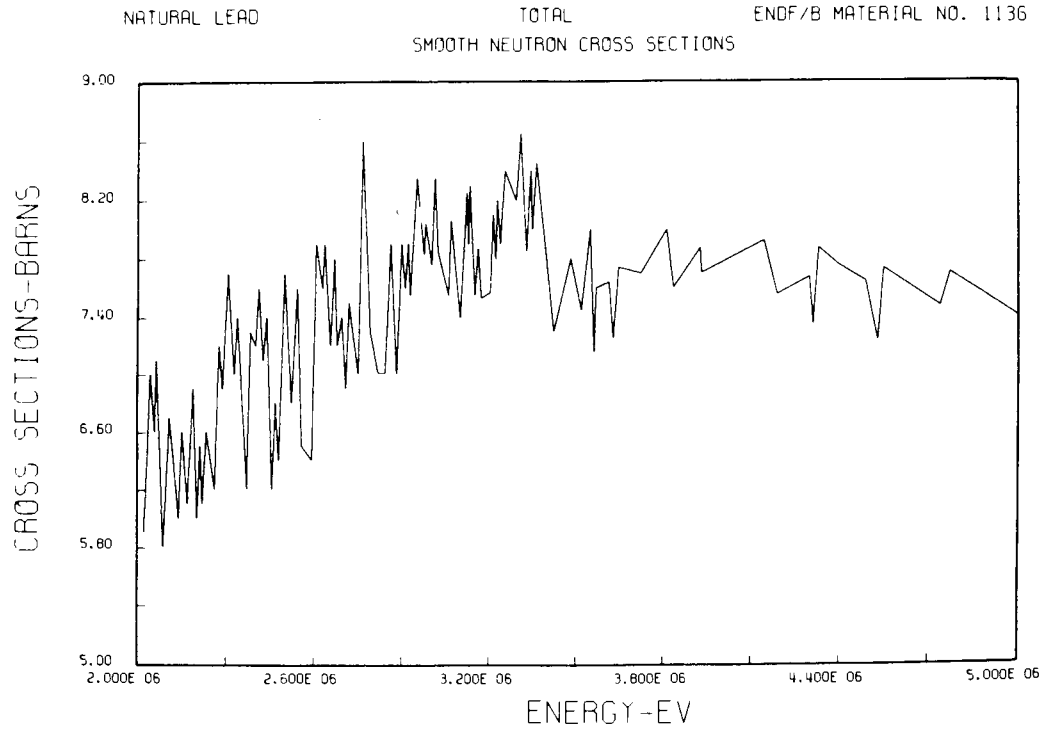

Fig. 34. Smoothed total cross sections from 2 MeV to 5 MeV.

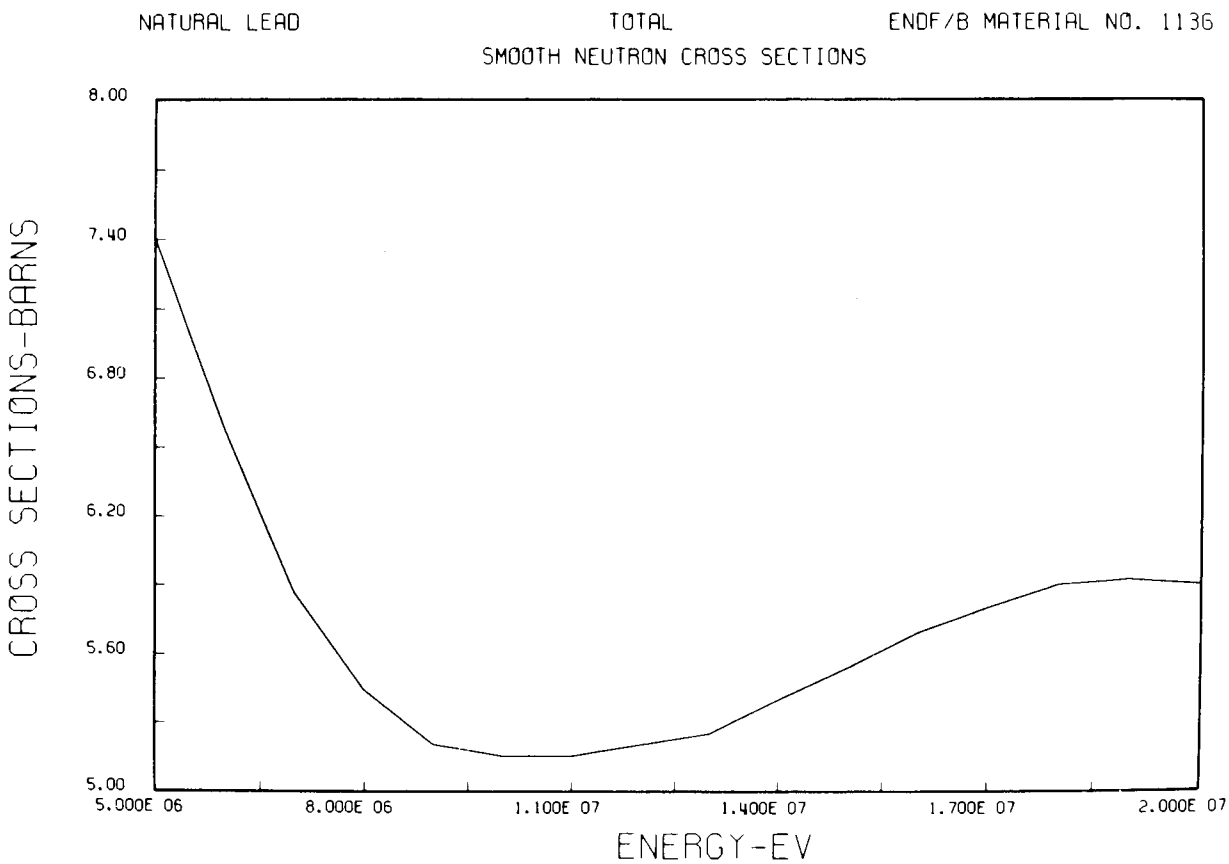

Fig. 35. Smoothed total cross sections from 5 MeV to 20 MeV.

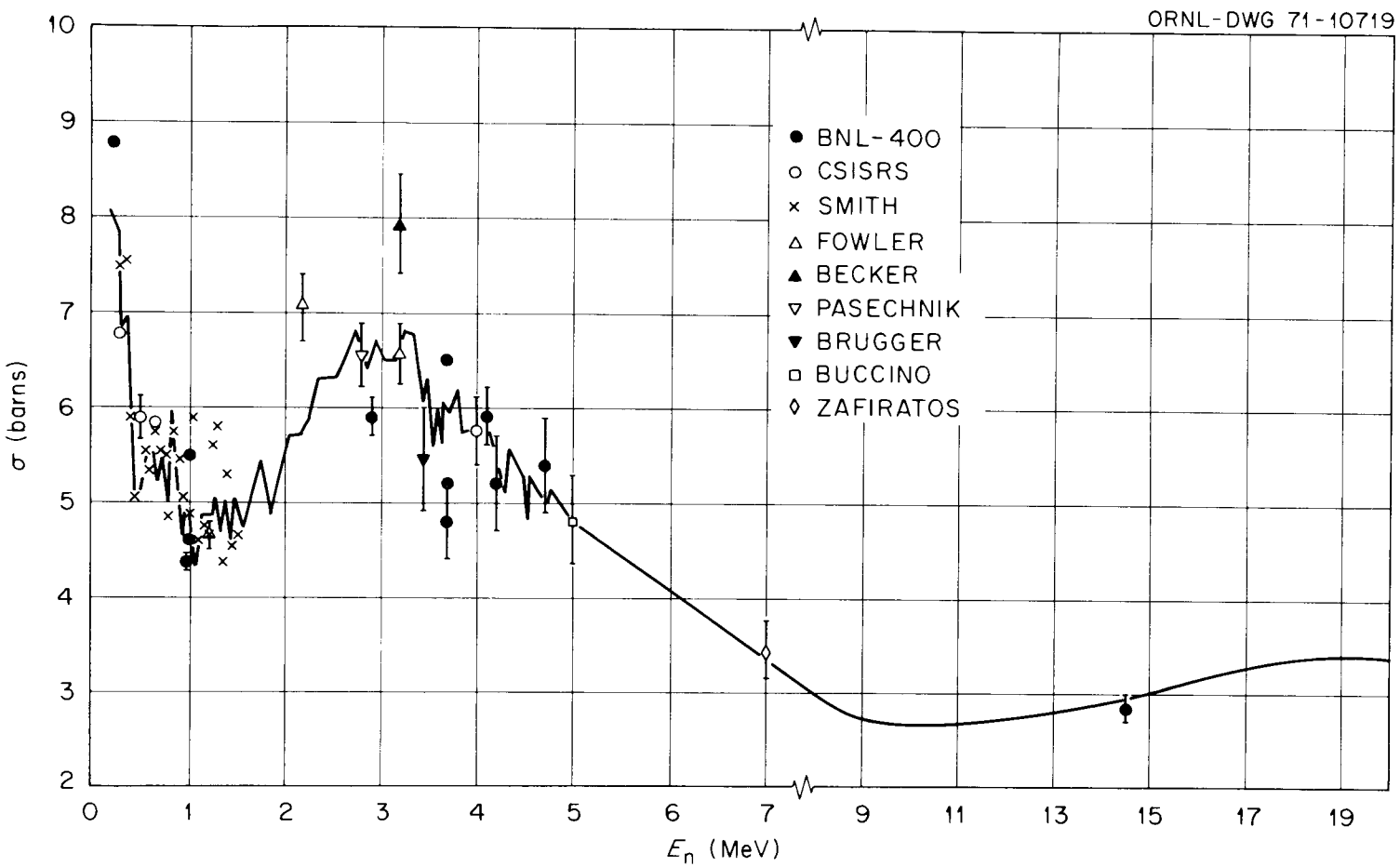

Fig. 36. Comparison of averaged (see text) elastic-scattering cross sections with experiment.

integrating their reported differential cross sections. Other data were obtained from BNL-400 (Ref. 42) and CSISRS data library.[52] The data of A. B. Smith were also taken from CSISRS but were singled out for easier recognition. The available data were measured with energy resolutions varying from 30 keV to 220 keV which are far greater than the widths of most resonances. Therefore, for the purpose of comparison, the curve shown in Fig. 36 is for elastic-scattering cross sections averaged over 50 keV intervals from 0.2 MeV to 1.5 MeV and over 100 keV intervals from 1.5 MeV to 3.5 MeV. Above 3.5 MeV, the curve shown in Fig. 36 corresponds exactly to the evaluated elastic-scattering cross sections. It is evident from Fig. 36 that the available data, while not sufficient to define the detailed structure of elastic-scattering cross sections, are consistent with the difference of the total cross sections and the nonelastic-scattering cross sections.

6.3. Nonelastic-Scattering Cross Sections

Nonelastic-scattering cross sections were taken to be the sum of $\sigma(n,X)$ and $\sigma(n,\gamma)$. $\sigma(n,X)$ was taken from the calculation which has been shown to be in good agreement with available data (see Fig. 18).

6.4. Inelastic-Scattering Cross Sections

Inelastic-scattering cross sections were taken from the calculation which has been shown to be in good agreement with experiment (see Fig. 18). Inelastic excitations of levels below 4.4 MeV were treated as discrete levels. Levels above 4.4 MeV were considered as a continuum. Comparisons of calculations with available data for the low-lying levels have been made and the agreement is generally good (see Figs. 12, 13, and 15). This justifies the adoption of calculated excitation cross sections.

for higher-lying levels. Below 4.4 MeV there are 48 excited states in ^{206}Pb, 49 in ^{207}Pb and 22 in ^{208}Pb which have been merged into 35 levels for natural lead. The structure of the level groups is given in Table 11. Direct-interaction contributions have been included in eleven of these level groups.

6.5. $\sigma(n,2n)$ and $\sigma(n,3n)$

These cross sections were calculated (see Fig. 5). Experimental data for $\sigma(n,2n)$ are available near 14 MeV and have been compared with the calculation in Section 5.4. The calculated cross sections were adopted for lack of alternatives.

6.6. Capture Cross Sections

Capture cross sections of neutrons of 0.0253 eV have been given in Table 1 for the lead isotopes. The weighted sum of these cross sections gives 176 mb for natural lead. The capture cross sections in the low eV region are assumed to be $\frac{1}{v}$ up to a certain energy to be determined. ^{207}Pb accounts for 91% of the thermal captures in natural lead.

In the keV and MeV region, the available data have been included in BNL-325 (Ref. 9) except that of Leipunsky[93] who reported 1 mb at 3 MeV. The data points are too few to define any resonances which are known to be numerous in this energy region. Therefore, smoothed capture cross sections have to be sought. By comparing the natural-lead data with the capture cross sections of ^{206}Pb measured by Macklin et al.[94] and those of ^{207}Pb measured by Allen and Macklin,[95] it is seen that some of the natural-lead data hit the resonance peaks. It is thus rather difficult to obtain smoothed cross sections from the sparse natural-lead data alone. From

Table 11. Level Groups for Inelastic Scattering

Level	^{208}Pb	^{207}Pb	^{206}Pb
1		0.570	
2			0.803*
3		0.898	
4			1.175
5			1.341
6			1.462
7		1.633	
8			1.682*
			1.700
9			1.762
10			1.998
11			2.160
			2.200
			2.210
			2.250
12		2.340	
13			2.385
			2.500
			2.526
14	2.615*		
15		2.624*	
		2.662*	
		2.726	
16			2.634*
17			2.783
			2.800
			2.820
			2.940
18			3.017
			3.050
			3.125
			3.200
19		3.057	
		3.180	
		3.202	
		3.222	
		3.267	
		3.298	
20	3.198*		
21			3.250
			3.280
			3.300
			3.404
22		3.382	
		3.409	
		3.426	

Table 11 cont.

Level	^{208}Pb	^{207}Pb	^{206}Pb
23		3.471	3.453
		3.499	3.500
		3.503	
		3.522	
24	3.475		
25		3.580	3.560
		3.620	3.600
		3.632	
		3.645	
26	3.708*	3.725	3.708
			3.721
27		3.817	3.776*
28		3.854	3.900
		3.891	3.961
29	3.920		
	3.946		
	3.961		
	3.998		
	4.038		
	4.050		
30		3.989	4.005
		4.040	4.075
		4.060	4.125
		4.113	
		4.120	
31	4.076*	4.089*	4.128*
		4.127*	
32	4.125	4.140	4.191
	4.161	4.160	
		4.181	
33	4.204	4.200	4.253
	4.231	4.220	4.259
	4.243	4.240	
	4.258	4.260	
34	4.316	4.288*	4.368*
	4.323*	4.300	
		4.310	
		4.314	
35	4.357	4.339*	4.382
	4.382	4.380*	4.386*
	4.425*	4.388	

*Levels for which direct interactions have been included.

research in nucleosynthesis, Maxwellian averaged cross sections for kT = 30 keV are available.[94-96] These are tabulated in Table 12 for natural lead and the four natural isotopes. Removing the $\frac{1}{v}$ component from the average, the smoothed cross section for natural lead is approximately 5.0 $\pm$ 1.2 mb in the neighborhood of 30 keV. The onset of statistical region for neutron capture in natural lead is probably somewhere around 1 MeV. The data of Diven et al.[97] near 1 MeV vary from 3.3 mb to 3.6 mb. We thus took 3.5 mb as the smoothed cross section at 1 MeV and 5.0 mb at 30 keV. These two points were connected by a straight line on a log-log scale. This line intersects the $\frac{1}{v}$ line at approximately 10 eV. From 1 MeV on, the capture cross sections were defined by a straight line going through 1 mb at 3 MeV on a log-log scale.

6.7. Angular Distribution of Secondary Neutrons

The angular distributions of secondary neutrons from elastic-scattering and inelastic-scattering exciting discrete levels were represented by Legendre coefficients (normalized in the ENDF/B sense) in the center of mass system. The angular distributions of secondary neutrons for (n,n' continuum), (n,2n), and (n,3n) reactions were assumed isotropic.

Above 5 MeV, the angular distributions of elastically scattered neutrons were taken from the calculation (see Section 5.1). Below 5 MeV, the experimental data were best-fitted by Legendre polynomials. The data considered were taken from Smith,[52] Fowler et al.,[89] Becker et al.,[90] Buccino et al.,[43] Pasechnik et al.,[91] Brugger et al.,[92] Bostrom et al.,[74] Whitehead and Snowdon,[98] Gorlov et al.,[48] and Walt and Beyster.[46] The resulting Legendre coefficients were compared with those from calculation in Fig. 37. It is seen from Fig. 37 that the calculated coefficients are slightly higher than

Table 12. Maxwellian-Averaged Capture Cross Sections for kT = 30 keV

Isotope	$\sigma(kT)$ (mb)	Percentage	Reference
Natural	4.6±1.5	---	96
	5.183	100	*
204	43.0±5.0	10.3	94
206	9.6±3.0	43.7	96
207	9.8±2.0	42.7	95
208	0.33±0.07	3.3	94

* Obtained from combining the isotopes.

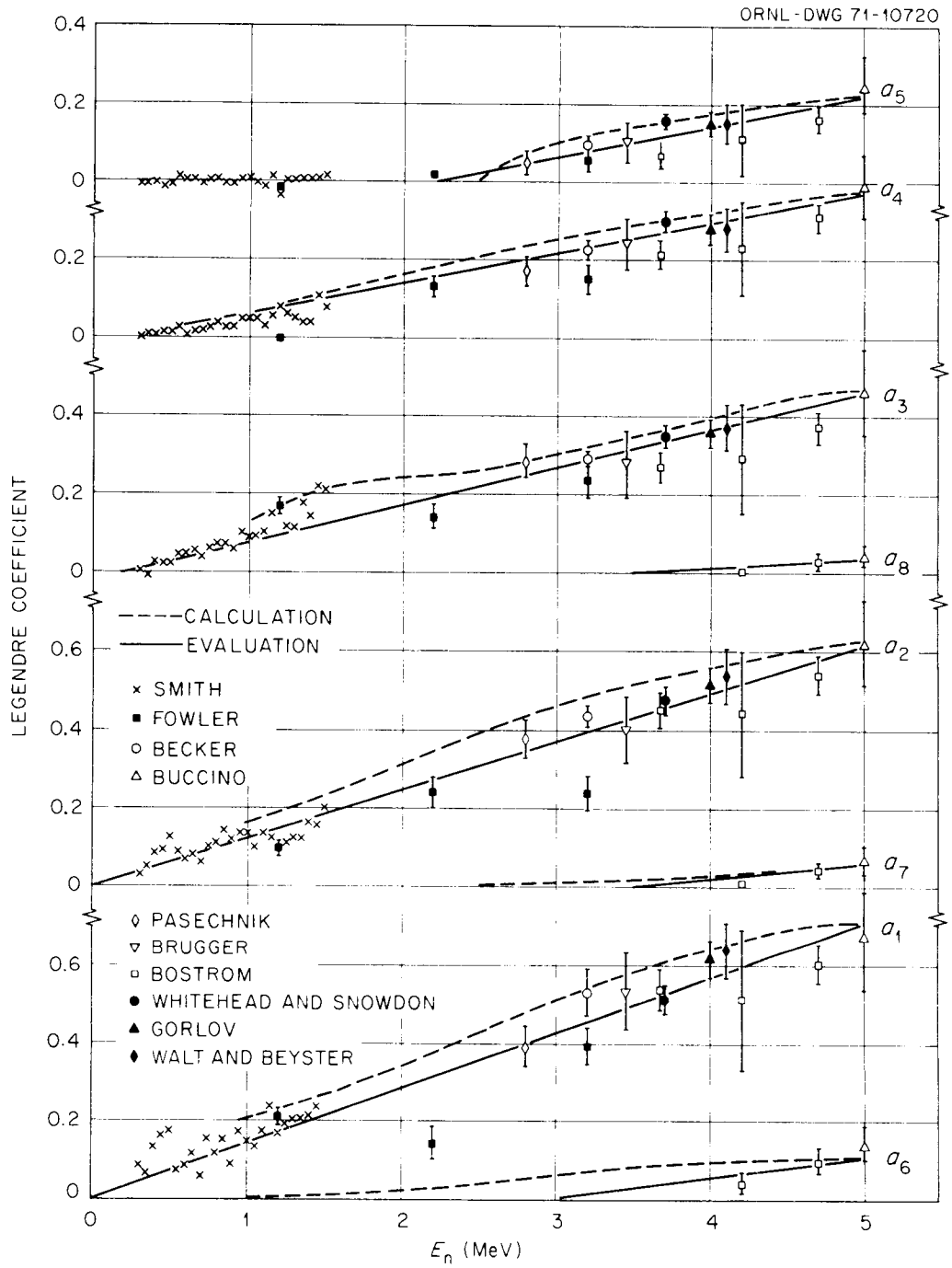

Fig. 37. Legendre expansion coefficients for the angular distributions of elastically scattered neutrons for incident neutrons of energy below 5 MeV.

the experimental data for all coefficients. Therefore, the evaluated Legendre coefficients were determined by linearly fitting the experimental coefficients. It should be noted that most of the measured data do not cover the angles from 150° to 180°. In these cases, extra data points were added, with guidance from calculation, to the measured data for the purpose of obtaining reasonable fittings to the back angles. The extra data were assigned somewhat larger errors than those of the experimental data in order to maintain the essence of the measurements.

The angular distribution of secondary neutrons from inelastic scattering exciting discrete levels were calculated and were given for each level group listed in Table 11. Comparisons of the calculation with avaiable data have been made in Figs. 8, 14, 16, and 17. Agreement between calculation and experiment is quite good.

6.8. Energy Distribution of Secondary Neutrons

The energy distributions of secondary neutrons from (n,n' continuum), (n,2n), and (n,3n) reactions were obtained from theoretical considerations explained in Section 5.5.

6.9. Gamma-Ray-Production Cross Sections

The gamma-ray-production cross sections for the sums of (n,n'), (n,2n), and (n,3n) reactions were taken from the calculation (see Section 5.6). Comparisons of the calculation with the available data have been made in Figs. 20, 21, 22, and 28, and agreement is generally good.

The gamma-ray-production cross sections for neutron capture were taken to be proportional to the capture cross sections with a multiplicity of unity from 10^{-5} eV to 10 eV (the range of $\frac{1}{v}$ capture), and a multiplicity

of 1.407 from 1 keV to 573 keV. From 10 eV to 1 keV, the multiplicity was linearly interpolated. Above 573 keV the capture cross sections are so small that the gamma-ray-production from capture is negligible compared to that from (n,n'), (n,2n), and (n,3n) reactions.

6.10 Angular Distribution of Secondary Gamma Rays

Angular distribution of secondary gamma rays is available to some extent as listed in Table 9 and can be calculated with the method of Sheldon and Van Patter[83] and modifications thereof.[99] However, there has yet been no transport code that can handle anisotropic gamma rays. Therefore, the angular distributions of secondary gamma rays were assumed isotropic in the cross section file. For certain simple problems, corrections for the anisotropy of gamma rays can be made, using the information given in Table 9, after the transport calculation is completed.

6.11. Energy Distribution of Secondary Gamma Rays

The energy distribution of gamma rays from capture of neutrons from 10^{-5} eV to 10 eV is assumed to be that of thermal capture measured by Rasmusen et al.[100] which contains only two gamma rays: 94.91% of E_γ = 7.3677 MeV and 5.09% of E_γ = 6.7364 MeV. From 1 keV to 573 keV, a single gamma-ray spectrum was assumed valid for all resonance captures. In between these two regions, the gamma-ray spectrum was linearly interpolated. The spectrum from resonance captures was determined in the following way.

In their measurement of capture cross sections of ^{207}Pb from 3 keV to 640 keV, Allen and Macklin[96] also reported the fraction of ground state transition to total transitions for each of 36 resonances. Weighting these fractions by the resonance areas for resonances below 573 keV, we obtained

that 83% of the total gamma rays resulted from ground-state transitions. From the spins of the capture states (1 and 2), it is conceivable that the rest of the gamma rays arise dominantly from decays to the 3^-(2.615 MeV) state. This we assumed. Then it is possible to construct an average gamma-ray spectrum for resonance captures in ^{207}Pb, which is shown in Table 13. An average energy of 30 keV was assumed for the captured neutrons.

For captures in ^{206}Pb, Biggerstaff et al.[101] have measured the gamma-ray spectra for seven resonances from 10 keV to 72 keV. These spectra were averaged with equal weight for each resonance because areas under the resonances were not available. The result is also given in Table 13. The observed gamma rays indicate a mean of 27 keV for the captured neutrons.

Resonance captures in ^{204}Pb were assumed to produce the same gamma rays as thermal captures measured by Jurney et al.[100] for lack of experimental information. Fortunately, ^{204}Pb contributes only 10% of resonance captures. Capture cross sections of ^{208}Pb are very small and thermal capture in ^{208}Pb does not produce gamma rays; we therefore ignored resonance capture in ^{208}Pb.

The average gamma-ray spectrum for resonance captures in natural lead was obtained by weighting the spectra of the isotopes by the Maxwellian-averaged capture cross sections given in Table 12. The resulting spectrum as shown in Fig. 38, was assumed valid for capture of all neutrons in the range 1 keV to 573 keV. The spectrum is seen to be drastically different from that of thermal capture. This approach is by no means accurate but it is believed to be far better than the usual assumption that nonthermal captures generate the same gamma rays as thermal captures.

The energy distributions of gamma rays from the sum of (n,n'), (n,2n), and (n,3n) were taken from the calculation. Comparisons of the calculations

Table 13. Average Gamma-Ray Spectra For Resonance Captures in ^{207}Pb and ^{206}Pb

Isotope and Multiplicity	E_γ(MeV)	Gamma Rays per 100 Capture
^{207}Pb	7.406	83.0
	4.791	17.0
1.170	2.615	17.0
^{206}Pb	6.76	32.6
	6.19	17.6
1.674	5.86	20.9
	4.15	12.1
	3.55	16.8
	3.21	16.8
	2.61	12.1
	0.90	20.9
	0.57	17.6

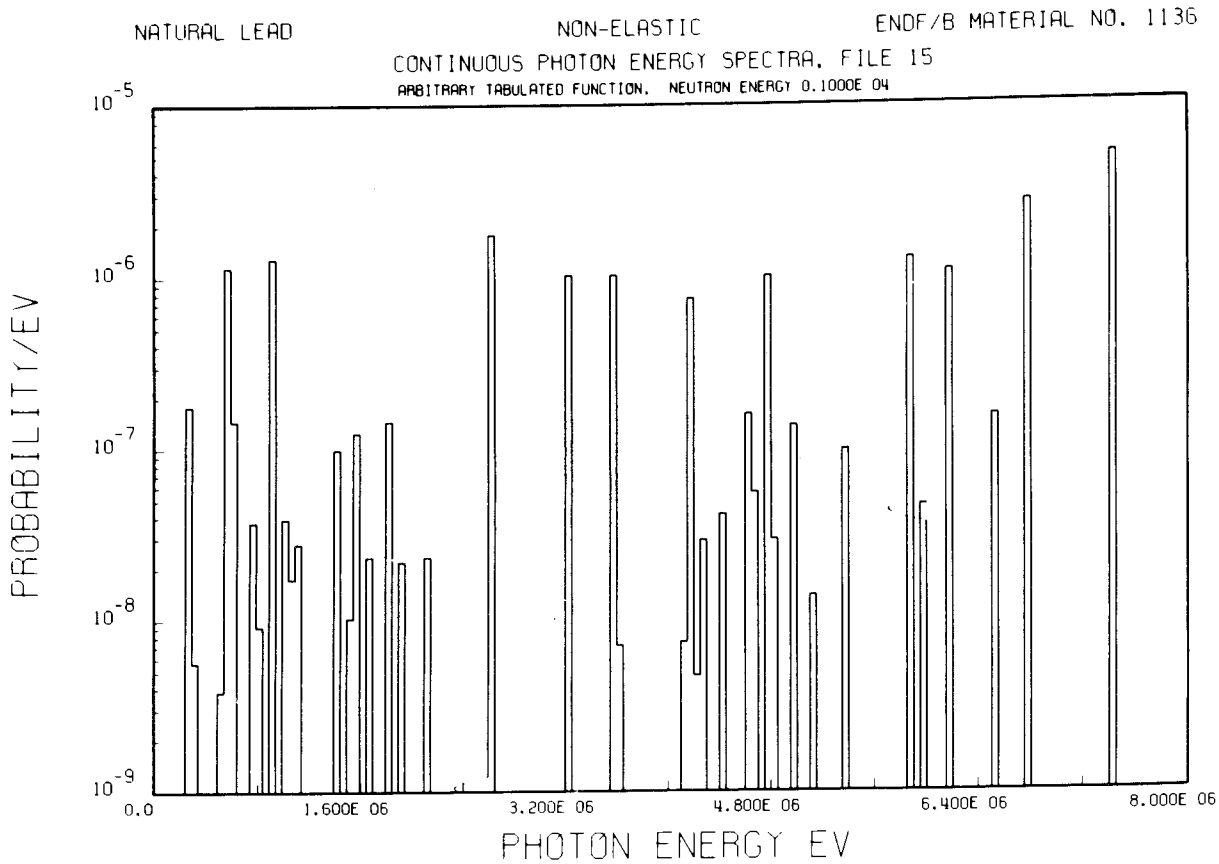

Fig. 38. Representative energy distribution of gamma rays from resonance capture.

with experiment have been discussed in Section 5.6 and shown in Figs. 20 - 27.

6.12. Photon Interaction Cross Sections

Photon interaction cross sections were taken from an evaluation by McMaster et al.[102] in the energy range 1 keV to 1 MeV and from a compilation by Plechaty and Terral[103] for the range 1 MeV to 100 MeV. The interactions considered were total, coherent scattering, incoherent scattering, pair production plus triplet production, and photo-elastic. Only the integrated cross sections were incorporated into the evaluation.

7. CONCLUSION AND DISCUSSIONS

In Section 2 we briefly described the extent of the present evaluation for the purpose of helping those who are familiar with and have used the previously available cross section sets. The nuclear properties of the lead isotopes needed for model calculations were established in Section 3. In Section 4 we outlined the computer codes used and the procedures adopted for the calculations. Details of the calculations and comparisons of the calculated cross sections with experiments were presented in Section 5. The way the final data sets were chosen was given in Section 6.

It has been obvious that the status of experimental data in lead is such that heavy reliance had to be placed with calculations. The calculated cross sections, when adopted, have been shown to be strongly favored by available data. Most of the calculations have been known from experience to be trustworthy for interpolation and extrapolation into energies and angles not covered by measured data. However, the following areas of calculation are believed the weakest and assumptions embodied in the calculations need to be tested:

1. The gamma-ray-production cross sections and the energy distributions of secondary gamma rays for the sum of (n,n'), (n,2n), and (n,3n) reactions for incident neutrons above 8 MeV.

2. The energy distributions of secondary neutrons for (n,n' continuum), (n,2n), and (n,3n) reactions.

3. The (n,3n) cross sections right above the threshold.

In cases the evaluation had to be dependent upon experimental data alone and the data are sparse or large discrepancies exist among various measurements; the evaluation was, of course, weakened. The most severe cases are:

1. Capture cross sections in the nonthermal range.

2. Gamma-ray spectra from resonance captures.

3. Total cross sections in several portions of the range 1 keV to 470 keV.

Some of these weaknesses of the evaluation may be removed by measurements currently being performed at Oak Ridge National Laboratory:

1. Inelastic scattering exciting levels and the resulting gamma rays for ^{206}Pb, ^{207}Pb, and ^{208}Pb for incident neutrons from 5.5 MeV to 8.5 MeV by J. K. Dickens and F. G. Perey.

2. Capture cross sections of ^{206}Pb and ^{204}Pb from 3 keV to 900 keV by B. J. Allen and R. L. Macklin.

3. Remeasurement of total cross sections from 1 keV to 1 MeV by W. M. Good.

4. Gamma rays from resonance captures by G. G. Slaughter.

These new data when available will strengthen the evaluation substantially.

We would appreciate being informed of any discrepancies among experiments and calculations using this evaluation, since we plan to revise the evaluation as new information becomes available.

8. ACKNOWLEDGEMENTS

We are grateful to S. K. Penny of the ORNL Mathematics Division for his providing the code HELGA and for many useful discussions. We gratefully acknowledge the help of R. Q. Wright, also of ORNL Mathematics Division, in his deriving some of the redundant cross sections and in the plotting of the total cross sections. We are indebted to R. B. Schwartz of NBS and W. M. Good of ORNL Physics Division in sending their total cross section data prior to publication.

REFERENCES

1. M. K. Drake, (ed.), Data Formats and Procedures for the ENDF Neutron Cross Section Library, Preliminary Report, Brookhaven National Laboratory (1970). Revision of BNL-8381 (ENDF) and BNL-50066 (ENDF-102).

2. D. J. Dudziak, ENDF/B Formats and Procedures for Photon Production and Interaction Data, Preliminary Report, Los Alamos Scientific Laboratory (1970). Revision of LA-3801 or ENDF-111.

3. B. R. S. Buckingham, K. Parker, and E. D. Pendlebury, Neutron Cross Sections of Selected Elements and Isotopes for Use in Neutronic Calculations in the Energy Range 0.025 eV - 15 MeV, United Kingdom Atomic Energy Authority Report AERE-O-28/60 (1961).

4. E. P. Barrington, A. L. Pope, and J. S. Story, The Data in the Winfrith Nuclear Data Library, United Kingdom Atomic Energy Authority Report AEEW-R-351 (1964).

5. M. C. Bertin et al., Neutron Cross Sections of ^{238}U, ^{235}U, ^{237}U, ^{239}U, ^{234}U, ^{236}U, ^{239}Pu, ^{240}Pu, W, Pb, Ni, Cr, C, ^{6}Li, ^{7}Li, and T, United Nuclear Corporation Report UNC-5099 (1964).

6. F. R. Mynatt, Oak Ridge National Laboratory, Private Communication.

7. W. E. Ford, III, The POPOP4 Library of Neutron Induced Secondary Gamma Ray Yield and Cross Section Data, Union Carbide Corporation Report CTC-42 (1970).

8. C. A. Rohrmann, "Chart of the Nuclides," (May 1969) prepared by Battelle Northwest.

9. M. D. Goldberg et al., Neutron Cross Sections, Vol. 11C, Z = 61 to 87, BNL-325, 2nd Edition, Supplement No. 2 (1966).

10. J. H. E. Mattauel, W. Thiele, and A. H. Wapstra, Nucl. Phys. 67, No. 1, 32 (1965).

11. C. Maples, G. W. Goth, and J. Cerny, "Nuclear Reaction Q-Values," Nuclear Data, Section A, Vol. 2, Nos. 5 and 6 (1966).

12. Nuclear Data Sheets compiled by K. Way, et al., Printing and Publishing Office, National Academy of Sciences, National Research Council, Washington, D. C. (1965).

13. D. A. Lind and R. B. Day, Ann. Phys. 12, 485 (1961).

14. L. Cranberg et al., Phys. Rev. 159, 969 (1967).

15. D. E. Alburger and M. H. L. Pryce, Phys. Rev. 95, 1482 (1954).

16. J. Saudinos et al., Nucl. Sci. and Appl. 3, 22 (1967).

17. R. L. Auble, Nuclear Data Sheets, A=207, Preprint (1970).

18. L. Cranberg and C. D. Zafiratos, Phys. Rev. 142, 775 (1966).

19. E. Grosse et al., Z. Physik 218, 213 (1969).

20. M. B. Lewis, Nuclear Data Sheets, A=208, Preprint (1970).

21. D. O. Nellis, I. L. Morgan, and E. L. Hudspeth, "Gamma Rays from $^{208}Pb(n,n'\gamma)$," Texas Nuclear Corp. Preprint (1970).

22. P. H. Stelson and L. Grodzins, "Nuclear Transition Probability, B(E2), for $D^{f}_{9.5} \rightarrow 2^{f}_{first}$ Transitions and Deformation Parameter, β_2," Nuclear Data 1, No. 1, 21 (1965).

23. P. H. Stelson et al., Nucl. Phys. 68, 97 (1965).

24. A. Gilbert and A. G. W. Cameron, Can. J. Phys. 43, 1446 (1965).

25. S. K. Penny, HELENE - A Computer Program to Calculate Nuclear Cross Sections Employing the Hauser-Feshbach Model, Porter-Thomas Width Fluctuations and Continuum States, ORNL-TM-2590 (1969).

26. H. Baba, Nucl. Phys. A159, 625 (1970).

27. F. G. Perey, Computer Code GENOA, not published (1969).

28. F. G. Perey and B. Buck, Nucl. Phys. 32, 353 (1962).

29. S. K. Penny, Computer Code HELGA is an advanced version of HELENE, Reference 25.

30. W. Hauser and H. Feshbach, Phys. Rev. 87, 366 (1952).

31. C. E. Porter and R. G. Thomas, Phys. Rev. 104, 483 (1956).

32. R. H. Bassel, R. M. Drisko, and G. R. Satchler, The Distroted Wave Theory of Direct Nuclear Reactions. I = 'Zero Range' Formalism Without Spin-Orbit Coupling, and the Code SALLY., Oak Ridge National Laboratory Report ORNL-3240 (1962).

33. G. R. Satchler, Nucl. Phys. 55, 1 (1964).

34. C. Y. Fu, Computer Code NNNGAM, unpublished (1971).

35. H. Goldstein, "Statistical-Model Theory of Neutron Reactions and Scattering," Fast Neutron Physics, Part II, ed. by J. B. Marion and J. L. Fowler, Interscience Publishers, N. Y. 1963.

36. E. S. Troubetzkoy, Phys. Rev. 122, 212 (1961).

37. D. Wilmore and P. E. Hodgson, Nucl. Phys. 55, 673 (1964).

38. C. D. Zafiratos et al., Phys. Rev. Letters 14, 913 (1965).

39. B. Y. Guzhovskii, Soviet J. of Atomic Energy 11, 1041 (1962).

40. J. H. Coon et al., Phys. Rev. 111, 250 (1958).

41. J. D. Anderson et al., Phys. Rev. 110, 160 (1958).

42. M. D. Goldberg, V. M. May, and J. R. Stehn, Angular Distributions in Neutron-Induced Reactions, Volume 2, Z = 23 to 94, Brookhaven National Laboratory Report BNL-400 (1962).

43. S. G. Buccino et al., Z. Physik 196, 103 (1966).

44. R. W. Hill, Bull. Am. Phys. Soc. Ser. II, 1, 174 (1956).

45. R. W. Hill, Phys. Rev. 109, 2105 (1958).

46. M. Walt, and J. R. Beyster, Phys. Rev. 98, 677 (1955).

47. P. L. Okhuysen and J. T. Prud'homme, Phys. Rev. 116, 986 (1959).

48. G. V. Gorlov et al., Dokl Ak. Nauk 158, 574 (1964).

49. J. H. Towle and W. B. Gilboy, Nucl. Phys. 44, 256 (1963). Data taken from BNL-325 (1966).

50. R. F. Coleman et al., Proc. Phys. Soc. 73, 215 (1959).

51. S. Pearlstein, Nucl. Sci. Eng. 23, 238 (1965).

52. CSISRS data library, Brookhaven National Laboratory (1970).

53. M. Walt and H. H. Barschall, Phys. Rev. 93, 1062 (1954).

54. J. R. Beyster et al., Phys. Rev. 98, 1216 (1955).

55. J. R. Beyster, M. Walt, and E. W. Salmi, Phys. Rev. 104, 1319 (1956).

56. V. I. Strizhak, Zhur. Eksp. i Theoret. Fiz 31, 907 (1956). (Trans. in Soviet Phys. JETP 4, 769 (1957)).

57. H. L. Taylor, O. Lonsjo, and T. W. Bonner, Phys. Rev. 100, 174 (1955).

58. M. V. Pasechnik, First Geneva Conference 2, 3 (1955).

59. Yu. G. Degtyarev, Atomnaya Energiya 19, 456 (1965). (Transl. in Soviet J. Atomic Energy 19, 1426 (1966)).

60. T. W. Bonner and J. C. Slattery, Phys. Rev. 113, 1088 (1959).

61. Yu. G. Degtyarev and V. G. Nadtochii, Atomnaya Energiya 11, 397 (1961). (Transl. in Soviet J. Atomic Energy 11, 1043 (1962)).

62. A. Chatterjee and A. M. Ghose, Phys. Rev. 161, 1181 (1967).

63. M. H. MacGregor, International Congress on Nuclear Physics, Paris, P. 609 (1958).

64. B. Jönsson, Physica Scripta 2, 277 (1970).

65. A. Adams et al., Nucl. Phys. 49, 489 (1963).

66. N. M. Flerov and V. M. Talizin, Atomnaya Energiya 5, 657 (1958). (Transl. in J. Nuclear Energy 2, 174 (1959)).

67. P. P. Lebedov et al., J. Nucl. Energy, Part A = Reactor Science, Vol. 11, p. 39 (1959).

68. E. R. Graves and R. W. Davis, Phys. Rev. 97, 1205 (1955).

69. V. J. Ashby et al., Phys. Rev. 111, 616 (1958).

70. K. J. LeCouteur, Proc. Phys. Soc. A65, 718 (1952). See also Nuclear Reactions, Vol. 1, p. 318 ed. by P. M. Endt and M. Demur, North-Holland (1959).

71. S. C. Mathur, P. S. Buchanan, and I. L. Morgan, Phys. Rev. 186, 1038 (1969).

72. P. Huber et al., Phys. Letters 5, 202 (1963).

73. D. Thomson, Phys. Rev. 129, 1649 (1963).

74. N. A. Bostrom et al., Interaction of Fast Neutrons in Iron, Lead, Oxygen, and Nitrogen, WADC-59-31 (1959).

75. J. W. Boring and M. T. McEllistrem, Phys. Rev. 124, 1531 (1961).

76. R. M. Kiehn and C. Goodman, Phys. Rev. 95, 939 (1954).

77. R. B. Day, Phys. Rev. 102, 767 (1956).

78. I. L. Morgan et al., Nuclear Physics Division Annual Progress Report, Texas Nuclear Corporation Report TID-20657 (1963).

79. J. L. Perkin, Nucl. Phys. 60, 561 (1964).

80. R. J. Howerton and E. F. Plechaty, Nucl. Sci. Eng. 32, 178-183 (1968).

81. V. E. Scherrer, R. B. Theus, and W. R. Faust, Phys. Rev. 91, 1476 (1953).

82. M. E. Battat, R. W. Davis, and A. H. Frentrop, Gamma Rays from 14-MeV Neutron Bombardment of C, O, Al, Fe, and Pb, LA-1507 (1953).

83. E. Sheldon and D. M. Van Patter, Rev. Mod. Phys. 38, 143 (1966).

84. D. J. Hughes and R. B. Schwartz, Neutron Cross Sections, Brookhaven National Laboratory Report BNL-325 2nd ed. (1958).

85. R. B. Schwartz, National Bureau of Standards, private communication (1971).

86. H. W. Newson et al., Ann. Phys. 14, 346 (1961).

87. E. G. Bilpuch et al., Ann. Phys. 14, 387 (1961).

88. W. M. Good, Oak Ridge National Laboratory, private communication (1971).

89. J. L. Fowler and E. C. Campbell, Phys. Rev. 127, 2192 (1962).

90. R. L. Becker et al., Nucl. Phys. 89, 154 (1966).

91. M. V. Pasechnik et al., Second Geneva Conference, Vol. 15, p. 18 (1958).

92. H. R. Brugger et al., Helv. Phys. Acte. 28, 331 (1955).

93. A. I. Leipunsky et al., Second International Conference, Vol. 15, p. 50 (1958).

94. R. L. Macklin and J. H. Gibbons, Phys. Rev. 181, 1639 (1969).

95. B. J. Allen and R. L. Macklin, "The Neutron Capture Cross Section of ^{207}Pb," Transactions of Neutron Cross Section Conference ed. by R. L. Macklin, p. 764, Knoxville, Tennessee (March 1971).

96. B. J. Allen, J. H. Gibbons, and R. L. Macklin, "Nucleosynthesis and Neutron Capture Cross Section," to be published in Advances in Nuclear Physics (1971).

97. B. C. Diven et al., Phys. Rev. 120, 556 (1960).

98. W. D. Whitehead and S. C. Snowdon, Phys. Rev. 92, 114 (1953).

99. S. C. Mathur, P. S. Buchanan, and I. L. Morgan, Phys. Rev. 160, 816 (1967).

100. L. V. Groshev et al., "Compendium of Thermal-Neutron-Capture γ-Ray Measurements, Part III. Z=68 to Z=94 (Er to Pb)," Nuclear Data, Vol. V, Nos. 3-4 (1969).

101. J. A. Biggerstaff et al., Phys. Rev. 154, 1136 (1967).

102. W. H. McMaster et al., Compilation of X-Ray Cross Sections, UCRL-50174 (1969).

103. E. F. Plechaty and J. R. Terrall, An Integrated System for Production of Neutrons and Photonic Calculational Constants: Vol. VI, Photon Cross Sections 1 keV to 100 MeV, UCRL-50400 (1968).

ORNL-4765
UC-34 — Physics

INTERNAL DISTRIBUTION

1-3. Central Research Library
4. ORNL — Y-12 Technical Library Document Reference Section
5-54. Laboratory Records Department
55. Laboratory Records, ORNL R.C.
56. L. S. Abbott
57. R. G. Alsmiller, Jr.
58. C. E. Clifford
59. F. L. Culler
60. J. K. Dickens
61-70. C. Y. Fu
71. R. F. Hibbs
72. W. E. Kinney
73-74. F. C. Maienschein
75. G. McNeilly
76. R. W. Peelle
77. S. K. Penny
78-97. F. G. Perey
98. M. J. Skinner
99. D. A. Sundberg
100. A. M. Weinberg
101. J. E. White
102. R. Q. Wright
103. H. Feshbach (consultant)
104. H. Goldstein (consultant)
105. C. R. Mehl (consultant)
106. H. T. Motz (consultant)

EXTERNAL DISTRIBUTION

107. P. B. Hemmig, Division of Reactor Development and Technology, U.S. Atomic Energy Commission, Washington, D.C. 20546
108. W. H. Hannum, Division of Reactor Development and Technology, U.S. Atomic Energy Commission, Washington, D.C. 20546
109. K. O. Laughon, AEC Site Representative, ORNL
110. Department of Defense, Defense Nuclear Agency, Washington, D.C. 20305
111. P. G. Young, Los Alamos Scientific Laboratory, Los Alamos, New Mexico 87544
112. Norman Francis, Knolls Atomic Power Laboratory, General Electric, Schenectady, New York 12309
113. R. L. Howerton, Lawrence Radiation Laboratory, Livermore, California 94550
114. M. Drake, Brookhaven National Laboratory, Upton, L.I. New York 11973
115. Leona Stewart, Los Alamos Scientific Laboratory, Los Alamos, New Mexico 87544
116. Martin P. Fricke, Gulf Radiation Technology, P. O. Box 608, San Diego, California 92112
117-256. Given Special DNA Shielding Distribution
257. J. A. Swartout, Union Carbide Corporation, New York, N.Y. 10017
258-260. Director, Division of Reactor Licensing (DRL), U.S. Atomic Energy Commission, Washington, D.C.
261-262. Director, Division of Reactor Standards (DRS), U.S. Atomic Energy Commission, Washington, D.C.
263-267. Executive Secretary, Advisory Committee on Reactor Safeguards, U.S. Atomic Energy Commission, Washington, D.C.
268. Patent Office, AEC, ORO
269. Laboratory and University Division, AEC, ORO
270-496. Given distribution as shown in TID-4500 category under Physics category (25 copies — NTIS)